Transport and Density Fluctuations in Disordered Systems: Appliations to Atmospheric Dispersion

Rehab Bitane

Université de Nice–Sophia Antipolis - UFR Sciences

Ecole Doctorale de Sciences Fondamentales et Appliquées

THESIS

to obtain the title of

Ph.D. in Sciences

of the University of Nice-Sophia Antipolis

Discipline : Physics

presented and defended by

Rehab Bitane

Transport and Density Fluctuations in Disordered Systems

Applications to Atmospheric Dispersion

defended on the 22nd of November 2012

Committee :

Mr.	Mickaël Bourgoin	Referee
Ms.	Alessandra Lanotte	Referee
Mr.	Marc-Étienne Brachet	Member of the Commitee
Mr.	Alain Pumir	President of the Commitee
Mr.	Alain Noullez	Advisor
Mr.	Jérémie Bec	Co-advisor

Université de Nice–Sophia Antipolis - UFR Sciences
Ecole Doctorale de Sciences Fondamentales et Appliquées

THÈSE

pour obtenir le titre de
Docteur en Sciences
de l'Université de Nice-Sophia Antipolis

Discipline : Physique

présentée et soutenue par

Rehab Bitane

Transport et Fluctuations de Densité dans les Systèmes Désordonnés

Applications à la Dispersion Atmophérique

Thèse dirigée par Alain NOULLEZ
et co-dirigée par Jérémie BEC

soutenue le 22 Novembre 2012

Jury :

M.	Mickaël Bourgoin	Rapporteur
Mme.	Alessandra Lanotte	Rapporteur
M.	Marc-Étienne Brachet	Examinateur
M.	Alain Pumir	Président
M.	Alain Noullez	Directeur
M.	Jérémie Bec	Co-directeur

A mia nonna Immacolata

Résumé

Le transport turbulent de particules est un phénomène important qui intervient dans de nombreux processus naturels et industriels. Comprendre ses propriétés et, en particulier, la création de grandes fluctuations de densité, est fondamental pour améliorer les modèles et affiner les prévisions. Cela représente de nombreux enjeux économiques, environnementaux et de santé. Une étude Lagrangienne de la séparation de paires de traceurs a été menée en s'appuyant sur l'analyse des données de simulations numériques à très haute résolution. Elle a permis de souligner les défaillances des approches de type champ moyen qui sont à la base des modèles les plus couramment utilisés. Pour la séparation, on constate que la transition entre le régime balistique de Batchelor et le régime explosif de Richardson a lieu à des temps données par le temps moyen de dissipation de l'énergie cinétique turbulente. Aussi, il est montré que la loi de Richardson peut s'interpréter comme un comportement diffusif des différences de vitesse. Des arguments phénoménologiques permettent d'interpréter cet effet par la décorrélation de différences d'accélération et la stationnarité aux temps longs du taux local de transfert d'énergie cinétique. Les moments d'ordres élevés de la séparation et de la vitesse sont aussi étudiés pour aborder la question des "événements violents" dans la distribution des distances. Enfin, un modèle d'éjection de masse est proposé et utilisé pour examiner les fluctuations de la densité de particules lourdes transportées dans un environnement aléatoire.

Summary

The turbulent transport of particles is an important phenomena which appears in many natural and industrial processes. Understanding its properties, and, in particular, the creation of strong density fluctuations, is fundamental to improve models and refine forecasts. This can lead to significant benefits in issues related to economics, the environmental and health. A Lagrangian study of the tracer pair separation was carried out with the help of high resolution data analysis. This allowed us to point out the weaknesses of the mean-field approaches on which most models are based. For the separation, it is found that the transition from the regime of Batchelor (or ballistic) to that of Richardson (or explosive) occurs at times given by those typical of the turbulent kinetic energy dissipation. It is also found that Richardson's law can be reinterpreted in terms of diffusive behaviour of the velocity differences. Phenomenological arguments allow us to explain this effect through the decorrelation of the acceleration differences and the stationarity of the

kinetic energy transfer ratio at large times. The high-order moments of both separation and velocity are also investigated to address the question of “violent events" in the distribution of the distances. Finally, a one-dimensional mass ejection model is proposed and used to examine the density fluctuations of heavy particles transported by the random environment.

Contents

Chapter 1

Introduction

Almost all natural and industrial fluid flows are usually in a turbulent state. Their study has always attracted much attention in order to understand, for example, the hydro or aerodynamical properties of objects, to model winds in meteorology or fluxes in factory devices, and to quantify the timescales at which transported species are mixed and dispersed. During the last two decades turbulent transport has gathered a growing interest in the scientific community. This is due to the development of new societal concerns related to pollution and climate change and, at the same time, to the emergence of the scientific paradigm of Lagrangian turbulence. Turbulent transport is indeed ubiquitous in atmospheric physics, oceanography and astrophysics [Csanady, 1973, Seinfeld & Pandis, 2006, Battaner, 1996]. It plays a crucial role in modeling the dispersion of volcanic ashes [Peterson & Dean, 2008] or of pollutants [Arya, 1999, Cooper & Alley, 2002], the dynamics of plankton populations in seas [Lewis & Bala, 2006], the formation of clouds [Pinsky & Khain, 1997], the initiation of rain [Shaw, 2003] or the early stages of planet formation [De Pater & Lissauer, 2001, Charnoz et al., 2011]. Illustrations of such applications are shown in Fig. 1.1. The phenomena occurring in the atmosphere are the object of intense studies because, in addition to important economical and ecological implications, their precise understanding is needed to design efficient and reliable models in meteorology and climate sciences. In parallel to such a growth of interest, the last decades witnessed the development of new theoretical approaches for the problem of turbulent transport, or of Lagrangian turbulence. Such fundamental contributions have used tools taken from statistical physics and field theory [Shraiman et al., 2000, Falkovich et al., 2001, Cardy et al., 2008] and led to important results related, for instance, to the anomalous scaling of passive tracers [Bernard et al., 1996], to the improvement of collision kernels for warm clouds [Falkovich et al., 2002], and to the statistical properties of vor-

ticity contours in two-dimensional turbulence [Bernard et al., 2006]. These advances were intricately connected to simultaneous experimental developments. Recent optical and electronic technologies have been used to improve Lagrangian measurement techniques and to track transported particles in highly turbulent flows. Breakthroughs were then made on the determination of fluid element accelerations [La Porta et al., 2001], on the study of relative dispersion [Ott & Mann, 2000, Bourgoin et al., 2006] and on the scaling properties of Lagrangian velocity increments [Arnéodo et al., 2008].

The work presented in this thesis manuscript has the long-term objective to contribute to the study of atmospheric dispersion, with a particular emphasis on the transport of particulate pollutants. Such pollutants originate either from natural sources (suspension of dust by wind erosion, of salt by seawater evaporation, dispersion of pollen, of volcan ash, ...) or from human activities (combustion of organic compounds, dispersion of insecticides used in agriculture, emission of industrial and nuclear wastes, ...) [Harrison & Perry, 1986]. These particulate atmospheric pollutants are often called *aerosols*, as they are solid particles suspended in the air. They have direct and indirect effects on climate, which are still controversial and the source of many uncertainties [Pilewskie, 2007, Stevens & Feingold, 2009]. Also, the particulate pollutants represent a hazard for health. Their harmfulness often depends on their size [Valavanidis et al., 2008]. As we will see in more details later, very small particles (with sizes of the order of $1\,\mu$m or smaller) are extremely dangerous because they can reach and settle into the pulmonary alveoli, causing serious respiratory diseases. These particles are so small that, in good approximation, size effects do not enter their dynamics. They follow the fluid flow as trace markers and are usually referred to as *Lagrangian tracers*. In addition, when they are sufficiently dilute, these small particles do not influence the fluid motion and one then talks of *passive tracers*.

Turbulent transport enhances the dispersion of species. In addition to molecular diffusion and advection by a mean flow, the fluid flow fluctuations provide another mechanism of mixing, usually called *turbulent dispersion*, which is orders of magnitude more efficient. If we consider, for instance, the smoke of a cigarette in a room, experience suggests that few seconds are enough to "diffuse" its smell everywhere. However, even with the most accurate estimations on smoke diffusivity and on the convection effects due to temperature differences between smoke and air, one would obtain a diffusion time of the order of hours. Such a discrepancy occurs when one neglects the effects of turbulence. Since the pioneering work of Reynolds in 1883, there have been many efforts to understand and model how turbulent mixing interfere with both the large-scale advection by a mean flow and the small-scale molecular diffusivity. In a developed turbulent flow, the scales

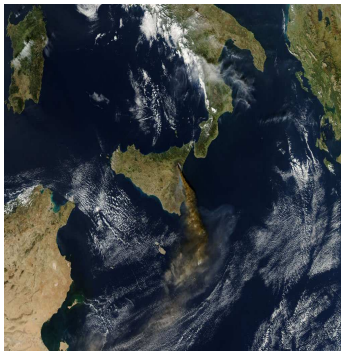

(a) Ash and dust plume carried away from Etna volcano in Sicily.

(b) Radioactive leak after the recent disaster in Fukushima Daiichi nuclear complex.

(c) Artist view of a protoplanetary disk gravitating around a young star. Credit: NASA/JPL-Caltech

(d) Phytoplankton bloom in the bay of Biscay. Credit: NASA

(e) Clouds formation in the high atmosphere.

(f) Pollution due to industrial activities.

Figure 1.1: Examples of situations involving turbulent particle transport.

associated to these two processes are generally widely separated and the turbulence spans all the intermediate range between them. This led Eckart in 1948 to decompose the process of turbulent dispersion in three main steps. The first concerns large scales, where particles are entrained, the second is responsible for the mixing process that happens at intermediate scales, and the last step is at small scales where stretching by the fluid strain creates large concentration gradients and diffusion becomes important.

The study of Lagrangian transport aims at describing the processes occurring in the intermediate range of length scales where turbulence is at play. Much work has been devoted to the study of tracer dynamics in turbulent flows. However, because of the large span of scales covered by turbulence (from millimeters to hundreds of meters in the atmosphere), the prediction

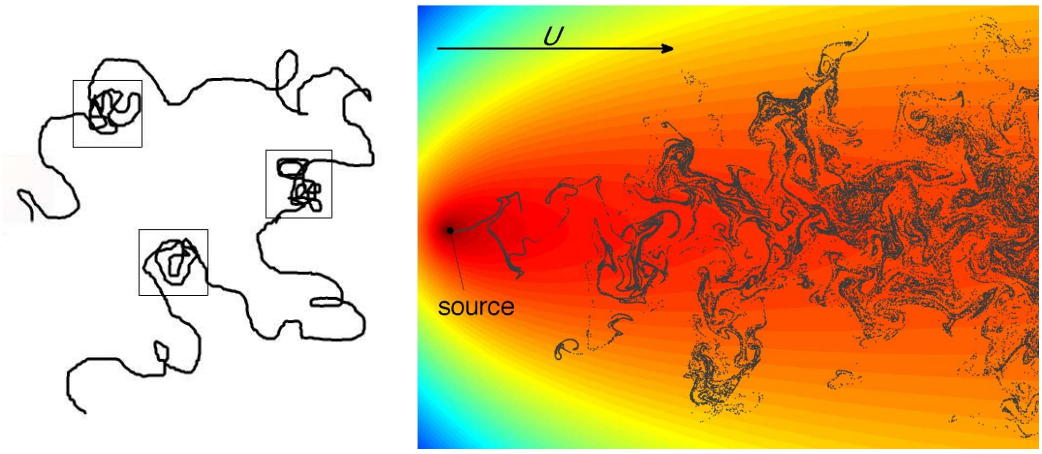

(a) (b)

Figure 1.2: (a) Schematic illustration of trapping events in turbulent flow. A particle finds along its path several vortices (here indicated by squares) that act like traps and interrupt the trajectory. (b) Gaussian vs meandering plume. The snapshot shows the positions of tracer particles (black dots) downstream a source. The plume contains regions with local high density than cannot be predicted from the solution of the mean field approximation (color background).

tools, which are expected to be operative in concrete situations, have to rely on modeling. Many approaches have thus been investigated in order to design efficient and reliable models for turbulent tracer dispersion and consequently the time evolution of their concentration fields (see, for instance, [Monin & Yaglom, 1971, Csanady, 1973, Majda & Kramer, 1999, Pope, 2000]). Despite the evident progresses that have been achieved, most of the models currently used to predict for instance air quality, provide pollutant concentration forecasts that are rather rough since they are simply based on the estimations of the *average* concentration fields. Transport is indeed usually treated via the so-called *mean-field approaches* [Opper & Saad, 2001]. They consist in approximating the transport through a combination of advection by the mean wind velocity and diffusion to model the effects of airflow turbulent fluctuations. These techniques give acceptable results on long-term averages. The resulting estimations are sufficient in many applications, as for instance when interested in the mean exposure to a given pollutant. In addition, they do not require sophisticated modeling as the balance between accuracy and efficiency is generally satisfactory. This partly explains the gap that currently

exists between state-of-the-art models and practical implementations.

However, in some cases, one could be interested in estimating the fluctuations that originate from the complex structure of the turbulent flow. An instance is the risk that a local pollutant concentration exceeds a given threshold. Often, local unexpected concentration fluctuations can indeed produce serious damages on health and predicting them would give great benefits for safety monitoring. The recent eruption of the Icelandic volcano Eyjafjallajökull in 2010 is another instance where such shortcomings had an important economical impact. The inability of meteorological models to predict the likelihood that an aircraft meets a concentrated ash puff led to completely close the North-European air traffic. Thus the importance of the strong fluctuations of mass concentration fields in monitoring and predicting atmospheric dispersion cannot be underestimated. In such situations, the relevant scales are then much smaller than those typically resolved by models. In addition, the information on an average value is not sufficient to directly determine the amplitude and the nature of the fluctuations. High concentrations are associated to the values of the tails of the probability distribution rather than to its core. A typical situation that can be encountered in turbulent transport is shown in Fig. 1.2(b), which represents the average concentration (colored background), together with the instantaneous positions of tracers emitted from a time-continuous source in a two-dimensional flow. The plume contains regions with local high density than cannot be predicted from the average concentration, which is a solution to the mean field approximation.

The creation of strong fluctuations in the distribution of transported particles can essentially be explained by two mechanisms. The first one is intrinsically related to the nature of the turbulent transport itself. It is known that for tracers advected by turbulent flows, the probability distribution of concentration has tails that are decreasing much slower than a Gaussian distribution [Warhaft, 2000]. Hence a Gaussian diffusive model is not suitable to describe them. The discrepancy can be explained by considering the eddies of the underlying turbulent flow as sort of traps in which trajectories spend more time than expected (see Fig. 1.2(a) for a schematic illustration). Such *trapping events* will then give high probabilities of finding high concentrations. Because this mechanism is intrinsic to the fluid flow, it would be important to identify and investigate the characteristics that are favoring or preventing it. It is still not clear whether this behavior is universal or depends on the features of the flow. Also the functional form of the resulting tails in the concentration probability distribution is unknown.

The second cause of strong fluctuations in the concentration field of transported species is the presence of inertia in the dynamics of certain suspended

particles. When the transport does not concern tracers but finite-size particles, heavier than the surrounding air, several effects occur. A first effect is due to gravity. Indeed, because of their weight, the particles settle and this process generally occurs with a *preferential sweeping* of their trajectories in the direction of the regions of downward airflow [Wang & Maxey, 1993]. This amplifies the formation of fluctuations in their distribution. Another important effect is due to the centrifugal inertial forces that act when heavy particles are inside vortices. Such particles are then ejected and this favors their concentration in the high-strain regions. This phenomenon of formation of voids and high-density fluctuations is known as *preferential concentration* [Squires & Eaton, 1991]. High concentration fluctuations have marked impacts on the monitoring of pollutant dispersion at small scales and, for this reason, quantifying the correlations between the flow turbulent structures and the particle concentration is important.

This thesis encompasses fundamental studies of transport properties in disordered environments. The objective is to provide new tools in order to qualify and quantify the fluctuations that are present in atmospheric turbulent transport. For that, I have mainly focused on the study of two problems that unveils some aspects of the two concentration mechanisms described above. The first concerns the relative motion of Lagrangian tracers in turbulent flows and relates to second-order statistics of a passively advected concentration field. The second concerns the effects of preferential concentration on the fluctuations in the density of heavy particles and uses a statistical formalism that relates them to mass ejection models in random scale-invariant environments. Both studies make use of notions and techniques borrowed from statistical physics, and combine them with the phenomenology of fluid mechanics and the development of numerical tools. The thread running throughout this thesis is to characterize with which universality the fluctuations of the turbulent flows, or more generally of a random medium, are responsible for the variability of the transport properties.

The rest of this dissertation is organized as follows.

The next two chapters give some background on turbulent transport. Chapter 2 contains a brief introduction to the main concepts on the dynamical and statistical properties of turbulence. It summarizes the scaling theories of turbulent velocity fields, relates them to kinetic energy transfers, and briefly discusses intermittency. Chapter 3 is focused on particle transport by turbulent flows. After introducing the equations that describe the dynamics of minute particles, it focuses on stochastic approaches for tracer

dispersion and discusses with some details the mechanisms leading to concentration fluctuations.

Chapters 4 and 5 are dedicated to the problem of tracer relative dispersion in turbulent flow and report work that was the subject of an article published on *Physical Review* E [Bitane et al., 2012b] and of another article submitted to *Journal of Turbulence* [Bitane et al., 2012a]. In Chapter 4, I first introduce the key concepts, such as Richardson's diffusive approach and Batchelor's ballistic regime. Then the rest of the chapter reports an original work on the study of the various timescales involved in this problem. The arguments that involve a scale-dependent effective diffusivity is revisited to explain the explosive separation of tracers according to the celebrated $t^{3/2}$ Richardson law. For that, state-of-the-art numerics are used. The Lagrangian correlation time of velocity differences is found to increase too quickly for validating this approach, but acceleration differences decorrelate on dissipative timescales. This results in an asymptotic diffusion $\propto t^{1/2}$ of velocity differences, so that the long-time behavior of distances is that of the integral of Brownian motion. The time of convergence to this regime is shown to be that of deviations from Batchelor's initial ballistic regime, given by a scale-dependent energy dissipation time rather than the usual turnover time. In Chapter 4, I also report the finding that the mixed moment, defined by the ratio between the cube of the longitudinal velocity difference and the distance, attains a statistically stationary regime on very short timescales. All these considerations are then put together and used to introduce a new one-dimensional stochastic model, which is studied and whose relevance to dispersion in real flows is discussed.

Chapter 5 reports thesis work on the study of violent events that occur in pair dispersion and provides a statistical and geometrical characterization of them. Evidence is obtained that the distribution of distances attains an almost self-similar regime characterized by a very weak intermittency. Conversely the velocity differences between tracers are displaying a strongly anomalous behavior whose scaling properties are very close to that of Lagrangian structure functions. Such violent fluctuations are interpreted geometrically and are shown to be responsible for a long-term memory of the initial separation. These results are brought together to address the question of violent events in the distribution of distances. It is found that distances much larger than the average are reached by pairs that have always separated faster since the initial time. They contribute a stretched exponential behavior in the tail of the inter-tracer distance probability distribution. The tail approaches a pure exponential at large times, contradicting Richardson's diffusive approach. At the same time, the distance distribution displays a

time-dependent power-law behavior at very small values, which is interpreted in terms of fractal geometry. It is argued and demonstrated numerically that the exponent converges to one at large time, again in conflict with Richardson's distribution. Finally, at the end of Chapter 5 some perspectives on the study of the specific problem of turbulent pair dispersion are reported.

In Chapter 6, I make use of statistical physics tools for characterizing fluctuations in the density of heavy inertial particles. This problem is related to random walks in random environments. A mass ejection model in a time-dependent random environment with both temporal and spatial correlations is then introduced. When the environment has a finite correlation length, individual particle trajectories are found to diffuse at large times with a displacement distribution that approaches a Gaussian. The collective dynamics of diffusing particles reaches a statistically stationary state, which is characterized in terms of a fluctuating mass density field. The probability distribution of density is studied numerically for both smooth and non-smooth scale-invariant random environments. A competition between trapping in the regions where the ejection rate of the environment vanishes and mixing due to its temporal dependence leads to large fluctuations of mass. These mechanisms are found to result in the presence of intermediate power-law tails in the probability distribution of the mass density. For spatially differentiable environments, the exponent of the right tail is shown to be universal and equal to $-3/2$. However, at small values, it is found to depend on the environment. Finally, spatial scaling properties of the mass distribution are investigated. The distribution of the coarse-grained density is shown to possess some rescaling properties that depend on the scale, the amplitude of the ejection rate, and the Hölder exponent of the environment. This work was the subject of a publication in the *New Journal of Physics* [Krstulovic et al., 2012].

Finally, Chapter 7 draws general conclusions on this thesis work. The stress is put on the perspectives and on the implications of the reported results on quantifying fluctuations in atmospheric transport.

Chapter 2

Basic concepts in turbulence

Turbulence is the largest unsolved problem in fluid dynamics and, more generally, in classical physics. If we consider that Leonardo Da Vinci was already studying turbulence in the 16th century, we can understand how complicated is this problem as five hundred years were not enough to solve it. His sketches (see Fig. 2.1), that are famous in the whole world, capture well the complex fluid motion involving a wide range of spatial scales. Such scale separations and chaoticity are typical of turbulent flows. The problem in "solving turbulence" basically comes from the presence of *nonlinear* terms in the Navier-Stokes equation, which governs the time evolution of an incompressible fluid. As a consequence, there is no simple general solutions for the fluid flow. The apparent paradox that a phenomenon described by the deterministic Navier-Stokes equation does not have a deterministic and unique solution was explained by Lorentz. He showed in 1963 that some nonlinear systems have a strong dependence on initial conditions, so that even undetectable differences of initial parameters can give extremely different solutions.

2.1 Phenomenology of turbulent flows

The concept of turbulence, which is present in everyday life (from a coffee cup to blowing wind), is well known to everybody. Despite this fact, the effect of turbulence on the global features of the fluid is far from being fully understood. In fluid dynamics, the level of turbulence in a fluid flow is characterized and measured by a dimensionless parameter, the *Reynolds number*

$$Re = \frac{UL}{\nu}, \tag{2.1}$$

where U is the typical velocity of the flow, L its typical lengthscale and ν the kinematic viscosity. The Reynolds number comes from a dominant-balance

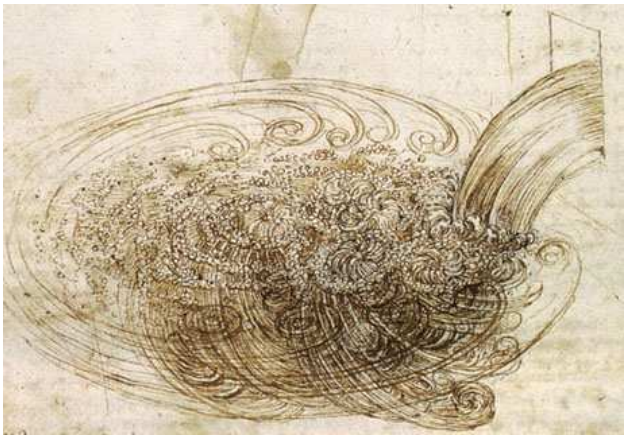

Figure 2.1: The first documented scientific study of turbulence is due to Leonardo Da Vinci in the sixteenth century. Here it is shown one of his drafts of a free water jet exiting from a square hole of a container into a pool.

analysis of the various terms in the Navier–Stokes equation and represents the ratio between the inertial and the viscous forces in the fluid.

When its value is larger than a certain threshold (which is somewhere between 40 and 75, [Frisch, 1996]), the regularity of motion is broken by the rise of vortical structures. In that case, the vortices that initially appear at the largest scale create regions where shearing is strong, which become unstable and are responsible (for instance by Kelvin–Helmholtz instability) for the formation of smaller vortices. Again, these structures create shear, destabilize and give rise to smaller eddies. This process is repeated as long as the local Reynolds number (defined with the iterated lengthscale and its associated typical velocity) is large enough. This process ends at small scales where kinetic energy dissipation by viscous damping becomes important. When the large-scale Reynolds number Re has a sufficiently large value, this process repeats many times and one usually talks of *fully-developed turbulence*. In this regime, the various symmetry properties of the Navier-Stokes equation are broken because of the presence of flow structures at every scales. However these symmetries are expected to be recovered in a statistical sense.

2.1.1 Kolmogorov 1941 theory

This conjecture led Kolmogorov to design a statistical theory of turbulence [Kolmogorov, 1941a, Kolmogorov, 1941b, Kolmogorov, 1941c], which is com-

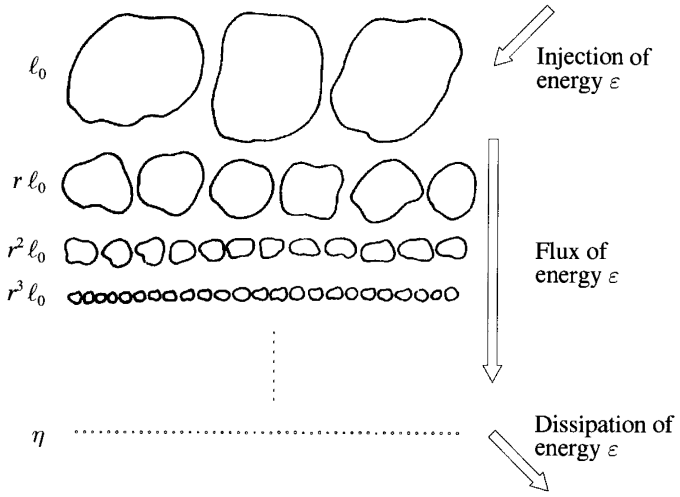

Figure 2.2: Schematic representation of the Richardson's cascade (from [Frisch, 1996]).

monly referred to as *K41 theory*. The basic idea is to classify all scales in three differet ranges. The range containing the largest scales, which is of the order of the domain size, is called the *injective range*, as energy is injected there. The smallest scales, where dominant viscous effects prevent the formation of additional vortices, is named the *dissipative range*, as it is the place where kinetic energy is dissipated. In between these two regions, there is an intermediate range in which energy is simply transported from the largest to the smallest scales. It is called the *inertial range*. This intermediate asymptotic region is very important because is the only one in which the symmetry of the Navier-Stokes equation are recovered in a statistical sense.

The process of energy transfer by the formation of eddies, which is at play in three-dimansional turbulent flows, is known as the *energy cascade*. It is also sometimes referred to as the *Richardson cascade*, since the concept was first introduced by the meteorologist L.F. Richardson in 1922. The path of kinetic energy in turbulent flows is schematically shown in Fig. 2.2. One notices that in three-dimansional turbulence is in principle a dissipative phenomenon and to keep it active, it is necessary to provide some injection of energy at the largest scales of motion. This is usually done in theoretical, experimental, and natural situations by either boundary conditions or volumic forcing. The basis of K41 theory is that the rate ε at which energy is transferred through the different eddy sizes is constant and independent of the fluid viscosity. By dimensional analysis, this implies that it is equal to

the ratio between the kinetic energy and the typical timescale given by the advection (namely L/U). It thus reads

$$\varepsilon \sim \frac{U^3}{L}. \tag{2.2}$$

Another important notion in K41 theory is the size of eddies where energy is no more transferred but just dissipated. This scale, that we denote η, is called the *dissipative* or *Kolmogorov scale* and depends, this time, on the fluid viscosity. Again from dimensional considerations, an estimation of such a scale comes out by imposing that the amount of energy transferred and of energy dissipated are equal. One then obtains

$$\eta \sim \left(\frac{\nu^3}{\varepsilon}\right)^{\frac{1}{4}} \tag{2.3}$$

where ν is the kinematic viscosity.

2.1.2 Similarity and scale invariance

A very important concept, on which K41 theory is based, is that of *similarity* [Frisch, 1996, Pope, 2000]. Essentially it states that for high value of Re the statistical properties of the turbulent fluid velocity field are universal at scales within the inertial range and only depend on the scale ℓ at which they are measured and on the rate of energy dissipation ε. In the dissipative range when $\ell \lesssim \eta$, they additionally depend on the viscosity ν. When $Re \to \infty$ with L fixed, the inertial range extends to all scales $\ell \ll L$ and the statistical properties become independent of ν. At very large Reynolds numbers, the inertial range is very wide and the energy cascade very long. As during the turbulent energy transfer eddies lose more and more memory about the initial configuration, it is easily comprehensible that the smallest structures present in any turbulent fluid display universal features.

For high Reynolds numbers the processes of energy injection and of viscous dissipation do not affect the inertial ranges. Under such hypotheses, one can demonstrate that the fluid velocity field is a solution to the incompressible Euler equation and it thus satisfies the scaling transformations

$$t \mapsto \lambda^{1-h} t \qquad \ell \mapsto \lambda \ell \qquad u \mapsto \lambda^h u \tag{2.4}$$

where λ is an arbitrary scaling factor and h any real exponent. When the viscous term is present, the only way Navier-Stokes equation is invariant by

such transformations is to impose $h = -1$. Indeed, with such a choice of h, the scaling transformation does not change the Reynolds number:

$$Re = \frac{UL}{\nu} \mapsto \frac{\lambda^{-1} U \lambda L}{\nu} = \frac{UL}{\nu} \tag{2.5}$$

However in the inertial range where the viscous term is negligible, any value of h is possible. To constrain this scaling exponent, one can make actually use of the only exact statistical relation that exists for turbulent velocity fields, namely Kolmogorov's 1941 *four-fifths law*. For that we introduce the *longitudinal velocity structure function* (or simply structure function) as the moment of the longitudinal velocity difference $\delta_\ell^{\parallel} u$ between two points separated by a distance ℓ. Under isotropy and homogeneity conditions, Kolmogorov showed that

$$S_3(\ell) = \langle \delta_\ell^{\parallel} u^3 \rangle = -\frac{4}{5} \varepsilon \ell. \tag{2.6}$$

If velocity fluctuations are self-similar, one has

$$\delta_\ell^{\parallel} u \sim \lambda^h \delta_{\lambda\ell}^{\parallel} u, \tag{2.7}$$

and this implies that

$$S_p(\ell) = \langle \delta_\ell^{\parallel} u^p \rangle \sim \ell^{h\,p}, \text{ when } \eta \ll \ell \ll L. \tag{2.8}$$

To comply with Kolmogorov 4/5 law (2.6) when $p = 3$, one has to impose $h = 1/3$. As we will see later, deviations to such a self-similar behavior are observed in experimental and numerical measurements. Qualifying the scaling properties of the structure functions is still an open issue which is of relevance since these statistical quantities provide information related to the energy transfer in the inertial range. Also, it worth stressing that, despite the fact the *four-fifths law* is an exact consequence of the Navier-Stokes equation, it is very hard to observe it experimentally or in direct numerical simulation. The discrepancy between theory and results is often due to contamination of inertial range by the diffusive effects or also to velocity fields scarcely isotropic and homogeneous [Biferale & Procaccia, 2005].

2.2 Energy budgets and transfers in turbulence

All the physics of turbulent flows and of the energy transport in the inertial range, so far represented from a phenomenological point of view, is contained in the incompressible Navier-Stokes equation

$$\begin{aligned} \rho \frac{\partial \mathbf{u}}{\partial t} + \rho\,(\mathbf{u} \cdot \nabla)\mathbf{u} &= -\nabla p + \mu\,\nabla^2 \mathbf{u} + \rho\,\mathbf{f}, \\ \nabla \cdot \mathbf{u} &= 0. \end{aligned} \tag{2.9}$$

This equation is nothing but the Newton's second law written in case of an incompressible fluid with constant density ρ and dynamical viscosity μ. The two terms in the left-hand side represent the inertial forces, while terms in the right-hand side are instead the pressure force, the viscous force and the last one represent the external (and not conservative) force. Gravity, if relevant, can be inserted in the pressure term. This equation describes the time evolution of each *fluid element* velocity and its terms have the dimension of a force per unit volume. The term $(\mathbf{u} \cdot \nabla \mathbf{u})$ is the nonlinear term responsible for a unstable chaotic fluid motion and thus for the creation of turbulence. It induces the generation of eddies at all scales and drives the energy transport through them. The pressure term is present to maintain the incompressibility condition $\nabla \cdot \mathbf{u} = 0$. One easily sees that all terms in the Navier–Stokes equation conserve the divergence-free nature of $\mathbf{u}$, except the non-linear term, which has a gradient component. The pressure is there to cancel it. It is given by the Poisson equation

$$\nabla^2 p = -\nabla \cdot (\mathbf{u} \cdot \nabla \mathbf{u}), \tag{2.10}$$

which is obtained by taking the divergence of Eq. (2.9). The pressure term depends thus non-locally on the velocity field and this is the cause of many difficulties encountered in the study of turbulence. This non-locality is absent from the viscous term. Despite its apparent simplicity, this term plays an essential role as it dissipates the energy injected by the external forcing and keeps the system in energy balance. As we already saw, the dimensional ratio between the non-linear term and this viscous term measures the level of turbulence via the Reynold dimensionless number.

The evolution equation for the total kinetic energy $K = \int_V \rho |\mathbf{u}|^2 \, \mathrm{d}v$, where the integration is over the whole spatial domain V, can be obtained multiplying Eq. (2.9) by $\mathbf{u}$

$$\frac{\partial K}{\partial t} = \int_V \rho \, \mathbf{f} \cdot \mathbf{u} \, \mathrm{d}v - \mu \int_V |\nabla \mathbf{u}|^2 \mathrm{d}v \tag{2.11}$$

The local rate of kinetic energy dissipation is defined as $\varepsilon(\mathbf{x}, t) = \nu |\nabla u|^2$, where $\nu = \mu/\rho$ is the kinematic viscosity of the fluid. Equation (2.11) can thus be also written in the form

$$\frac{\partial K}{\partial t} = \int_V \rho \mathbf{f} \cdot \mathbf{u} \, \mathrm{d}v - \rho \int_V \varepsilon \, \mathrm{d}v \tag{2.12}$$

From this expression it is clear that kinetic energy does not depend neither on the convective motion in the fluid nor on the pressure since the corresponding terms are no more present in Eq. (2.12). In fact, as already seen, they

conserve kinetic energy and only concern its transport through all scales. It is also important to point out that by definition, the local rate of energy dissipation is always positive and this means that in Eq. (2.12) there is a term that is continuously subtracted. Without the external force, the energy would be slowly dissipated till have a fluid with null velocity. Like the pressure, the dissipative term belongs to the paradigms of turbulence. Despite what could be naively thought, even when the Reynolds number goes to extremely high values, the dissipative effects do not disappear. In fact, even if the kinematic viscosity ν goes to 0, the velocity gradients increase in such a way that ε remains constant. This effect is sometimes called the "dissipative anomaly" and its proof is still one of the main open questions of turbulence. This concept is at the base of K41 theory. Indeed, to maintain ε constant when $\nu \to 0$, the former has to be independent of viscosity. It implies that the velocity gradients have to increase like $\varepsilon^{1/2}\nu^{-1/2}$. This gives the scalings of Kolmogorov dissipative scales introduced in previous section.

2.2.1 Direct and inverse cascades

Although the arguments so far discussed about turbulence are of general validity for all fluids with similar characteristics, it is needed to underline what actually depends on the space dimension. Important mechanisms in turbulence are related to the creation or not of vorticity. The latter is defined as $\boldsymbol{\omega} = \nabla \times \mathbf{u}$ and is generically different from zero for a fluctuating velocity fields. Its dynamics is however very different in two and three space dimensions. To see that let us consider again the Navier-Stokes equation (2.9). Taking its curl and recalling that $\mu/\rho = \nu$, one obtains the equation for the transport of vorticity by the velocity field $\mathbf{u}$

$$\frac{\partial \boldsymbol{\omega}}{\partial t} + (\mathbf{u} \cdot \nabla)\,\boldsymbol{\omega} = (\boldsymbol{\omega} \cdot \nabla)\,\mathbf{u} + \nu \nabla^2 \boldsymbol{\omega} + \nabla \times \mathbf{f} \tag{2.13}$$

The vorticity field gives an information about turbulence that is complementary to the velocity. In fact, while velocity cannot be localized in space because the pressure distributes it over the whole domain, the vorticity tends to localize in certain regions and it is transported across space by advection and diffusion. However, the first term in the right-hand side of Eq. (2.13) can be responsible for the creation of vorticity, depending on the space dimension.

In three dimensions, this term is generically different from zero and it is often called the *vortex stretching* (or also *twisting*). It stretches and squeezes the vortical structures and contributes, in dominant manner, to the overall variations of vorticity. When a vortex tube is stretched, for instance in its axial direction, the conservation of angular momentum implies that its

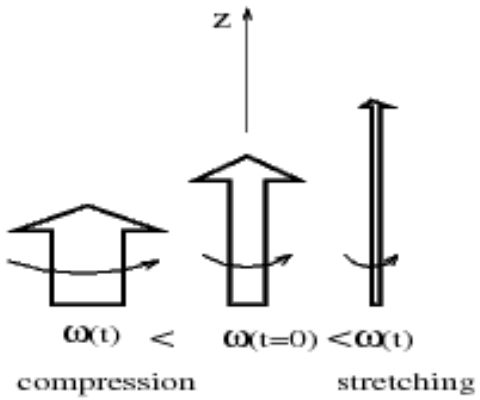

Figure 2.3: Qualitative sketch of the stretching vortex tube effect.

vorticity has to increase (see Figure 2.3). Such a mechanism is able to amplify vorticity through the velocity gradients without any external source. The increase in the parallel direction of the vorticity implies an decrease of the cross section area of the vortex. This means that the vortex tube has a smaller size because of this process. Thanks to the twisting term, large vortices are strongly stretched until their size reaches the scales at which the vorticity diffusion becomes strong enough to dissipate rotational energy. Although the term $(\boldsymbol{\omega} \cdot \nabla)\mathbf{u}$ can in principle increase or decrease vorticity, it can be shown that in a three dimensional fluid stretching occurs statistically more often than compression and, as a consequence, vorticity is in average amplified and concentrated at scales smaller and smaller. This materializes by a positive sign of the average stretching term. This is one of the explanation of the cascade of energy from large to small scales in three-dimensional turbulence and numerical simulations have confirmed this picture.

The situation drastically changes in two dimensions. The stretching term always vanishes and the vorticity equation (2.13) becomes simply

$$\frac{\partial \boldsymbol{\omega}}{\partial t} + (\mathbf{u} \cdot \nabla)\, \boldsymbol{\omega} = \nu \nabla^2 \boldsymbol{\omega} + \nabla \times \mathbf{f}. \tag{2.14}$$

If one neglects both the viscous and the external forcing terms, the vorticity remains constant in time along each fluid particle trajectory and just experiences pure advection. For this reason it is easy to understand that not only vorticity but all its moments will be conserved. Of particular interest is the second power of vorticity $\Omega(t) = \omega^2(t)$, which is a sort of energy related to vorticity, more commonly known as *enstrophy*. Such a conservation

determines the deep differences between two- and tree-dimensional turbulent dynamics and in particular in the ways energy is transferred among scales. In a three-dimensional flow there is a single definite-positive conserved quantity in the inertial range: the kinetic energy, which is transferred from larger to smaller scales. In two dimensions, both the kinetic energy and the enstrophy are conserved and this implies, as we will see, that energy transfer has not a preferential direction toward small scales or toward large scales. These phenomena are easily pictured by introducing the kinetic energy spectral density $E(k)$, which is roughly the kinetic energy content of a shell in Fourier space of radius $k \sim 1/\ell$. At the initial time there is a certain energy distribution centered on the mean wave number $\tilde{k}(t_0)$. The distribution changes when time goes on and the mean wave number takes either larger or smaller values. One can show that the time derivative of $\tilde{k}(t)$ is always negative in two dimensions, because both kinetic energy and enstrophy are conserved. This means that the mean wave number becomes preferentially smaller than its initial value, so that the energy transfer takes place from smaller to larger scales.

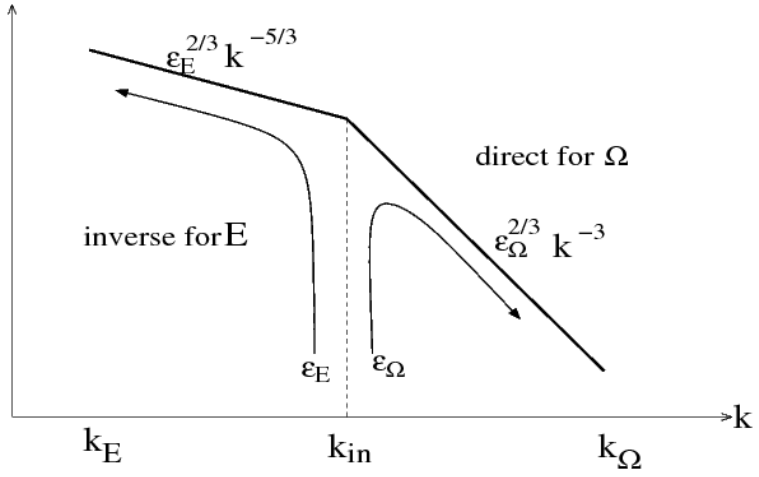

Figure 2.4: Direct and inverse cascade in two dimensional turbulence.

This energy transfer, which is proper to two dimensions, is usually referred to as the *inverse cascade*. It is usually accompanied by a *direct cascade* of the other conserved quantity, the enstrophy, from large to small scales (see Fig. 2.4 for a qualitative sketch).

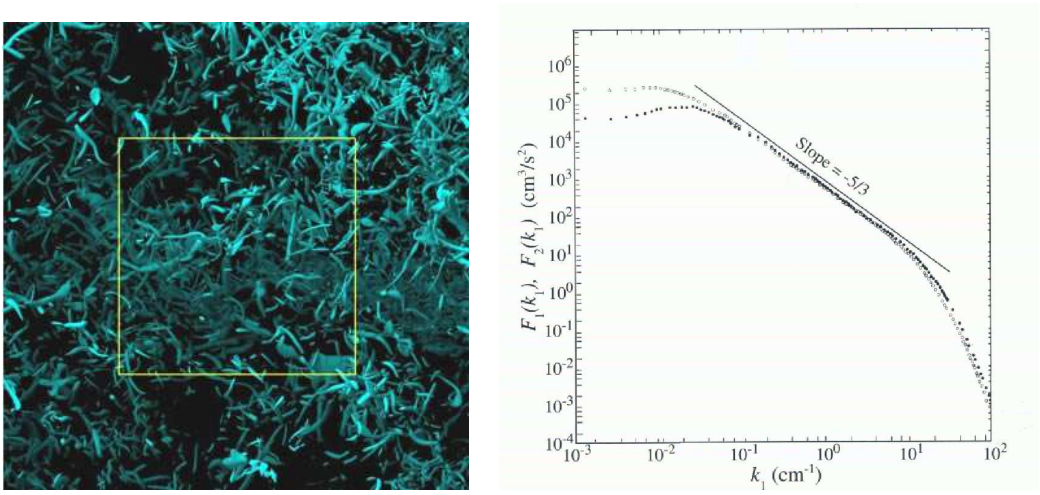

Figure 2.5: Left: snapshot of the vorticity contour surfaces in the direct numerical simulation of a three-dimensional turbulent flow (from [Ishihara et al., 2009]). Right: Kolmogorov energy spectra for very high Reynolds number (from [Frisch, 1996]).

2.2.2 Energy and enstrophy spectra

As for structure functions, dimensional analysis and K41 approach predict how the kinetic energy is distributed among the different wave lengths. In three dimensions it leads to the well-known power-law *Kolmogorov's spectrum*, which is represented in Fig. 2.5 (Right) and widely observed and measured in experimental data, valid for $Re \gg 1$ and $(1/\eta) \ll k \ll (1/L)$

$$E(k) \simeq C_K \, \varepsilon^{\frac{2}{3}} \, k^{-\frac{5}{3}}, \tag{2.15}$$

where ε is the average dissipation rate and C_K is a positive *universal* constant often called the *Kolmogorov constant*.

In two dimensions, as first pointed out by Kraichnan [Kraichnan, 1971] in the inviscid limit case, the situation is different. The conservation of both energy and enstrophy implies a universal characteristic feature for the energy spectrum. The rate at which energy is transferred toward the large scales is different from that at which enstrophy is toward the small scales. The two cascades are separated at the wave number k_0 at which the energy and the enstrophy are injected. Calling Ψ_E the rate at which energy is tranferred at scales $k < k_0$ and Ψ_Ω that at which enstrophy is transferred for $k > k_0$, one can check that they can be written as

$$\Psi_E \propto k^{(5+3\alpha)/2} \quad \text{and} \quad \Psi_\Omega \propto k^{(9+3\alpha)/2}. \tag{2.16}$$

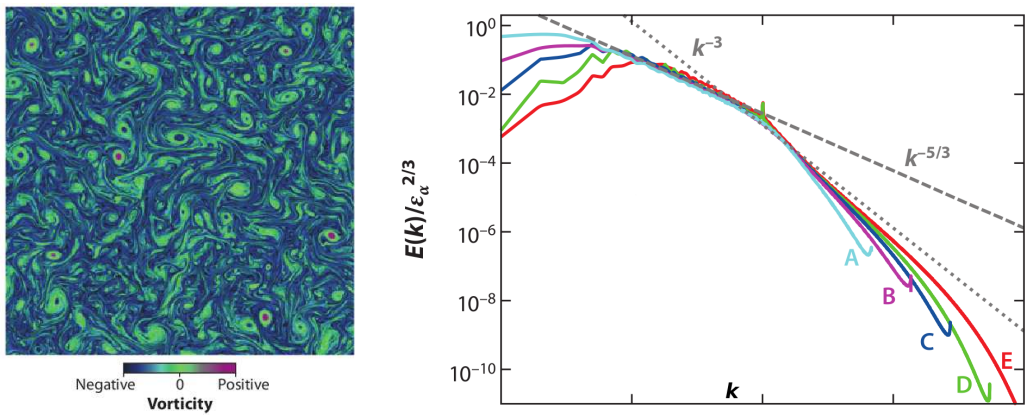

Figure 2.6: Left: snapshot of the velocity field in a two-dimensional direct numerical simulation of Navier–Stokes equation (from [Boffetta & Ecke, 2012]). Right: two-dimensional turbulent energy spectra from direct simulations and for different resolutions, showing both the $k^{-5/3}$ inverse and k^{-3} direct cascade regimes (from [Boffetta & Musacchio, 2010]).

Clearly there are two particular values of α, $-5/3$ and -3, for which either the energy and the enstrophy transfer is constant. When $\alpha = -5/3$, the energy transfer is independent of scales and enstrophy is not transferred. This first case corresponds to the inverse cascade and occurs when $k < k_0$. When $\alpha = -3$ the enstrophy transfer is independent of scales and energy is not transferred. This second case holds for $k > k_0$ and is referred to as *Kraichnan's spectrum*

$$E(k) \simeq C'_K \varepsilon_\Omega^{\frac{2}{3}} k^{-3}, \tag{2.17}$$

with possible logarithmic corrections and where ε_Ω is the average enstrophy dissipation rate. Remarkably the enstrophy cascade in two dimensions is very similar to that of energy in three dimensions. The *dual cascade* scenario is characteristic of two-dimensional flows and has been clearly observed in numerical simulations (see Fig. 2.6). In experiments the shapes of these power laws is not so regular because, on the one hand, the range of possible wavenumber is limited and, on the other hand, they are contaminated by other physical mechanisms, such as friction between the two-dimensional fluid layer and its surrounding.

2.2.3 Intermittency

For the sake of completeness, it is necessary to recall that, although there is a common agreement that K41 theory, and in particular the $k^{-5/3}$ Kolmogorov spectrum fairly describes velocity fluctuations in turbulent flows, there are many observations of discrepancies between such theoretical previsions and experiments. The K41 approach is surely the simplest theory that is able to catch the main features of turbulence but it still has several limits. Theory needs further developments in order to provide a more precise understanding of turbulence [Frisch, 1996]. Discrepancies from K41 are very small when interested in second-order moments of velocity fluctuations, as for instance in the case of spectral analysis. However, as pointed out by several experimental and numerical measurements (see, e.g., [Van Atta & Chen, 1970, Anselmet et al., 1984, Yoshimatsu et al., 2009]), larger and larger discrepancies appear when the order of moments increases. The scaling exponents of the structure functions behave clearly not linearly as a function of the moment, as it would be the case if K41 theory was valid.

Another observation is that the probability distribution functions of velocity increments are far from Gaussian. Experimental data give evidence that, even if Gaussianity can barely be seen at large scales (close to the integral scale), the tails at separations within the inertial range are much fatter [Castaing et al., 1990, Gagne et al., 1990]. This means that the probability of violent events (basically strong eddies in a localized region of space) is much larger than expected. As a consequence the configurations that contribute the most to structure functions depend on the order. Therefore the high-order statistics cannot trivially be related to those at lower orders, as it would be the case with a Gaussian distribution. Such an anomalous behavior, which relates to the presence of periods with strong fluctuations alternating with relatively quiet regions, takes the name of *intermittency*. This a feature is not captured by K41 theory, as it contradicts the hypothesis of self-similarity of the velocity (that is independence of the statistical properties from the scale at which they are observed). To account for intermittency, the representation of Richardson's cascade has to be corrected considering that only the total energy transfer rate is constant while locally it can present fluctuations (see the sketch in Fig. 2.7 Left). This approach was proposed by Kolmogorov [Kolmogorov, 1962] and is named the *refined self-similarity hypothesis*. It allows for the presence of regions with high activity and others with less. Another approach consists in formalizing this using a *multifractal* description of velocity increments statistics (see [Frisch, 1996] for more details).

A useful tool to observe and measure intermittency is the fourth-order

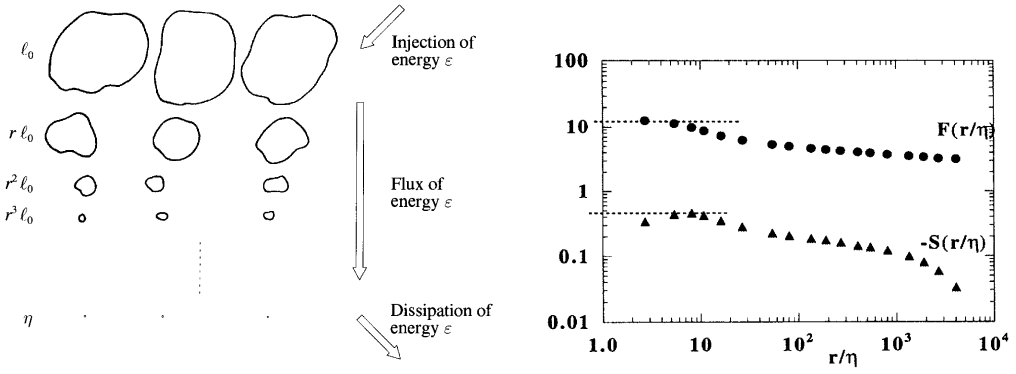

Figure 2.7: Left: sketch of the intermittent energy cascade (corresponding to the β multifractal model; from [Frisch, 1996]). Right: Skewness $\mathcal{S}$ and flatness $\mathcal{F}$ of three-dimensional turbulent velocity increments (from [Tabeling et al., 1996]).

structure function. One usually defines the *flatness* of the velocity increments probability distribution as

$$\mathcal{F}_\ell = \frac{\langle \delta_\ell^{\parallel} u^4 \rangle}{\langle \delta_\ell^{\parallel} u^2 \rangle^2}. \tag{2.18}$$

Fourth-order statistics give more weight to the tails of the probability density function and therefore measures how frequently events larger than the standard deviation occur. For Gaussian, the flatness is always equal to 3. Deviations from this value are usually called the *kurtosis* of the distribution. As seen from the experimental data shown in Fig. 2.7 (Right) velocity increment flatness approaches the value 3 at large scales. However, noticeable deviations from 3 are visible for smaller separations within the inertial range. For value close to the Kolmogorov scale η, the flatness is above 10. This indicates that the probability distribution of velocity gradients has tails that are much fatter than a Gaussian.

2.3 Mixing in a turbulent flow

We have seen that in the ideal case of homogeneous and isotropic turbulence, a flow is characterized by the presence of vortical structures that span all its spatial scales. When one is considering species transported by this flow, it is expected that turbulence will enhance the mixing properties with a "high rate of diffusivity" that can be two or three orders of magnitude larger than the molecular one. From considerations that are similar to the K41 approach

and the introduction of the Kolmogorov dissipative scale, one can estimate the scale below which molecular diffusion dominates. This scale is known as the Batchelor length and reads

$$\ell_B \sim \left(\frac{\nu D^2}{\varepsilon}\right)^{\frac{1}{4}}, \tag{2.19}$$

where D is the molecular diffusivity, ν is the kinematic viscosity of the flow and ε the mean rate of kinetic energy dissipation. The large velocity fluctuations are able to effectively transport all passive scalar quantities such as heat and concentration. The transport due to the fluctuations is usually modeled in terms of an effective diffusion coefficient, which is known as *eddy diffusivity*. As in the case of velocity, the impredictability of turbulent flows implies that the instantaneous value of a passive scalar at a given location in space is not enough to predict the expected value at the same point but after a brief time interval. For that reason a statistical approach is well adapted to address the issue of mixing by turbulent flows.

As already seen in the Introduction, the efficient mixing and diffusion by turbulent flows has many applications. For instance, turbulence is capable to dilute and spread strong concentrations of contaminants in the environment [Shraiman et al., 2000, Smyth et al., 2001]. Without a sustained level of turbulence, the transport and mixing mechanisms of the various regions of the fluid would be much slower than they normally are. This was first shown experimentally by Reynolds in 1883 through his studies on the dispersion of a dye injected in a turbulent pipe flow (the experimental equipment is schematically illustrated in Figure 2.8). The efficency of the mechanism is due to a peculiar feature of turbulent transport, which is currently not fully understood, that tends to separate very quickly two initially close fluid elements. Such a separation depends on the initial distance between the fluid elements only for a short time but the large-time separation is *explosive* in the sense that such a dependence on initial conditions disappears. Recently much work has been devoted to understand better the nature of this phenomena, and in particular on how fast the initial separation is forgotten [Ott & Mann, 2000, Biferale et al., 2005, Bourgoin et al., 2006]. Such an investment has led to several new results that clarify many aspects of turbulent mixing. However, a systematic description of this problem is still an open challenging theoretical and modeling question.

Normally the transported material self-generates local forces that have a significant influence back on the fluid but thankfully these two problems, transport induced by turbulent flow and local forces induced by particles, can be treated separately. In 1948 C. Eckart gave his description of the

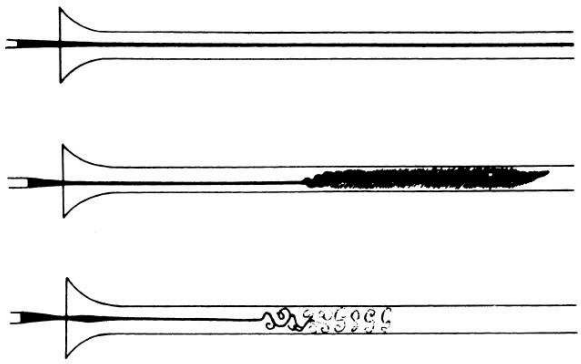

Figure 2.8: Sketches of the pipe flow used by Reynolds in 1883 to study the dispersion of a dye injected as a function of the level of turbulence in the flow (from [Acheson, 1990]).

turbulent mixing process by dividing it in three main and separate stages involving all spatial and temporal scales of the flow [Eckart, 1948]. The first stage, the so-called *entrainment*, relates to the large-scale mass movements that occur because of eddies. After this, follows the second stage, *stirring* or also *dispersion*, which is responsible for the creation, at intermediate scales, of large interfacial surfaces which enhance the mixing [Ottino, 1989]. Fluid elements are then deformed with a consequent increase of the concentration gradients. This leads in turn to a local increase of molecular diffusion. The last *mixing* stage happens at very small scales where the gradients are almost constant and molecular diffusion takes place.

From a conventional point of view, it is possible to distinguish, depending on the complexity of the system concerned, different "levels of mixing" [Dimotakis, 2005]. The cases of pollutants, of small-size particle clouds or in general simple passive tracers are included in the Level-1 mixing (the least intricate one). In this level, also called *one-way coupling*, the influence of mixing on the fluid dynamics is not considered. Infact to have a good description of mixing it is then necessary to understand carefully the turbulence of the flow but, on the contrary, depicting correctly the fluid dynamics does not require considering mixing with a high degree of accuracy. Levels 2 and 3 are concerned with more complicated cases in which mixing and fluid dynamics are coupled with subsequent changes in properties of the fluid itself. Such levels encompass what is also called *two-way* or *four-way coupling*.

In the following chapter we will see with more details, the main characteristics of tracer particles, of their diffusion and the turbulent transport

properties. A particular emphasis will be given to the two-particle relative dispersion problem and the issue of the statistics of fluctuations concentration. We do not take into account mixing caused by combined forces but we only consider the case of simple turbulent diffusion due to the irregular turbulent velocity field fluctuations.

Chapter 3

Particle Transport

Understanding the dynamics of particles transported by a fully-developed turbulent flow is very important for many fundamental physical processes. One typically distinguishes, depending on their size, several classes of particles, each of which having different interactions with the carrier fluid and thus behaving in a different way. A further level of difficulty can of course arise when interested in polydisperse systems composed of several species of particles. Such a situation, which occurs naturally in applications, is not considered here.

Precise studies of particle transport dynamics are necessary to validate and ameliorate the models used to describe and foresee particle concentrations and in particular their irregular fluctuations. This is a matter of enormous importance not only for engineering, but also for the problem of modeling pollution by particulate matter. Such an issue affects both the environment and human health. The atmospheric particulate pollutants are usually classified according to their size. The larger particles (*supercoarse*) are those whose diameter is larger than $10\,\mu$m. They settle quickly because of their massive size and thus have a short lifetime in the atmosphere. Also, their size is so large that they do not penetrate deeply the respiratory system and thus do not have an important effect on health. They are usually not included in standard models. The particles whose aerodynamic diameters are less than $10\,\mu$m are denoted PM_{10}. They are respirable and thus deserve much more attention. The class PM_{10} encompasses the *coarse* particles (with diameters larger than 2.5μm), and the *fine* particles (whose size is less than 2.5μm). The most dangerous particles for health are the smallest ones as they are able to penetrate deeply in the respiratory system and to possibly settle in the pulmonary alveoli. In addition to that importance, it is very difficult to measure and monitor them because of their small size, so that an important effort is required in their modeling. The size effects in the

dynamics of such particles can generally be disregarded. In this chapter we mainly focus on describing the turbulent transport of such particles, whose individual trajectories are more commonly referred to as *Lagrangian tracers* and whose concentration field is a *passive scalar*.

3.1 Dynamics of tiny particles in turbulent flows

3.1.1 Equations of motion

The dynamics of finite-size particles transported in a turbulent flow is an intrinsically complicated model as it requires to solve the full Navier–Stokes equation with the proper boundary condition at the possibly rough particle surface. As we have seen in previous Chapter, unsteady solutions for the dynamics of a fluid in a turbulent state are still unknown and display very unstable properties. For this reason, one usually restricts the problem to very small particles whose velocity difference with the fluid is sufficiently small. More precisely, let us assume, in a turbulent flow, that the particle is spherical, with a radius a much smaller than the Kolmogorov dissipative scale η and that the particle Reynolds number, defined as $Re_\mathrm{p} = W\,a/\nu$ where W is the particle slip velocity, is much less than one. One can then neglect non-linear terms in the Navier–Stokes equation, integrate the Stokes equation in the vicinity of the particles and use matched-asymptotics techniques to write a Newton equation for the particle position

$$m_\mathrm{p}\frac{\mathrm{d}^2\mathbf{X}_\mathrm{p}}{\mathrm{d}t^2} = -6\pi a\nu\rho\left[\frac{\mathrm{d}\mathbf{X}_\mathrm{p}}{\mathrm{d}t} - \mathbf{u}(\mathbf{X}_\mathrm{p},t)\right] + m_\mathrm{f}\frac{\mathrm{D}\mathbf{u}}{\mathrm{D}t}(\mathbf{X}_\mathrm{p},t) + (m_\mathrm{p}-m_\mathrm{f})\,\mathbf{g} \quad (3.1)$$
$$-\frac{m_\mathrm{f}}{2}\left[\frac{\mathrm{d}^2\mathbf{X}_\mathrm{p}}{\mathrm{d}t^2} - \frac{\mathrm{d}}{\mathrm{d}t}\mathbf{u}(\mathbf{X}_\mathrm{p},t)\right] - 6\sqrt{\pi\nu}a^2\rho\int_0^t \frac{\mathrm{d}s}{\sqrt{t-s}}\frac{\mathrm{d}}{\mathrm{d}s}\left[\frac{\mathrm{d}\mathbf{X}_\mathrm{p}}{\mathrm{d}s} - \mathbf{u}(\mathbf{X}_\mathrm{p},s)\right].$$

Here $\mathbf{X}_\mathrm{p}(t)$ is the particle position, $\mathbf{u}(\mathbf{X}_\mathrm{p},t)$ the fluid velocity at the particle location, ρ is the fluid mass density, m_p the particle mass, m_f the mass of fluid displaced by the particle, and $\mathbf{g}$ is the acceleration of gravity. The first force on the right-hand side of Eq. (3.1) is the Stokes viscous drag. The second term is the force exerted on the undisturbed fluid. The third is buoyancy, the fourth added mass and the last term is the Basset-Boussinesq history force, which comes from the interaction between the particle and its own wake. A first version of this equation was written in [Stokes, 1850] and was then refined in [Boussinesq, 1885] and in [Basset, 1888]. Further development were performed in [Faxén, 1922] and perfected in [Maxey & Riley, 1983] and [Gatignol, 1983], to express the corrections due to fluid velocity variations on lengths of the order of the particle size.

The complexity of the terms appearing in Eq. (3.1), and in particular of the last one that makes this equation integro-differential, motivated many fluid dynamicists to perform further simplifications. In the limit when, in addition to small size and moderate velocity difference with the fluid, one assumes that the particles are much denser than the fluid, the dynamics simplifies to

$$\frac{\mathrm{d}^2\mathbf{X}_\mathrm{p}}{\mathrm{d}t^2} = -\frac{1}{\tau_s}\left[\frac{\mathrm{d}\mathbf{X}_\mathrm{p}}{\mathrm{d}t} - \mathbf{u}(\mathbf{X}_\mathrm{p},t)\right] + \beta\frac{\mathrm{D}\mathbf{u}}{\mathrm{D}t}(\mathbf{X}_\mathrm{p},t) + (1-\beta)\,\mathbf{g}, \tag{3.2}$$

where $\tau_s = a^2/(3\beta\nu)$, $\beta = 3m_\mathrm{f}/(m_\mathrm{f}+2m_\mathrm{p}) \ll 1$. Such an approach is for instance relevant to describe particulate pollutants. Note that this model is sometimes used for particles that are lighter than the fluid. However, for such finite values of β, neglecting the history term requires additional assumptions, as for instance, prescribing a small response time τ_s.

Because of the Stokes viscous drag, the dynamics described by (3.2) is *dissipative* in the phase space. This is true even if the carrier flow is incompressible. As we will see in Sec. 3.2.2 this is responsible for the formation of strong fluctuations in the particle spatial distribution. This aspect is further discussed in Chapter 6. In an incompressible turbulent flow, the degree of dissipation in the particle dynamics is measured by the *Stokes number* $St = \tau_s/\tau_\eta$ which is defined as the ratio between the particle response time and the turnover time associated to Kolmogorov dissipative scale. When $St \to \infty$, the particles do not feel the underlying fluid and the viscous drag does not act on them. On the contrary, when $St \to 0$ the velocity difference between the particle and the flow is instantaneously dissipated.

In the case of a vanishing Stokes number, the particle dynamics becomes infinitely dissipative. However, in this singular limit, they distribute uniformly in space. The full dynamics of particles takes place in the position-velocity phase space, which is six-dimensional. For finite values of St the six-dimensional particle trajectories concentrate in phase-space on an *attractor* because of a dissipative dynamics. When $St \to 0$, there is a reduction of dimensionality of the particle dynamics: the particle velocity is assigned to be equal to that of the fluid. This implies that in this limit the attractor becomes the full position space and the particle dynamics becomes to leading order

$$\frac{\mathrm{d}\mathbf{X}_\mathrm{p}}{\mathrm{d}t} = \mathbf{u}(\mathbf{X}_\mathrm{p},t). \tag{3.3}$$

The particles are then called *tracers* of the turbulent flow. When the flow is incompressible, they distribute uniformly in space.

Note that we have here neglected the molecular thermal diffusion that acts in principle on the particles and comes from the microscopic collisions

of the considered macro-particle with the molecules that constitute the surrounding fluid. This effect is responsible for an additional Brownian motion of the particle that has to be added to the full dynamics (3.1). Such a term can be disregarded when the particle is large enough. However, in many situation when the particles is so small that they can be considered as tracers, molecular diffusion becomes important. In that case the tracer equation becomes

$$\frac{\mathrm{d}\mathbf{X}_\mathrm{p}}{\mathrm{d}t} = \mathbf{u}(\mathbf{X}_\mathrm{p}, t) + \sqrt{2\kappa}\,\eta(t), \tag{3.4}$$

where η is the standard three-dimensional white noise (defined in next subsection) and κ is the diffusion constant (related to mass, temperature, and the response time τ_s by Einstein's formula, see, e.g., [Csanady, 1973]). The overall behavior of such tracer particles is mainly due to the combined effect of transport, that is the physical displacement caused by the mean velocity of the flow, mixing by its turbulent fluctuations and finally molecular diffusivity, which tends to smooth out an initially concentrated field.

3.1.2 Generalities on stochastic processes

The use of mathematical models appeared in the study of physical problems because of the difficulty to know by direct measurements the spatial and temporal distributions of the variables we are interested in. Although exact theoretical results can be derived from them, these models provide only a coarse approximation of real situations; one hence frequently encounters predictions that are in disagreement with measurements. In many cases, the time evolution of the variable of interest depends on many factors that the models are not able to catch with the same accuracy. This is why there are many models, each of them being more or less efficient depending on the considered problem. The paradigmatic mathematical approach associated to the problem of particle transport by turbulent flow is *stochastic (or statistical) modeling* that makes probabilistic predictions for the future considering the values that the variable has taken in the past [Van Kampen, 2007].

The function that defines the value taken by a random variable at each instant of time is called a *stochastic process*. When a process has no memory, that is when the future does not depend on the past but only on the present, one talks about a *Markovian process* [Gillespie, 1992]. In high-Reynolds-number flows, we will see in next subsection that the larger timescale is given by the Lagrangian integral time T_L, which is defined as the time integral of the velocity two-times correlation along tracer trajectories (see [Monin & Yaglom, 1971]). When interested in processes that occur on timescale much larger than T_L, we can in general decompose the dynamics as a sum of decorrelated

events. In that case, the considered problem can be approximated by a Markovian process.

Let us consider a given stochastic process $X(t)$. If we consider that this process has the value x at time t, we can write that at the time $t + \mathrm{d}t$

$$X(t + dt) = x + \mathrm{d}X(\mathrm{d}t; x, t) \tag{3.5}$$

where we have introduced the stochastic process $\mathrm{d}X(\mathrm{d}t; x, t)$ that gives the transition of the process $X(t)$ between time t and $t + \mathrm{d}t$ knowing that the process was in x at time t. Through a number of mathematical steps [Gillespie, 1992] it is possible to show that, for all processes that are continuous with respect to t, the increment dX can be written as

$$\mathrm{d}X = a(X, t)\,\mathrm{d}t + b(X, t)\,\mathrm{d}W_t, \tag{3.6}$$

where W_t is the standard Wiener process, that is the Gaussian process with zero mean and correlation $\langle W_t\, W_s\rangle = \min(t, s)$ and $\mathrm{d}W_t = W(t+\mathrm{d}t) - W(t)$. Note that we have adopted here the *Itō formalism* as we have decided to express $\mathrm{d}X$ as a function of x, that is the value of the process at time t. The *Stratonovich* formulation would have consisted in using the value of X at time $t+\mathrm{d}t/2$ (see, e.g., [Gardiner, 1985]). Equation (3.6) decomposes the variation of a stochastic process as the sum of a deterministic part due to $a(X, t)\,\mathrm{d}t$, which is called the *drift term*, and a random part, which is the product of a *diffusion coefficient* $b(X, t)$ by the increment of the Wiener process. This noise changes quickly in time. It relates to the *white noise process* (that can be informally written as $\eta(t) = \mathrm{d}W_t/\mathrm{d}t$), which is a stochastic process characterized by being completely decorrelated in time, with zero mean and a constant variance.

The stochastic equation (3.6) gives us a framework to model the particle motion when assuming that their dynamics is a Markovian process. Such an approach, which consists in following particles along their path, belongs to the class of *Lagrangian* descriptions. Equivalently, one can also obtain an equation for the time evolution of the *transition probability density* $p(x, t|x_0, t_0)$ associated to the process $X(t)$. It is defined such that the probability that $x \leq X(t) \leq x + \mathrm{d}x$, knowing that $X(t_0) = x_0$, is equal to $p(x, t|x_0, t_0)\,\mathrm{d}x$. Thus not only one but all particles that are at the position x_0 at time t_0 are involved and we therefore switch from an individual description to a collective description, which is typical of *Eulerian* approaches. The process X is completely determined by this transition probability density function. One can show that this quantity satisfy the *Fokker-Planck (or forward-Kolmogorov)* equation

$$\partial_t p + \partial_x[a(x, t)\, p] = \frac{1}{2}\partial_x^2[b^2(x, t)\, p]. \tag{3.7}$$

This equation describes a forward evolution as it is associated to the initial condition $p(x, t_0|x_0, t_0) = \delta(x - x_0)$ at time $t = t_0$. This formulation is particularly useful when the initial condition for the particles is fixed and the question is to know were the particles are after a given time. An example of such settings is when interested in the forward-in-time evolution of a spot of pollutant.

Similarly, one can also write an equation for the reversed-time evolution of the transition probability density. This equation is usually called the *backward-Kolmogorov* equation and reads

$$\partial_{t_0} p - a(x_0, t_0)\, \partial_{x_0} p = \frac{1}{2} b^2(x_0, t_0)\, \partial^2_{x_0} p, \tag{3.8}$$

which is this time associated to the final condition $p(x, t|x_0, t) = \delta(x - x_0)$ at time $t_0 = t$. This backward approach is relevant to describe situations where the final condition is prescribed for instance by a measurement. An instance is the case in which one wants to know where a given observed concentration of pollutant is coming from.

The Markovian stochastic processes can be equivalently described in terms of individual solutions to a stochastic equation or in terms of fields by the Fokker-Planck equation. These two approaches are just different ways to portray the same phenomenon. However both have their own advantages and disadvantages. Considering individual trajectories requires to perform statistics by multiplying the number of individual realizations of the noise. This is referred to as a *Monte-Carlo* approach , which can be rather involved. A field approach in terms of Fokker–Plack equation does not have such a pitfall but requires understanding the evolution of the full probability transition for all possible values of the initial and final positions. This is often impossible numerically. Nevertheless, depending on the type of question that one wants to address, one or the other method can be chosen. All these approaches are widely used to study particle transport and diffusion and belong to what is called *Lagrangian stochastic models*.

The particular case of simple diffusions

To finish this section, we recall some results on diffusions. They correspond to the case where the drift term vanishes $a(x, t) = 0$ and the diffusion coefficient is constant $b(x, t) = \sqrt{2D}$. The case when $D = 1/2$ and $X(0) = 0$ coincides with the Wiener process, i.e. $X(t) = W(t)$. Such simple diffusions have zero mean and a variance

$$\langle X^2(t) \rangle = 2\, D\, t. \tag{3.9}$$

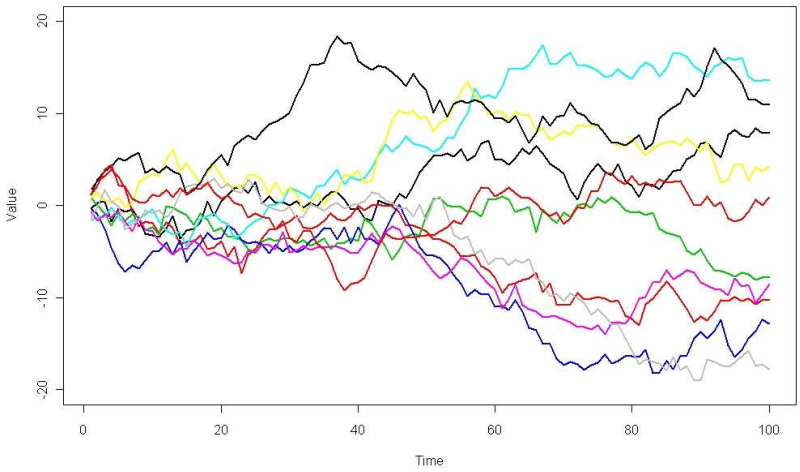

Figure 3.1: Example of the time-evolution of random walks in one dimension. Each color represents a different initial condition for the random walks.

All simple diffusions can be written as $X(t) = X(0) + \sqrt{2D}\,W(t)$. The probability distribution of $W(t)$ is Gaussian and its increments are independent of each other. Its infinitesimal increments can be written as $\mathrm{d}W(t) = \eta(t)\,\mathrm{d}t$, where η is the white-noise process. Hence the Wiener process can be seen as the continuous limit of a *Random Walk*, which is a discrete stochastic process. These two processes are related to each other and the convergence of the second one towards the first, after a large number of steps, is guaranteed by the *central-limit theorem* [1].

Random walks consist of a set of trajectories on a lattice that jump a random length in a random direction at each time step, in a way that is independent from the previous steps. For that reason the random walk is a Markovian process. A good review on the topic is given in the third chapter of the book [Feller, 1971]. Classical examples of random walk are the *drunkard's walk* and the more particular case of *Lévy flight*, in which the jump lengths have a certain probability distribution. The Wiener process is obtained when the distribution of jumps do not have too fat tails. Random walks display basically two peculiar features that are independent of the microscopic aspects (in other words at scales where the single steps are indistinguishable,

[1] The *central limit theorem* states that, independently of the initial distribution, a sum of n independent random variables, distributed with mean μ and variance σ^2, tends to have a normal distribution as n goes to infinity

all random walks behave in a similar way). The first characteristic is that they satisfy the diffusion equation and the second one is that after a time lapse long enough every random walk becomes scale invariant. Denoting by ℓ the average step-length and by N the number of steps, one has that the average squared distance covered by the trajectory satisfies

$$\langle X_N^2 \rangle = \ell^2 \, N. \tag{3.10}$$

In Chapter 6 we will consider with more details the problem of random walks on a one-dimensional lattice but with a random, time- and space-dependent distribution of jumps. Such settings are usually referred to as random walks in random environments. As we will see such models are relevant to describe the diffusive properties of heavy inertial particles in a turbulent flow.

3.1.3 Single-particle diffusion in turbulent flow

There are two different cases where tracer transport can be exactly related to a stochastic equation.

The first case is when the randomness comes from the molecular diffusion, but the realization of the fluid velocity field $\mathbf{u}(\mathbf{x}, t)$ is fixed. In that case, we have seen in Subsection 3.1.1 that, when the molecular diffusivity is equal to κ, the particle trajectories are solutions to (3.4), which through the stochastic equation mathematical formalism can be written as

$$\mathrm{d}\mathbf{X}_\mathrm{p} = \mathbf{u}(\mathbf{X}_\mathrm{p}, t) \, \mathrm{d}t + \sqrt{2\kappa} \, \mathrm{d}\mathbf{W}_t. \tag{3.11}$$

In such case, the drift is given by the particular realization of the velocity and the diffusion coefficient is constant. All the tools of stochastic equations introduced in previous subsection can be applied. In particular, the effect of molecular diffusion on the tracer motion can be described in terms of a transition probability density.

A second case where stochastic formalism applies to tracer motion concerns the use of *eddy diffusivity*. As already anticipated in previous subsection, such approaches are of particular relevance to describe the turbulent transport on very large timescales. This fact has been first stressed in [Taylor, 1921] and is nowadays widely used in both industrial and environmental situations. To understand the key concepts of such approaches, let us neglect the molecular diffusivity and write the equation for a Lagrangian tracer (3.4) in its integral form:

$$\mathbf{X}_\mathrm{p}(t) = \mathbf{X}_\mathrm{p}(0) + \int_0^t \mathbf{u}(\mathbf{X}_\mathrm{p}(s), s) \, \mathrm{d}s. \tag{3.12}$$

From this formulation, one can write the component-wise mean-squared displacement as

$$\left\langle [X_{\mathrm{p}}^i(t) - X_{\mathrm{p}}^i(0)]^2 \right\rangle = \int_0^t \int_0^t \langle u_i(\mathbf{X}_{\mathrm{p}}(s), s)\, u_i(\mathbf{X}_{\mathrm{p}}(s'), s') \rangle \, \mathrm{d}s \, \mathrm{d}s'. \tag{3.13}$$

Contrarily to the previous case, the average $\langle \cdot \rangle$ is now with respect to the realizations of the velocity field. With this formulation, the observation of Taylor is rather simple. Let us assume that the velocity is statistically stationary and introduce the Lagrangian integral time, defined as

$$T_L = \frac{1}{u_{\mathrm{rms}}^2} \int_0^\infty \langle u_i(\mathbf{X}_{\mathrm{p}}(s), s)\, u_i(\mathbf{X}_{\mathrm{p}}(0), 0) \rangle \, \mathrm{d}s, \tag{3.14}$$

where $u_{\mathrm{rms}}^2 = \langle u_i^2(\mathbf{x}, t) \rangle$. It is then easily seen that in the limit of large times

$$\left\langle [X_{\mathrm{p}}^i(t) - X_{\mathrm{p}}^i(0)]^2 \right\rangle \simeq \int_0^t T_L \, u_{\mathrm{rms}}^2 \, \mathrm{d}s = T_L \, u_{\mathrm{rms}}^2 \, t. \tag{3.15}$$

This is true as soon as t is larger than the Lagrangian correlation time of $\mathbf{u}$. In turbulence, this correlation time is of the order of T_L. The expression (3.15) tells us that the long-term mean-squared displacement of tracer particles is proportional to time. This means that the tracers have a behavior similar to that of simple diffusions with $D = T_L \, u_{\mathrm{rms}}^2/2$. This quantity is usually referred to as *eddy diffusivity*.

In addition to this average behavior, one can see from Eq. (3.12) that the displacement on times larger than T_L can be written as a sum of independent random variables. Indeed, it is sufficient to decompose the integral in a sum of integrals over time intervals of length T_L. Each of them is identically distributed and independent as the Lagrangian correlation time is of the order of T_L. This implies that we can apply the central-limit theorem to show that the probability distribution of the displacement is Gaussian with zero mean, when the mean velocity is zero, and a variance given by (3.15).

This approach is widely used in several applications where one is concerned with modeling the diffusion over timescales much larger than those of the underlying turbulence. An instance is the case of atmospheric transport in meteorological models. Typically the mesh size in such models is several kilometers, while the integral scale is of the order of one hundred meters. This scale separation implies that modeling is required and that Taylor's diffusive approach works. The transport of pollutants is then modeled by a diffusion. However the mean velocity in the grid is not zero and this gives a resulting drift term. The particle trajectories can then be approximated by the solutions to

$$\mathrm{d}\mathbf{X}_{\mathrm{p}} = \mathbf{U}(\mathbf{X}_{\mathrm{p}}, t) \, \mathrm{d}t + \sqrt{T_L} \, u_{\mathrm{rms}} \, \mathrm{d}\mathbf{W}_t, \tag{3.16}$$

where **U** denotes the mean velocity of wind. This formulation of turbulent transport in terms of an eddy diffusivity is only exact when interested in very large time scales (larger than the Lagrangian correlation time of the velocity). However, the concept of eddy diffusivity is also largely used in applications to model tracer concentrations on spatial and temporal scales within the inertial range (see, e.g., [Pope, 2000]). Usually, such approaches are designed to study the time evolution of average concentration fields. They provide in general satisfactory results but require to fit some parameters.

There are many other applications of turbulent transport where such an approach has shortcomings. This is the case when one needs to control not only the mean but also the fluctuations in the concentration of a transported specie. As we will see in next section, such problematics require to study dispersion properties on timescales not larger than T_L but rather within the inertial range of turbulence. Moreover, they necessitate understanding the relative motion of several tracer particles.

3.2 Concentration properties

3.2.1 Fluctuations of an advected passive scalar

We have seen in previous section that the motion of tracer particles in a turbulent flow can be described either by a Lagrangian approach, which consists in following their individual tracks, or by an Eulerian approach, where one considers the transition probability density. Now, if we are interested in describing not tracers but rather their concentration field $\theta(\mathbf{x}, t)$, it is generally more convenient to adopt an Eulerian approach and to write the advection-diffusion equation

$$\partial_t \theta + \mathbf{u} \cdot \nabla \theta = \kappa \nabla^2 \theta. \tag{3.17}$$

This formulation in terms of concentration carries less information than the determination of the full transition probability density (where, in that case, randomness is due to the molecular diffusion). Indeed, Eq. (3.17) has to be associated to a given initial condition $\theta(\mathbf{x}, t_0) = \theta_0(\mathbf{x})$, while the transition density $p(\mathbf{x}, t|\mathbf{x}_0, t_0)$ allows one to consider an arbitrary initial condition for tracers. In other terms, p is the *Green function* associated to the advection-diffusion operator. All solutions to Eq. (3.17) can be written as

$$\theta(\mathbf{x}, t) = \iiint \theta_0(\mathbf{x}_0)\, p(\mathbf{x}, t|\mathbf{x}_0, t_0)\, \mathrm{d}\mathbf{x}_0. \tag{3.18}$$

Note that the formulation that we have used here is that corresponding to the transport of a density (or concentration) field. The formulation will be

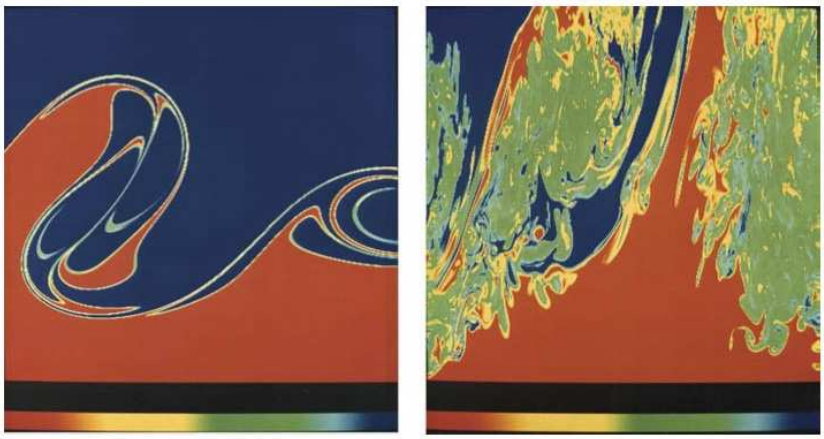

Figure 3.2: Slices of a passive scalar in a turbulent shear layer at two different times. Initially, the lower half plane is red ($\theta = 0$) and the upper is blue ($\theta = 1$). Left: After a small time, stretching and bending create fluctuations at small scales. Right: Later, diffusion becomes important and makes the field uniform. This figure is taken from [Koochesfahani & Dimotakis, 1986] (see also [Dimotakis, 2005]).

different if θ was a passive scalar in a compressible flow (see [Falkovich et al., 2001] or Chap. 2 of [Cardy et al., 2008] for more precisions). However, as we focus on incompressible flows, a density field and a passive scalar obey the same advection equation.

Incompressible flow preserve volumes. This implies that an initial concentration that is uniform in space (i.e. $\theta_0(\mathbf{x}) = 1$ in the whole domain) remains uniform at any later time. However concentration fluctuations appear when the initial condition is not uniform. In the terminology of atmospheric transport, the problem of advection-diffusion with a given initial condition is usually referred to as the problem of an *instantaneous source* and is relevant when interested, for instance, in the dispersion of a spot of pollutant. If we assume for instance that θ_0 is localized in space (say $\theta_0(\mathbf{x}) = 1$ within a given domain and 0 otherwise), turbulent mixing will stretch and bend progressively the lines of constant concentration under the action of the non-uniform velocity field (see Fig. 3.2 Left). After a short time interval, such a mechanism will create small-scale variations in the concentration field and the velocity at which mixing occurs will be dramatically increased. Local concentration gradients become stronger and stronger until they are dissipated by the molecular diffusivity (see Fig. 3.2 Right). It very important to stress that the transport as well as the mixing rate are independent of

molecular diffusivity in the case of fully-developed turbulent flow. However it is well known that, even if it is very weak, the diffusivity will dominate the turbulent advection in the long run as smaller and smaller-scale variations of θ are created. This makes the process of turbulent mixing irreversible as the system cannot recover its initial state by infinitesimal backwards changes without some energy cost. An exhaustive review of these basic concepts on turbulent mixing is given in [Monin & Yaglom, 1971] and in [Dimotakis, 2005].

Through dimensional analysis it is possible to portray in quite detail the typical timescales of mixing. Nevertheless such a simple phenomenological description is not sufficient to understand the statistics of the large fluctuations that appear in the concentration field. For instance, dimensional arguments are not able to explain the deviations from a Gaussian behavior of the probability density functions of θ that are observed experimentally and numerically. This was for instance evidenced in the experiment reported in [Jayesh & Warhaft, 1991] where the fluctuations of a passive scalar released upstream in a turbulent wind tunnel were measured in several locations downstream (see Fig. 3.3 Left). It is generally believed that such deviations from a Gaussian distribution are due to the creation by turbulence of strong gradients in the concentration field.

Historically, such probability distribution functions were not immediately considered a useful statistical tool, unlike the spectrum or the structure functions. It was widely believed that in homogeneous flows the concentration is always distributed according to the normal law, because the turbulent mixing would act as a sum of independent small-scale stretching events and the *central-limit theorem* would then applies. Later, several experimental evidences showed that the probability distributions are not necessarily Gaussian and their study started to gather an increasing interest. Through either simple phenomenological and rigorous theoretical models it was confirmed that the probability distribution function of a scalar field displays exponential tails when a mean scalar gradient is present [Pumir et al., 1991, Shraiman & Siggia, 1994] (for a complete argumentation on passive scalars see [Sreenivasan, 1991]). These tails are due to some rare events during which the tracers travel distances much larger than those expected in the case the of a random diffusive motion. Such violent fluctuations are responsible for what is called *anomalous mixing* (see [Shraiman & Siggia, 1994]). The exponential behavior in the probability distribution of a passive scalar can be observed experimentally in large-Reynold-number flows with a sufficiently wide inertial range [Jayesh & Warhaft, 1991, Gollub et al., 1991].

Large fluctuations of a passive scalar can also be observed when interested in problems of *time-continuous sources* rather than instantaneous sources.

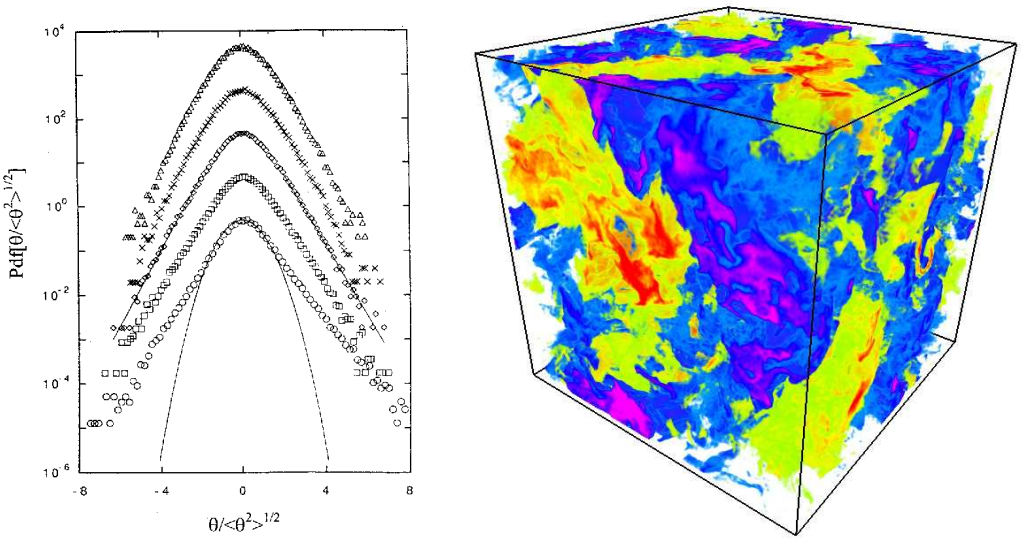

Figure 3.3: Left: normalized probability density functions of a passive scalar θ obtained from the experiment in [Jayesh & Warhaft, 1991] in a wind tunnel increasing (from bottom to top) the distance downstream the location where it is injected; the solid line is a Gaussian distribution. Right: typical snapshot of a passive scalar in a developed turbulent three-dimensional flow; high concentrations are shown in red/yellow and low ones in blue/magenta (courtesy of G. Krstulovic).

This is the case when a pollutant is emitted with a given constant rate at a fixed location (for instance at the nozzle of a chimney or above a highway). To model that, a forcing term $\phi(\mathbf{x}, t)$ has to be added to Eq. (3.17). Due to the linearity of the advection-diffusion operator, the solution can then still be written in terms of the Green function. When the forcing is statistically stationary, the passive scalar attains also a statistical steady state and can be written as

$$\theta(\mathbf{x}, t) = \int_{-\infty}^{t} \iiint \phi(\mathbf{x}_0, t_0)\, p(\mathbf{x}, t|\mathbf{x}_0, t_0)\, \mathrm{d}\mathbf{x}_0\, \mathrm{d}t_0. \tag{3.19}$$

As seen in Fig. 3.3 (Right), such a field develops very strong fluctuations, even if the force is very smooth in space and time. The strong variations are due to the fact that trajectories with very different histories, and thus experiencing different forcings, can in principle arrive very close to each other at a given time. This mechanism is responsible for the presence of *fronts* or *cliffs* in the concentration where its value has strong variations over very small scales. These structures are responsible for strongly intermittent scalar statistics.

For instance, the scaling exponents ξ_p of the scalar structure functions, i.e. such that $S_p^\theta(r) = \langle[\theta(\mathbf{x}+\mathbf{r}) - \theta(\mathbf{x})]^p\rangle \sim |\mathbf{r}|^{\xi_p}$, saturate to a constant for sufficiently high orders [Celani et al., 2000].

The p-th order structure function relates to p-th order correlations of the concentration field. This is for instance evident for $p = 2$ where, for a statistically homogenous distribution,

$$\begin{aligned} S_2^\theta(r) &= \langle[\theta(\mathbf{x}+\mathbf{r}) - \theta(\mathbf{x})]^2\rangle = 2\langle\theta^2(\mathbf{x})\rangle - 2\langle\theta(\mathbf{x}+\mathbf{r})\,\theta(\mathbf{x})\rangle \\ &= 2[C_2(0) - C_2(r)], \end{aligned} \tag{3.20}$$

where $C_2(r) = \langle\theta(\mathbf{x}+\mathbf{r},t)\,\theta(\mathbf{x},t)\rangle$ is the second-order correlation of the passive scalar field. This quantity relates to the two-point motion of the tracers. In general, the p-th order structure function can be determined by studying the joint motion of p tracer trajectories. This can be seen for $p = 2$ from the relationship (3.18) between the transition probability and the solutions to the advection-diffusion equation (assuming for instance that the problem is not forced). Considering that

$$\theta(\mathbf{x}_1,t)\,\theta(\mathbf{x}_2,t) = \iint \theta_0(\mathbf{x}_1^0)\,\theta_0(\mathbf{x}_2^0)\,p(\mathbf{x}_1,t|\mathbf{x}_1^0,t_0)\,p(\mathbf{x}_2,t|\mathbf{x}_2^0,t_0)\,\mathrm{d}\mathbf{x}_1^0\,\mathrm{d}\mathbf{x}_2^0,$$

one can take the average with respect to the flow realization to write the correlation C_2 as

$$C_2(r) = \iint \theta_0(\mathbf{x}_1^0)\,\theta_0(\mathbf{x}_2^0)\,p_2(\mathbf{x}+\mathbf{r},\mathbf{x},t|\mathbf{x}_1^0,\mathbf{x}_2^0,t_0)\mathrm{d}\mathbf{x}_1^0\,\mathrm{d}\mathbf{x}_2^0, \tag{3.21}$$

where

$$p_2(\mathbf{x}_1,\mathbf{x}_2,t|\mathbf{x}_1^0,\mathbf{x}_2^0,t_0) = \langle p(\mathbf{x}_1,t|\mathbf{x}_1^0,t_0)\,p(\mathbf{x}_2,t|\mathbf{x}_2^0,t_0)\rangle. \tag{3.22}$$

The latter is the joint transition probability of two trajectories, that is the density probability that two tracers, which were initially in $\mathbf{x}_1^0$ and $\mathbf{x}_2^0$ at time t_0, are located in $\mathbf{x}_1$ and $\mathbf{x}_2$ at time t. If in addition the flow is statistically stationary and homogeneous, p_2 depends only on $\mathbf{r} = \mathbf{x}_1 - \mathbf{x}_2$, on $\mathbf{r}_0 = \mathbf{x}_1^0 - \mathbf{x}_2^0$ and on $t - t_0$. Note that in Eq. (3.22), p_2 is defined as the average of the product of one-point transition probabilities. This is different from the product of averages, so that the two-point motion cannot be trivially deduced from single-point dispersion and deserves its own study. The relationship between concentration correlations and two-point dynamics motivates the study of the relative dispersion of tracers in a turbulent flow. As we will see in Chap. 4, the question is then to understand the evolution as a function of time of the separation $\mathbf{r}$ between two tracers that were initially separated by $\mathbf{r}_0$.

3.2.2 Preferential concentration of inertial particles

We have seen in previous subsection that the fluctuations that appear in the concentration of passive tracers are due to an amplification of the spatial inhomogeneities of the source (the initial condition or the forcing) by the turbulent flow. The situation is very different when the transported particles cannot be considered as tracers but have inertia. In that case, the particle dynamics itself is not volume-preserving and concentration fluctuations appear even if the initial condition is homogeneous and the fluid is incompressible.

As we have seen in Subsection 3.1.1, when the particles have a too large size, their dynamics cannot be approximated by that of tracers. When in addition, they are heavier than the fluid, their dynamics is described by Eq. (3.2) and they do not follow the fluid motion exactly and have a delay on it. Such an *inertia* is responsible for the presence of correlations between the particle positions and the structure of the underlying flow that cause the formation of particle clusters. These concentrations are at the center of many studies because quantifying them is crucial for many applications in planet formation [De Pater & Lissauer, 2001], in cloud physics [Shaw, 2003], and in engineering [Post & Abraham, 2002]. In all these cases, the transported particles are dust or droplets in a gas. They are heavier and have a too large size to be simply tracers. The strong inhomogeneities appearing in their distribution play an important role as they will alter the interactions among such particles. Modeling reaction rates, collisions, and gravitational interactions thus requires quantifying clustering. Moreover it is important to stress that light particles also distribute in a non uniform manner. This is for instance the case of bubbles in fluids, which settle, merge, or dissolve differently depending on their clustering properties.

The mechanisms that are responsible for clustering are often heuristically explained in terms of the interactions between an inertial particle and a vortex of the flow [Maxey, 1987]. It is indeed well known that, while light particles tend to concentrate inside the vortical structures, heavy particles are ejected out (see Fig. 3.4). These properties have frequently been used to visualize fluid flows. Small bubbles were for instance used in order to give evidence for the presence of vortex filaments in turbulence [Douady et al., 1991] (see Fig. 3.4 Right). The mechanism leading to ejection or concentration in the vortices can be easily understood in terms of the centrifugal or centripetal forces that act on the particle. This phenomenon is usually referred to as *preferential concentration* [Squires & Eaton, 1991]. It is responsible for fluctuations of the particle density at all scales spanned by the eddies of the turbulent flow. In addition to this mechanism, the dissipative dynamics of inertial particles is responsible for small-scale concentration properties. As

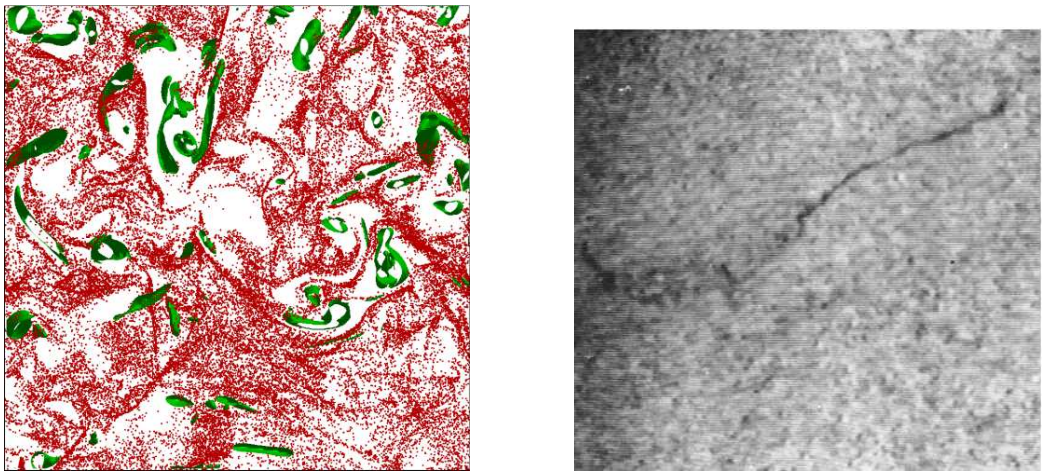

Figure 3.4: Left: snapshot of the position of heavy inertial particles (in red) in a slice of a three-dimensional developed turbulent flow (from [Homann et al., 2009]). The green structures are vorticity iso-surfaces and show the strong vortices of the flow. Right: instantaneous picture of bubbles concentrating in the core of a vortex filament in a Von Karman flow [Douady et al., 1991].

we can see from Fig. 3.4 (Left), the fluctuations in the distribution of heavy particles do not consist only in an anti-correlation between their position and the fluid vortices. In the regions where particles are present, their distribution actually resembles a folded fractal set. This can be explained by their dissipative dynamics that makes trajectories converge to a strange attractor [Bec, 2003]. In a turbulent flow, this attractor moves due to velocity fluctuations but its small-scale properties are stationary in a statistical sense. These properties determine the small-scale interactions among particles and can be measured and sometimes derived analytically as a function of the Stokes number St introduced in Subsection 3.1.1.

The large-scale properties of particle distribution are understood in a less systematic manner. The density fluctuations inside the inertial range are due to a cumulative effect of ejection/concentration by the vortical structures that span all the spatial scales of the turbulent flow. If the turbulent velocity is assumed to be scale-invariant, it can be shown that particle clustering at a given scale ℓ depends only on a *scale-dependent* Stokes number $St(\ell) = \tau_s/\tau_\ell$, in which the particle response time τ_s is non-dimensionalized by the turnover time τ_ℓ [Bec et al., 2007a, Bec et al., 2007b]. Also, it is observed there that the probability distribution of the coarse-grained density of particles behaves

as a power law at small values and has a tail fatter than Gaussian at large values. Such properties are reproduced by simple mass ejection models on a lattice [Bec & Chétrite, 2007]. As we will see in Chap. 6, a part of the work developed in this thesis consisted in extending this last work to settings where the rate at which particles are ejected depends continuously on space and time and displays scale-invariance properties.

Chapter 4

Diffusivity in turbulent pair dispersion

Relative dispersion in a turbulent flow gives rise to a considerable interest since, as seen in previous chapter, it is one of the main key to describe second-order statistics in turbulent transport and mixing. It is important to understand the physical mechanisms behind pair dispersion in order to improve the models used for instance to predict pollutant dispersion in the atmosphere as well as in the seas. The time evolution of the separation between two tracer particles was first studied in [Richardson, 1926]. Since then, much work has been devoted to understand the statistics of pair dispersion (see for instance [Batchelor, 1952, Kraichnan, 1966, Monin & Yaglom, 1971] and for recent reviews [Falkovich et al., 2001, Sawford, 2001, Salazar & Collins, 2009]). However several questions remain today without a definite answer. For example, the dependence on the initial separation of the probability density function of the distance between two particles is still the matter of some debate [Bourgoin et al., 2006, Rast & Pinton, 2011, Scatamacchia et al., 2012]. To address this issue, one has to consider in addition to the initial separation, the influence of the initial condition of the velocity and acceleration differences and to possibly identify different regimes of separation. This chapter reports thesis work on the time evolution of the mean square distance between two tracers. This study is the subject of an article published on *Physical Review* E [Bitane et al., 2012b]. The results of this study open the way to new possible explanations of the mechanisms leading to Richardson–Obukhov law, which are an alternative to the commonly-accepted scenario based on a scale-dependent effective diffusivity.

4.1 The regimes of tracer separation

Turbulence has the feature of strongly enhancing the dispersion and mixing of the species it transports. Also, as explained in Chap. 3, tracers transported by a turbulent flow approach a diffuse behavior on time scales much longer than the Lagrangian correlation time of the flow [Taylor, 1921]. These ideas are now commonly used in applications, as for instance in air quality control, to model effective mixing properties in terms of an eddy diffusivity. Such models give a good handle on long-term averages and are successfully used to determine, for instance, possible health hazards linked to a long exposure downstream a pollutant source. However they are unable to capture strong local fluctuations stemming from the complex structure of the turbulent flow. Such events cannot be directly predicted from the averaged concentration field as they relate to higher-order moments. Accessing these fluctuations is crucial in order to quantify for instance the likeliness of finding a local concentration exceeding a high threshold.

As we have seen in Sec. 3.2.1, second-order statistics, such as the variance of a transported concentration field and more generally the spatial correlation of a passive scalar, are statistically related to the relative motion of tracers. In turbulence, the distance $|\boldsymbol{R}(t)|$ between two Lagrangian trajectories follows the Richardson–Obukhov superdiffusive law

$$\langle |\boldsymbol{R}(t)|^2 \rangle \sim \varepsilon\, t^3, \tag{4.1}$$

where ε is the mean rate of kinetic energy dissipation and the average is performed over all the realizations. The long-term behavior of such a separation becomes independent of the initial separation $|\boldsymbol{R}(0)| = r_0$, whence the designation of *explosive* pair separation. This superdiffusive separation is much faster and less predictable than in any chaotic system. Some incertitudes remain on the validity and the possible convergence to this law, because such an explosive behavior is very arduous to observe both in numerics and in experiments. This is basically due to the difficulty to have a huge scale separation between the dissipative lengths, the initial separation of tracers, the observation range and the integral scale of the flow (the reader can refer to [Sawford, 2001] and [Salazar & Collins, 2009] for reviews on that questions). Much effort has been devoted to test the universality of this law, which was actually retrieved in various turbulent settings, such as the two-dimensional inverse cascade [Jullien et al., 1999, Boffetta & Sokolov, 2002b], buoyancy-driven flows [Schumacher, 2008], and magnetohydrodynamics [Busse & Müller, 2008].

4.1.1 Richardson's diffusive approach

In the commonly accepted sense, studying turbulent relative dispersion consists in considering the evolution of the separation

$$\boldsymbol{R}(t) = \mathbf{X}_1(t) - \mathbf{X}_2(t) \tag{4.2}$$

between two tracers $\mathbf{X}_1(t)$ and $\mathbf{X}_2(t)$. In these settings the initial distance $r_0 = |\boldsymbol{R}(0)|$ is fixed. Richardson's original arguments [Richardson, 1926] can be reinterpreted by assuming that the velocity difference $\boldsymbol{V}(t)$, defined as

$$\boldsymbol{V}(t) = \mathbf{u}(\mathbf{X}_1, t) - \mathbf{u}(\mathbf{X}_2, t), \tag{4.3}$$

between the two tracers has a short correlation time. This means that the central-limit theorem applies and that, for sufficiently large timescales, one has

$$\frac{\mathrm{d}\boldsymbol{R}}{\mathrm{d}t} = \boldsymbol{V} \simeq \sqrt{2\,\tau_L(\boldsymbol{R})}\;\boldsymbol{U}(\boldsymbol{R})\,\boldsymbol{\xi}(t), \tag{4.4}$$

where $\boldsymbol{\xi}$ is the standard three-dimensional white noise, $\boldsymbol{U}$ is the Eulerian velocity difference correlation tensor (such that $\boldsymbol{U}^{\mathsf{T}}\boldsymbol{U} = \langle \delta\mathbf{u} \otimes \delta\mathbf{u} \rangle$, where $\delta\mathbf{u}$ is the Eulerian velocity increment computed over a separation $R = |\boldsymbol{R}|$), and τ_L the Lagrangian correlation time of velocity differences between pair separated by R. Note that the product is here understood in the Stratonovich sense. This formulation in terms of a stochastic equation can equivalently be written for the two-point transition probability density $p_2(\boldsymbol{r}, t|\boldsymbol{r}_0, 0)$ (see Sec. 3.1.2 for details on these notions). The density p_2 is thus a solution to the Fokker–Planck equation

$$\partial_t p_2 = \partial_{r_i}\left[\tau_L\,\boldsymbol{U}^{\mathsf{T}}\,\boldsymbol{U}\partial_{r_j} p_2\right], \tag{4.5}$$

where τ_L and $\boldsymbol{U}$ are evaluated at the separation $\boldsymbol{r}$.

As stressed in [Obukhov, 1941], when assuming Kolmogorov 1941 scaling we can approximate

$$\tau_L \sim r^{2/3}, \quad \boldsymbol{U} \sim r^{1/3}, \tag{4.6}$$

where $r = |\boldsymbol{r}|$. In addition, because of isotropy and when integrating over angles, the transition probability depends only on r and r_0. The Fokker–Planck equation can then be rewritten as

$$\partial_t p_2 = \frac{1}{r^2}\partial_r\left[r^2 K(r)\,\partial_r p_2\right], \tag{4.7}$$

where K is the scale-dependent diffusivity of the separation diffusive process. For separations r within the inertial range of turbulence one has

$$K(r) \propto \varepsilon^{1/3} r^{4/3}. \tag{4.8}$$

Equation (4.7) exactly corresponds to that derived by Richardson for the transition probability density $p(r,t\,|\,r_0,0)$ at large times

$$p_2(r,t\,|\,r_0,0) \propto \frac{r^2}{\langle|\boldsymbol{R}(t)|^2\rangle^{3/2}}\ \exp\left[-\frac{A\,r^{2/3}}{\langle|\boldsymbol{R}(t)|^2\rangle^{1/3}}\right], \tag{4.9}$$

where A is a positive constant. The transition probability density is thus entirely determined by the second-order moment of the separation $|\boldsymbol{R}(t)|$ that, according to Eq.(4.7), is satisfying at large times

$$\langle|\boldsymbol{R}(t)|^2\rangle \simeq g\,\epsilon\,t^3, \tag{4.10}$$

where g is a positive constant (usually called the *Richardson constant*) related to A. The average is here taken over all pairs that are initially at a distance $|\boldsymbol{R}(0)| = r_0$.

The key hypothesis in order to derive a Fokker–Planck equation of the form in Eq. (4.5) for the separation $\boldsymbol{R}$ is that velocity differences $\boldsymbol{V}(t)$ between tracers are correlated over timescales much smaller than those of interest, so that $\tau_L(r) \ll t$. As noticed for instance in [Falkovich et al., 2001], this assumption can hardly be invoked. It is indeed expected that the Lagrangian turnover time τ_L will be of the order of the correlation for eddies of size r. It is known in turbulence that such eddies are correlated over a time of the order of their *turnover time* given by

$$\tau_r = \frac{r}{\delta_r u} \sim \varepsilon^{-1/3} r^{2/3}. \tag{4.11}$$

Hence for separations that, according to Eq. (4.10), grow like $r \sim (\varepsilon t^3)^{1/2}$, one has $\tau_L \sim \tau_r \sim t$, so that the dominant flow structures in the separation dynamics are in principle correlated over timescales of the order of the observation time. This implies that the central limit theorem cannot be applied and that the approximation in Eq. (4.4) does not hold. This is an issue in justifying the stochastic approach that we have just mentioned.

Despite such shortcomings, the diffusive approach proposed by Richardson and in particular the explicit form in Eq. (4.9) for the transition probability density, have proven being relevant in some asymptotics [Ott & Mann, 2000, Biferale et al., 2005, Ouellette et al., 2006, Salazar & Collins, 2009, Eyink, 2011]. Also, much work on relative dispersion has used it as a basis. For instance, improvements of Eq. (4.9) were proposed using modified versions of the eddy diffusivity $K(r)$, adding a time dependence [Batchelor, 1952, Kraichnan, 1966] or, more recently, including finite Reynolds number effects [Scatamacchia et al., 2012]. All of these improvements strongly alter the functional form of the large-r tail of the transition probability density.

Nevertheless, the physical mechanisms leading to the de-correlation of velocity differences and to models based on eddy diffusivity are still unclear and many questions remain open. In this chapter, we mainly focus on the mechanisms that justify a convergence to the Richardson–Obukhov law. In particular we address the questions of the speed at which such a convergence occurs and of the form of subleading terms, which is still not known. In this light, we will come back in next chapter on the problem of the form of the transition probability density, with a focus on the mechanisms giving extreme fluctuations.

4.1.2 Batchelor's ballistic regime

The first work dealing with the way pair separation converges to the Richardson superdiffusive behavior is due to G.K. Batchelor [Batchelor, 1950]. He argued that the explosive t^3 law is preceded by a ballistic phase during which the tracers keep their initial velocity and separate as

$$\langle |\boldsymbol{R}(t) - \boldsymbol{R}(0)|^2 \rangle \simeq t^2 S_2(r_0), \tag{4.12}$$

where $S_2(r) = \langle |\delta_r \mathbf{u}|^2 \rangle$ is the Eulerian second-order structure function over a separation r, computed with absolute values. This regime holds till a time scale that is a function of the initial separation r_0, known as *Batchelor's time* [Biferale et al., 2005, Bourgoin et al., 2006]

$$t_B(r_0) = \tau_{r_0} \sim \varepsilon^{-1/3} r_0^{2/3}, \tag{4.13}$$

which is equal to the eddy turnover time associated to the initial separation r_0. After this time, there is a transition to the Richardson regime and the dynamics loses all memory on the initial condition. In this Batchelorś regime, the velocity remains strongly correlated, so that it can clearly not be described by an eddy-diffusivity approach.

Various stochastic models have been designed to catch both Batchelor's and Richardson's regimes. Most of them are based on the observation that the acceleration difference between the two tracers is shortly correlated but they do not assume that velocity differences get uncorrelated. The pair separation and the velocity difference can then be approximated as coupled Markovian diffusive processes (see [Kurbanmuradov, 1997, Sawford, 2001] for reviews). The usual path for designing such models requires imposing some constraints on the drift and the diffusion terms. Thomson argued that they should satisfy the well-mixed condition [Thomson, 1987]: when averaging over uniformly separated pairs inside the whole inertial range, the statistics

of velocity differences between the two tracers has to recover Eulerian two-point statistics. Definitively, devising an admissible model requires an input from Eulerian statistics [Borgas & Yeung, 2004]. We have seen in Chap. 2 that, in turbulence, the distribution of velocity differences is neither self-similar nor Gaussian. Because of that, such models become so complicated that they can hardly be used to improve the understanding of the underlying phenomenology and, at the same time, they are not easily amenable for an analytical treatment.

To clarify when and where Richardson's approach might be valid, it is important to understand the timescale of convergence to the explosive t^3 law. Much work has recently been devoted to this issue: it was for instance proposed to make use of fractional diffusion with memory [Ilyin et al., 2010], to introduce random delay times of convergence to Richardson scaling [Rast & Pinton, 2011], or to estimate the influence of extreme events in particle separation [Scatamacchia et al., 2012]. The last point will be studied in detail in the next chapter. All these approaches consider as granted that the final behavior of separations is given by Richardson's diffusive approach. As we will see here, many aspects of the convergence to Richardson's law for pair dispersion can be clarified in terms of a diffusive behavior of velocity differences.

4.2 Timescales of two-particle dispersion

We focus in this section on determining the various timescales that are involved in the problem of tracer relative dispersion.

4.2.1 Settings of the numerical simulations

To investigate such issues, we have used the data from direct numerical simulations of the incompressible Navier–Stokes equation in the three-dimensional 2π-periodic domain. These simulations were performed with the code *LaTu* developed by H. Homann [Homann et al., 2007]. This code uses a standard pseudo-Fourier-spectral solver for calculating the spatial derivatives in the various terms of Navier–Stokes equation, together with a third-order Runge–Kutta scheme for the temporal evolution. Such a method is well adapted to incompressible homogeneous and isotropic turbulence at high Reynolds numbers with an extended inertial range of scales. It has the advantages of combining a high degree of accuracy with very good performances on massive parallel supercomputers such as BlueGene systems and large Intel/AMD

Table 4.1: Parameters of the numerical simulations

N	R_λ	δx	δt	ν	ε	$u_{\rm rms}$	η	τ_η	L	τ_L
2048^3	460	$3.7{\cdot}10^{-3}$	$6{\cdot}10^{-4}$	$2.5{\cdot}10^{-5}$	$3.6{\cdot}10^{-3}$	0.19	$1.4{\cdot}10^{-3}$	0.083	1.85	9.9
4096^3	730	$1.53{\cdot}10^{-3}$	$1.2{\cdot}10^{-3}$	$1.0{\cdot}10^{-5}$	$3.8{\cdot}10^{-3}$	0.19	$7.2{\cdot}10^{-4}$	0.05	1.85	9.6

N is the number of grid points, R_λ the Taylor-based Reynolds number, δx the grid spacing, δt the time step, ν the kinematic viscosity, ε the averaged energy dissipation rate, $u_{\rm rms}$ the root-mean square velocity, $\eta{=}(\nu^3/\varepsilon)^{1/4}$ the Kolmogorov dissipative scale, $\tau_\eta = (\nu/\varepsilon)^{1/2}$ the associated turnover time, $L = u_{\rm rms}^3/\varepsilon$ the integral scale and $\tau_L = L/u_{\rm rms}$ the associated large-scale turnover time.

clusters. One of the main advantages of the code *LaTu* is that it uses a pencil representation of the domain. While traditionally in pseudo-spectral codes the domain is divided in two-dimensional slabs, a decomposition in one-dimensional elements is here used. This allows one to use a maximum number of processors, which is given by the square number of grid-points in one direction, instead of this number itself when using slab decompositions. For instance, while in a 1024^3 simulation traditional codes can usually use a maximum of 1024 processes where two-dimensional fast Fourier transforms are performed, the code *LaTu* can use up to 1024^2 processes in which one-dimensional transforms are carried out. The code is parallelized using *MPI* and, because of its pencil representation of the domain, can run on massively parallel computers using up to several tens of thousands processors.

We have used two sets of simulations whose parameters are summarized in Table 4.1 (more details on these specific simulations can be found in [Grauer et al., 2012]). In both simulations, the resolution is such that $k_{\rm max}\,\eta = (N/3)\,\eta \approx 1$. As we are interested in inertial-range quantities, we do not need a very high resolution of the dissipative scales. To maintain a statistical steady state, the flow is forced by keeping constant the energy content of the two first shells of wavenumbers in Fourier space. This implies that in both simulations the forcing scale is $L_{\rm f} = \pi$. The Eulerian second-order structure function measured from these two simulations are represented in Fig. 4.1. As seen there, the largest one develops a significant scaling range where deviations from Kolmogorov 1941 scaling start to be visible. For each value of the Reynolds number, the flow is seeded with 10^7 tracer particles whose motion is integrated using tri-linear interpolation. Positions, velocities, and accelerations of tracers have been stored with enough frequency for studying

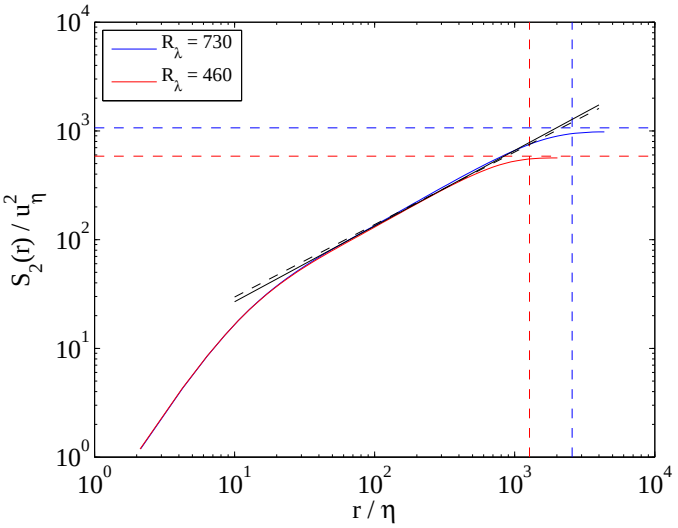

Figure 4.1: Second-order Eulerian absolute-value structure function $S_2(r) = \langle |\boldsymbol{u}(\boldsymbol{x}+\boldsymbol{r},t) - \boldsymbol{u}(\boldsymbol{x},t)|^2 \rangle$ for the two values of the Reynolds number investigated in this thesis. The dashed line represents Kolmogorov 1941 scaling $S_2(r) \simeq (11/3)\, C_2 (\varepsilon\, r)^{2/3}$ with $C_2 = 2.13$. The solid line corresponds to She-Lévêque anomalous scaling with $\zeta_2 \approx 0.696$ (see [She & Lévêque, 1994]). The vertical and horizontal colored dashed lines indicate the integral scale L and the large-scale velocity, respectively.

relative motion. These simulations were performed on the BlueGene machine *JuGene* of the German computer Center of Jülich in the framework of the XXL project HBO28. They required more than ten millions of CPU hours. All the statistical studies reported in this chapter and in the next one have been done using these datasets.

To provide a first insight on the numerical simulations that we have used and on the typical values of the timescales and lengthscales that are used throughout this and next chapter, let us shortly report some measurements on relative dispersion. One of the major difficulties encountered when approaching numerically this problem is that it requires a huge timescale separation. Indeed, to observe Richardson–Obukhov t^3 superdiffusive regime, one needs at least to follow particle pairs on a time t much longer than the Kolmogorov dissipative time $\tau_\eta = (\nu/\epsilon)^{1/2}$ and much shorter than the eddy turnover time τ_L associated to the integral scale L. Also, in order to observe possibly universal mechanisms of convergence to Richardson's explosive behavior, it is in principle required that the initial distance r_0 belongs to the inertial range. In particular, a possible proper rescaling in terms of r_0 of transients to the t^3 law

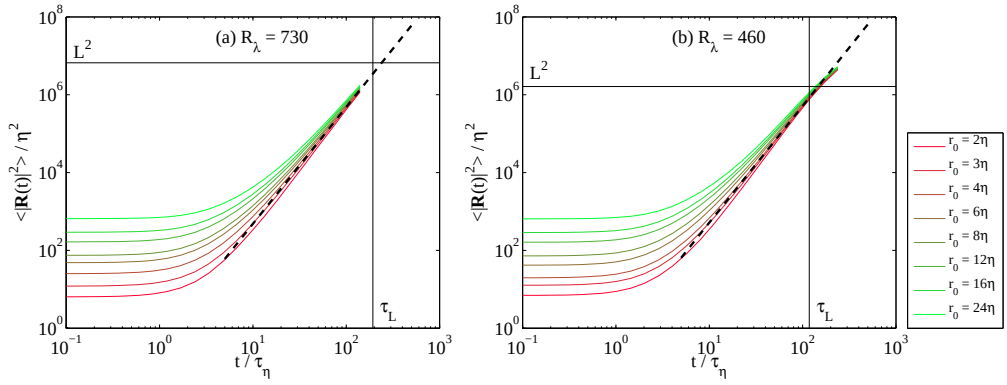

Figure 4.2: Time-evolution of the mean-squared distance for $R_\lambda = 730$ (a) and $R_\lambda = 460$ (b) for various initial separations r_0 as labeled. The horizontal and vertical solid lines represent the integral scale L and its associated turnover time τ_L, respectively. The dashed line corresponds to the explosive Richardson-Obukhov law given by Eq. (4.10) with $g = 0.52$.

can only be valid if the observation time t is much longer than the turnover time $\tau_{r_0} \sim \varepsilon^{-1/3} r_0^{2/3}$ associated to the initial separation $|\boldsymbol{R}(0)| = r_0$, which itself has to be longer than τ_η. We should thus have $\tau_\eta \ll \tau_{r_0} \ll t \ll \tau_L$. To give a concrete idea, if we require that these timescales are separated by at least a decade, this implies that one should have a Taylor-based Reynolds number $R_\lambda = \sqrt{15}\,(\tau_L/\tau_\eta) \gtrsim 4000$. Such a high level of turbulence is still far from present-day experimental setups where accurate particle tracking techniques can be used (see [Salazar & Collins, 2009, Toschi & Bodenschatz, 2009] for recent reviews). Also, such large values of the Reynolds number are unreachable by state-of-the-art direct numerical simulations. At the moment there is no simulations of lagrangian tracers in homogeneous isotropic turbulence with more than 4096^3 grid points. As we have seen in Table. 4.1, with such a resolution, we have attained $R_\lambda = 730$ as it was decided to resolve well the dissipative scales. Decreasing such a precision can help in reaching at maximum $R_\lambda \approx 1100$, with the risk of missing violent small-scale intermittent structures [Ishihara et al., 2009]. For this reason, there is an important need for understanding the full process of convergence to the t^3 law in order to predict and detect for instance possible subleading corrections. This is the spirit whereby this thesis work is presented.

After a time sufficiently long to have converged to a statistical steady state (around one large-scale turnover time), we start the analysis of the dispersion of tracer pairs. For this, we label at a fixed initial time (that we set here to be $t = 0$) all couples whose distance $|\boldsymbol{R}(0)| = |\boldsymbol{X}_1(0) - \boldsymbol{X}_2(0)|$

is equal to $r_0 \pm \eta$ for $r_0 \leq 16\,\eta$ and equal to $r_0\,(1 \pm 2\%)$ for $r_0 > 16\,\eta$ with $r_0 = 2, 3, 4, 6, 8, 12, 16, 24, 32, 48, 64, 96, 128$, and 192η. This bining was chosen such that each family indexed by r_0 contains a few hundreds of thousands of pairs. We then track forward in time all indexed pairs and perform statistics conditioned on their initial separation r_0. Figure 4.2 shows for the two simulations the time evolution of the mean squared distance $\langle |\boldsymbol{R}(t)|^2 \rangle$ for various values of the initial separation r_0. Time and space are there represented in dissipative-scale units. After a transient (which roughly corresponds to Batchelor's ballistic regime), the mean-squared distance approaches the explosive Richardson–Obukhov regime $\langle |\boldsymbol{R}(t)|^2 \rangle \simeq g\,\varepsilon\,t^3$ written in Eq. (4.10). We observe for both values of the Reynolds number a Richardson–Obukhov constant $g \approx 0.52 \pm 0.05$. In the next two subsections, we will see how to characterize the time at which the convergence to this regime occurs.

4.2.2 Timescale of departure from Batchelor's regime

As already motivated in Sec. 4.1, the objective is here to understand better the timescale at which the average separation between tracers converges to the t^3 Richardson scaling observed in previous subsection. Let us begin with rewriting the initial ballistic behavior Eq. (4.12) of the average squared separation, together with its subleading term. For that we follow the same algebraic steps as in [Ouellette et al., 2006]. A Taylor expansion at short times of the separation leads to

$$\big\langle |\boldsymbol{R}(t) - \boldsymbol{R}(0)|^2 \big\rangle_{r_0} = t^2 \langle |\delta_{r_0}\mathbf{u}|^2 \rangle + t^3\, \langle \delta_{r_0}\mathbf{u} \cdot \delta_{r_0}\mathbf{a} \rangle + \mathrm{O}(t^4). \tag{4.14}$$

We have here denoted by $\langle \cdot \rangle_{r_0}$ the average over all tracer pairs that are initially at a distance r_0 from each other. This notation is useful to distinguish this *Lagrangian average* from the *Eulerian average*, which is denoted by the simple brackets $\langle \cdot \rangle$. We have also used $\delta_r\mathbf{u}$ to designate the Eulerian increment $\mathbf{u}(\mathbf{x}+\mathbf{r},t) - \mathbf{u}(\mathbf{x},t)$, where $r = |\mathbf{r}|$. Finally, $\delta_r\mathbf{a}$ is the Eulerian increment of the fluid acceleration, defined as $\delta_r\mathbf{a} = [\partial_t\mathbf{u} + \mathbf{u}\cdot\nabla\mathbf{u}](\mathbf{x}+\mathbf{r},t) - [\partial_t\mathbf{u} + \mathbf{u}\cdot\nabla\mathbf{u}](\mathbf{x},t)$.

As long as the first term (proportional to t^2) in the right-hand side of Eq. (4.14) is dominant, the tracers separate ballistically. Clearly the expansion fails when the second subleading term in the right-hand side becomes of the same order as that giving the ballistic separation. This happens when the time is of the order of

$$t \;\approx\; t_0 = \frac{S_2(r_0)}{|\,\langle \delta_{r_0}\mathbf{u} \cdot \delta_{r_0}\mathbf{a} \rangle\,|}\,, \;\text{ where } S_2(r_0) = \langle |\delta_{r_0}\mathbf{u}|^2 \rangle. \tag{4.15}$$

It is known [Ott & Mann, 2000,Falkovich et al., 2001] that in a turbulent flow and for separations inside the inertial range, i.e. $\eta \ll r_0 \ll L$, the correlation between velocity and acceleration differences relates exactly to the average energy dissipation rate, namely

$$\langle \delta_{r_0}\mathbf{u} \cdot \delta_{r_0}\mathbf{a} \rangle \simeq -2\varepsilon. \tag{4.16}$$

This relation, which is exact and does not rely on K41 theory, can be seen as a Lagrangian version of the celebrated 4/5 law (see Chap. 2). It implies that for initial separations r_0 within the inertial range, the ballistic regime ends at a time of the order of

$$t_0 \simeq \frac{S_2(r_0)}{2\varepsilon}. \tag{4.17}$$

This timescale can be interpreted as the time required to dissipate the typical kinetic energy contained at the scale r_0 with the average rate ε. It is expected to be of the order of the correlation time of the initial velocity difference between tracers.

The definition of this timescale is actually different from that of the turnover time τ_{r_0} associated to the scale r_0. The latter is defined as the ratio between the initial separation r_0 and the typical turbulent velocity at that length scale. Using for instance as a typical velocity at scale r_0 the root-mean-squared value of the increment modulus $|\delta_{r_0}\mathbf{u}|$, one can write

$$\tau_{r_0} = \frac{r_0}{S_2(r_0)^{1/2}}. \tag{4.18}$$

When Kolmogorov 1941 scaling is assumed, the two time scales t_0 and τ_{r_0} have the same dependency on r_0. However, using standard estimates of the Kolmogorov constant C_2, one obtains that the ratio between these two times is of the order of

$$\frac{t_0}{\tau_{r_0}} \approx \frac{1}{2}\left[\frac{11}{3}C_2\right]^{3/2} \approx 11. \tag{4.19}$$

Also, we can note that intermittency corrections to the scaling behavior of $S_2(r_0)$ should in principle decrease this ratio. Indeed, let us assume that

$$S_2(r_0) \propto (\varepsilon\, r_0)^{2/3} \left(\frac{r_0}{L}\right)^{\zeta_2 - 2/3}, \tag{4.20}$$

where ζ_2 is the anomalous scaling exponent of second order. One then has

$$\frac{t_0}{\tau_{r_0}} \propto \left(\frac{r_0}{L}\right)^{(3/2)\zeta_2 - 1}. \tag{4.21}$$

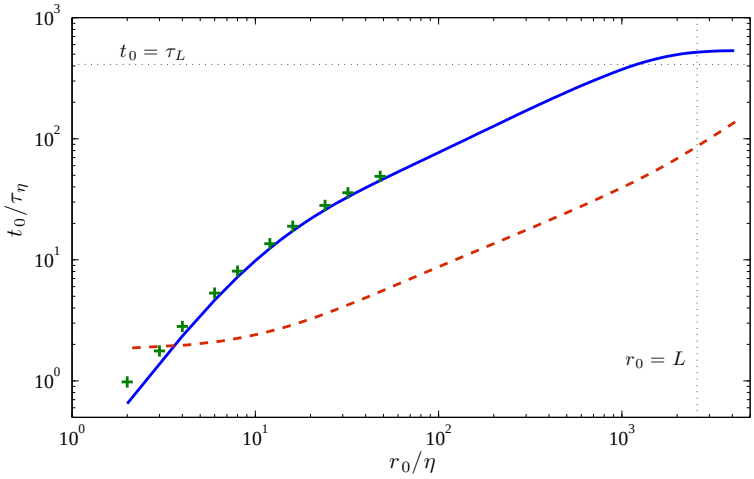

Figure 4.3: "Dissipation time" t_0 as a function of r_0 in dissipative-scale units. Here the blue solid line is obtained by Eulerian averages, while the green cross marks are the actual Lagrangian measurements. The red dashed line shows the turnover time $\tau(r_0) = r_0/[S_2(r_0)]^{1/2}$. Here and in the sequel we have used the Lagrangian data to estimate second-order structure function $S_2(r_0)$ and t_0. The two vertical and horizontal dotted lines show the large scale L and its associated turnover time τ_L (obtained from K41).

We know from experimental and numerical measurements in turbulent flows (see, e.g., Fig. 4.1), that $\zeta_2 \approx 0.7 > 2/3$. This implies that the ratio between the "dissipation time" t_0 and the turnover time in Eq. (4.21) increases as a function of r_0.

The two timescales are shown in Fig. 4.3 for the simulation with $R_\lambda = 730$ ($N = 4096^3$ grid points). One clearly sees a discrepancy between the two definitions. This difference increases when r_0 increases and decreases at scales of the order of the integral scale L. In the sequel, to measure t_0 as a function of r_0, we have not used its Eulerian estimate but rather a Lagrangian average where the second-order structure function $S_2(r_0)$ is obtained by taking the mean of $\delta\mathbf{u}$ over all pairs that are labeled at a distance r_0.

Turning back to our calculation of the subleading terms in Batchelor's ballistic regimes, we introduce in Eq. (4.14) the time scale t_0. For times t much smaller than t_0, we can then write

$$\left\langle |\boldsymbol{R}(t) - \boldsymbol{R}(0)|^2 \right\rangle_{r_0} = t_0^2\, S_2(r_0) \left[\frac{t}{t_0}\right]^2 \left[1 - \frac{t}{t_0}\right] + \text{h.o.t.}, \tag{4.22}$$

where h.o.t. stands for higher-order terms. Figure (4.4) shows the time evo-

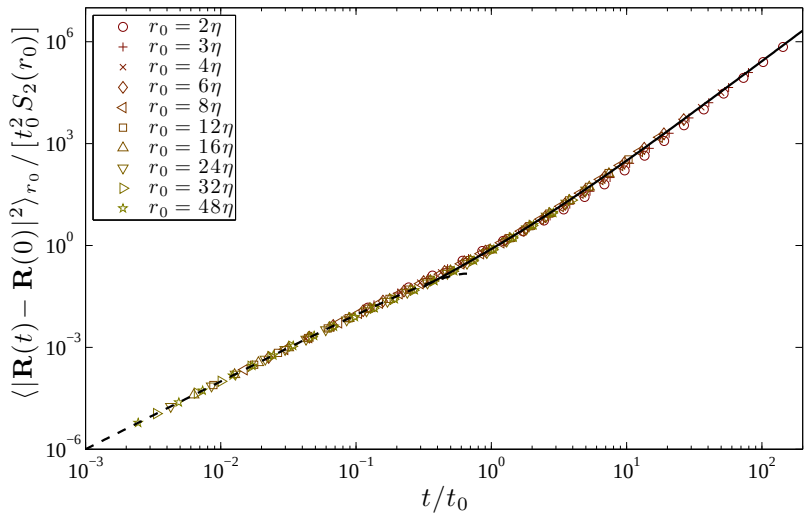

Figure 4.4: Rescaled mean-square separation between two trajectories as a function of time for $R_\lambda = 730$ and different initial separations r_0. The dashed line represents the two leading terms of the ballistic behavior (4.22). The solid line is a fit to the Richardson's regime, Eq. (4.23), with $g = 0.525$ and $C = 2.5$.

lution of the mean-squared displacement for various values of the initial separation r_0. Here and in the sequel the figures are shown for $R_\lambda = 730$, unless specified. It is clearly visible that, once that the time t has been rescaled by t_0 and the squared distances by $t_0^2 S_2(r_0)$, all measurements collapse almost perfectly onto a single curve when r_0 is far enough in the inertial range. Further, data are in rather good agreement with the departure from the ballistic regime predicted by Eq. (4.22).

4.2.3 Convergence to the super-diffusive behavior

It is important to note that the data collapse observed in Fig. 4.4 extends to times larger than t_0 when the mean squared separation tends to Richardson t^3 regime. Such unexpected fact implies that t_0 is not only the timescale of departure from the ballistic regime, but also that of convergence to Richardson's law. In particular, numerical data suggest that the large-time behavior takes the form

$$\left\langle |\boldsymbol{R}(t) - \boldsymbol{R}(0)|^2 \right\rangle_{r_0} = g\,\varepsilon\,t^3 \left[1 + C\,\frac{t_0}{t}\right] + \text{h.o.t.} \tag{4.23}$$

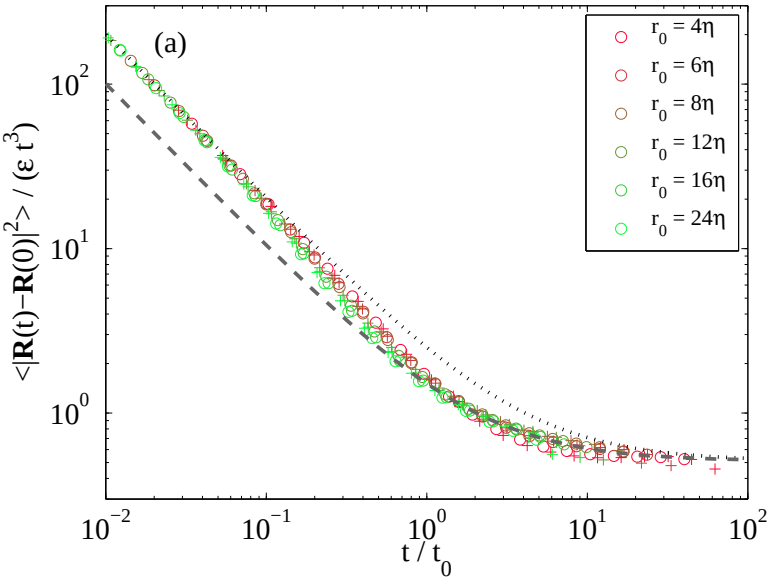

Figure 4.5: Compensated mean-squared displacement $\langle|\boldsymbol{R}(t)-\boldsymbol{R}(0)|^2\rangle/(\varepsilon\, t^3)$ as a function of t/t_0, with $t_0 = S_2(r_0)/(2\varepsilon)$, for various initial separations and $R_\lambda = 730$ ($\circ$) and $R_\lambda = 460$ ($+$). The two curves show behaviors of the form $\langle|\boldsymbol{R}(t)-\boldsymbol{R}(0)|^2\rangle \simeq g\,\varepsilon\, t^3 + A\, t^2$, with $A = S_2(r_0)$, given by Batchelor's ballistic regime (black dotted line), and $A = 2.5\, g\, /t_0^2$ (grey dashed line).

The term C appearing here does not strongly depend on the Reynolds number and actually, for both values of the Reynolds number, we obtain the same results, up to statistical errors. This is evidenced in Fig. 4.5, which shows the compensated mean squared increase of the distance $\langle|\boldsymbol{R}(t) - \boldsymbol{R}(0)|^2\rangle/(\varepsilon\, t^3)$ for the two investigated values of the Reynolds number. In this figure, the time has been again rescaled by $t_0 = S_2(r_0)/(2\varepsilon)$. Data confirm that the subdominant terms in Richardson explosive regime are $\propto t^2$, as postulated in Eq. (4.23). One also observes that the constant C is independent of r_0 when $r_0 \gg \eta$. The subleading terms, appearing at large times from the compensated plot in Fig. 4.5, are clearly different from those coming from a subleading ballistic regime. We indeed see on the figure that the two black lines do not coincide. The dotted line, which corresponds to Batchelor's regime, gives a good approximation to the data up to a few hundredth of t_0. On the contrary, the dashed line corresponds to the proposed formula of Eq. (4.23) with $C \approx 2.5$ and is valid only for $t \gg t_0$.

Systematic measurements of the constant C as a function of the initial separations have been performed and are shown in Fig. 4.6. This was done

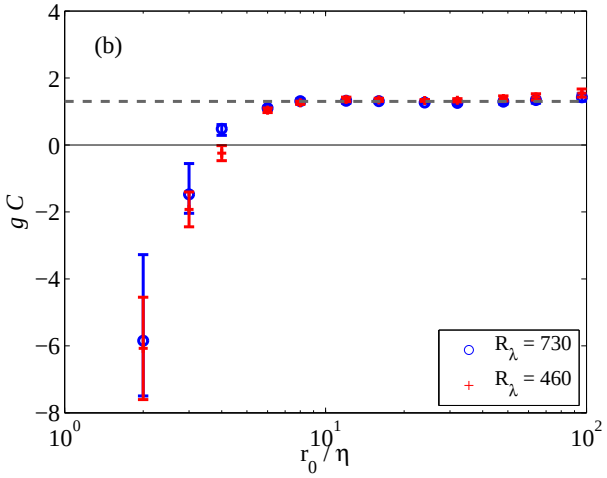

Figure 4.6: Measured value of the constant gC in front of the subleading term as a function of the initial separation. It stabilizes to $C \approx 1.3/g \approx 2.5$ for $r_0 \gg \eta$; this value is represented as a dashed line.

by estimating numerically the product of the constants g and C in the compensated mean-squared displacement. We find that C is negative when r_0 is of the order of the Kolmogorov scale η. In this case, the convergence to the Richardson law occurs from below and it is thus contaminated by tracer pairs that spend long times close together before sampling the inertial range. This is also consistent with the recent findings of [Scatamacchia et al., 2012].

The convergence to Richardson's law from below for such values of r_0 leads to an intermediate time range where the mean squared distance grows even faster than the explosive t^3 law, as for instance observed in [Biferale et al., 2005]. When r_0 is instead far-enough in the inertial range ($r_0 \gtrsim 8\eta$), we find that $C \approx 1.3/g \approx 2.5$ becomes independent on the initial separation and, on the contrary, the convergence to Richardson law is from above. Moreover, when the initial separation r_0 approximates the value of 4η we have that $C = 0$, independently of the Reynolds number. The only subleading terms present in Eq. (4.23) are then of lower order (i.e. $\propto t$ instead of t^2). As a consequence, the mean-squared separation converges much faster to the Richardson regime for such an initial separation than for others. This observation indicates that the initial separation $r_0 \approx 4\eta$ could be an "optimal choice" for choosing setups in order to observe the t^3 behavior in experiments. However, such small values of r_0 are clearly not representative of the inertial-range behavior. We can note in Fig. 4.6 that the overlap between the constants C obtained from the two values of Reynolds number is not observed for $r_0 = 4\eta$. As in that

case C is very small, this is certainly due to the fact that the fitting form used there ceases to give a good representation of the data. A better estimate of C would require accounting for next-order subleading terms.

4.3 Statistics of velocity differences

4.3.1 A diffusive behavior?

In this section, we are interested in the behavior of the velocity difference $\boldsymbol{V}(t) = \mathbf{u}(\mathbf{X}_1(t), t) - \mathbf{u}(\mathbf{X}_2(t), t)$ between two tracers as a function of time. Richardson's t^3 law for separations implies that the mean-squared velocity differences should behave at large times as

$$\langle |\boldsymbol{V}(t)|^2 \rangle_{r_0} \simeq h\,\epsilon\,t, \tag{4.24}$$

where h is a positive constant that cannot be straightforwardly expressed as a function of the Richardson constant g that appears in Eq. (4.10). As we have seen in Chap. 3, a behavior $\propto t$ of a mean-square quantity is a key feature of purely diffusive stochastic processes. In the rest of this chapter, we give some evidence that the large-time velocity difference between two tracers can indeed be understood as a diffusion. Before presenting our arguments for that, we report the results of numerical simulations on this quantity.

Initially, the statistics of $\boldsymbol{V}(0)$ are exactly given by the Eulerian statistics of velocity increments at a separation r_0. We have used such an argument to derive the ballistic regime behavior of Eq. (4.14). At large times, the behavior is expected to be given by Eq. (4.24). A naive picture would consist in interpolating between these two behaviors by assuming that

$$\langle |\boldsymbol{V}(t)|^2 \rangle_{r_0} \simeq S_2(r_0) + h\,\epsilon\,t. \tag{4.25}$$

Assuming such a form, it can be expected that one of the two regimes is dominant when t is much smaller or much longer than $t_0 = S_2(r_0)/(2\,\epsilon)$. As seen from Fig. 4.7 such a form with $h = 2.4$ (represented as a dashed line) seems to be a good first-order approximation. However, this picture is not completely satisfactory. When zooming closer to the initial times (see inset), one observes that the averaged pair kinetic energy $\langle |\boldsymbol{V}(t)|^2 \rangle_{r_0}$ first starts by decreasing for a time of the order of a few tens of t_0. We indeed know that initially

$$\boldsymbol{V}(t) = \boldsymbol{V}(0) + t\boldsymbol{A}(0) + \mathcal{O}(t^2), \tag{4.26}$$

where $\boldsymbol{A}(0) = (\partial_t \mathbf{u} + \mathbf{u}\cdot\nabla\mathbf{u})(\mathbf{X}_1(0), 0) - (\partial_t \mathbf{u} + \mathbf{u}\cdot\nabla\mathbf{u})(\mathbf{X}_2(0), 0)$ denotes the initial difference of fluid acceleration between the two tracer positions. This

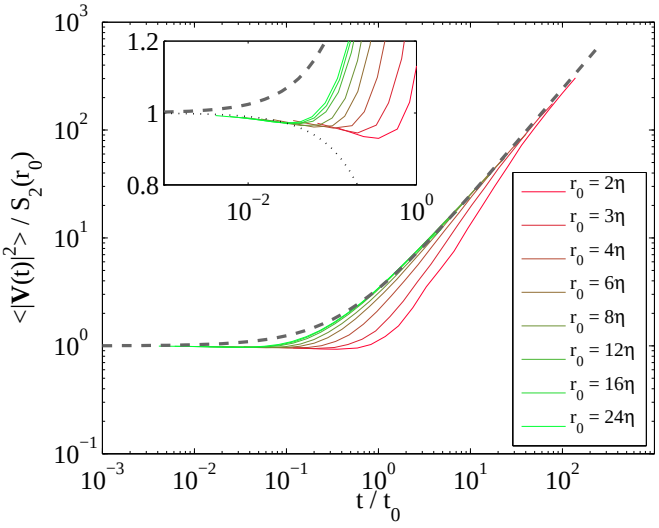

Figure 4.7: Time behavior of the mean-squared velocity difference $\langle |\boldsymbol{V}(t)|^2 \rangle_{r_0}$ for $R_\lambda = 730$. It is here normalized by its initial value and represented as a function of the rescaled time t/t_0. The gray dashed line is the behavior given by Eq. (4.24) of the form $\langle |\boldsymbol{V}(t)|^2 \rangle_{r_0} \simeq S_2(r_0) + h\,\varepsilon\,t$ with $h = 2.4$. Inset: same but zoomed at short times; the black dotted line is the initial decrease associated to kinetic energy dissipation: $\langle |\boldsymbol{V}(t)|^2 \rangle_{r_0} \simeq S_2(r_0) - 4\,\varepsilon\,t$.

approximation leads to

$$\langle |\boldsymbol{V}(t)|^2 \rangle_{r_0} \simeq S_2(r_0) - 4\,\epsilon\,t. \tag{4.27}$$

According to our numerical data, this regime seems to reproduce well what is happening for times up to $\approx 0.01\,t_0$ — see inset of Fig. 4.7. The fact that this prediction ceases to describe the data after such a short timescale (that is significantly smaller than t_0 instead of being of its order) indicates that the subleading terms in Eq. (4.26) become important. As a consequence, depending on the quantity we are interested in, Batchelor's ballistic regime might end very quickly.

After this subtle initial decrease, the averaged squared velocity difference amplitude tends asymptotically to a behavior $\propto t$. However this process occurs in a noticeably different manner to that of convergence of squared separation to Richardson t^3 law: irrespective of the initial separation r_0, the quantity $\langle |\boldsymbol{V}(t)|^2 \rangle_{r_0}$ always approaches from below the asymptotic behavior. In other terms, we observe that for a fixed value of t/t_0, the pair kinetic energy $\langle |\boldsymbol{V}(t)|^2 \rangle_{r_0}$ is an increasing function of r_0/η and seems to converge to the behavior given in Eq. (4.24) only in the limit $r_0/\eta \to \infty$.

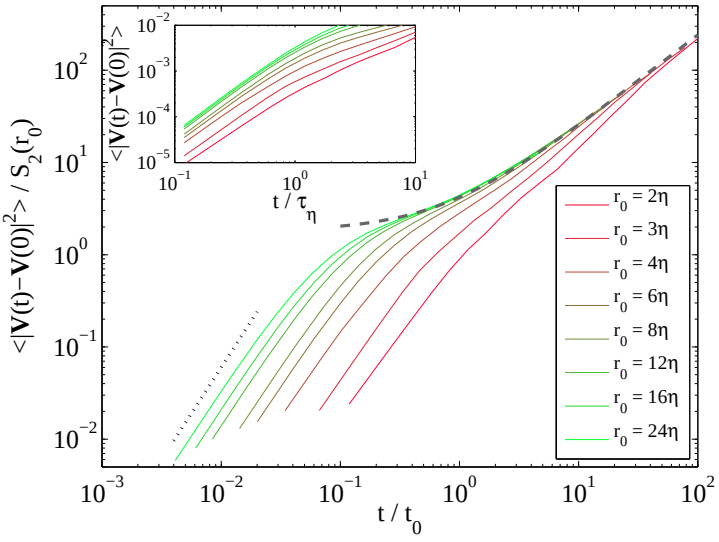

Figure 4.8: Time behavior of the velocity change $\langle|\boldsymbol{V}(t) - \boldsymbol{V}(0)|^2\rangle_{r_0}$; the dashed curve is $\langle|\boldsymbol{V}(t) - \boldsymbol{V}(0)|^2\rangle_{r_0} \simeq S_2(r_0) + h\,\epsilon\,t$; the dotted line has slope 2 and corresponds to the initial abrupt variation of the velocity difference. Inset: same but rescaling time by τ_η.

At large times, the mean-squared velocity difference grows linearly. This behavior suggest that velocity differences have a diffusive behavior for $t \gg \tau_\eta$. We will come back later on arguments supporting this observation. If this was exact, it would lead to the behavior in Eq. (4.25) as the temporal increments of $\boldsymbol{V}$ would be independent of its initial value. Also, a purely diffusive behavior of $\boldsymbol{V}$ would result in the fact that its mean-squared temporal increment $\langle|\boldsymbol{V}(t)-\boldsymbol{V}(0)|^2\rangle_{r_0}$ is $\propto t$ for all times $t \gg \tau_\eta$. As seen in Fig. 4.8, this is clearly not the case. Actually, data show that $\boldsymbol{V}(t)$ initially changes on times of the order of τ_η by a factor of the order of its typical initial value $[S_2(r_0)]^{1/2}$. This abrupt evolution can be interpreted phenomenologically. With some finite probability, one of the two tracers is within a vortex filament at time t_0. The typical energy content of this filament will contribute to the value of $S_2(r_0)$. However, after a time t of the order of τ_η, the trajectory of this tracer will have turned around this filament, so that its velocity will have completely changed orientation (without changing much its amplitude). This will result in $|\boldsymbol{V}(t)-\boldsymbol{V}(0)| \sim |\boldsymbol{V}(t)|$, explaining the observed behavior. As a result of this sudden kinematic variations of velocity differences, $\langle|\boldsymbol{V}(t)-\boldsymbol{V}(0)|^2\rangle_{r_0}$ behaves in a very similar manner to $\langle|\boldsymbol{V}(t)|^2\rangle_{r_0}$ for times $t \gg \tau_\eta$ (compare the dashed lines in Fig. 4.7 and Fig. 4.8). Let us also notice that the convergence to this behavior is again from below, irrespective of the initial separation r_0.

There is hence an abrupt change (occurring on timescales of the order of τ_η) that prevent from determining an effective initial velocity difference and thus from observing a clear diffusive behavior of $\boldsymbol{V}(t)$. However, data suggest that the timescale of convergence to this behavior is, as for separations, of the order of t_0. To understand further this question, we next turn to investigating the behavior of the longitudinal velocity difference between the tracers.

4.3.2 Geometry of longitudinal velocities

We are here interested in the evolution of the longitudinal component $V^{\parallel}(t) = \boldsymbol{R}(t)\cdot\boldsymbol{V}(t)/|\boldsymbol{R}(t)|$ of the velocity difference as a function of time. This quantity is important to characterize pair separation as $\mathrm{d}|\boldsymbol{R}|/\mathrm{d}t = V^{\parallel}$. Initially, the averaged longitudinal velocity vanishes, i.e. $\langle V^{\parallel}(0)\rangle_{r_0} = 0$; this is due to the statistical stationarity of the fluid flow. For times $t \ll t_0$ in the Batchelor's ballistic regime, the pairs are keeping their initial velocity difference and one can easily check that

$$\langle V^{\parallel}(t)\rangle_{r_0} \simeq t\,\frac{\langle|\boldsymbol{V}^{\perp}(0)|^2\rangle_{r_0}}{r_0}, \tag{4.28}$$

where $\boldsymbol{V}^{\perp}$ denotes the components of $\boldsymbol{V}$ that are transverse to $\boldsymbol{R}$. It is thus clear that the average velocity at which tracer trajectories separate immediately becomes positive. Figure 4.9, which represents the time evolution of $\langle V^{\parallel}(t)\rangle_{r_0}$, shows without doubt this initial linear growth.

This increase of the longitudinal velocity difference has an interesting geometrical interpretation. If all pairs were to maintain indefinitely their initial velocity differences $\boldsymbol{V}(0)$, it is clear that they would eventually all separate at large times. Indeed, they will reach a minimal distance at a finite time

$$t_* = -\frac{[\boldsymbol{R}(0)\cdot\boldsymbol{V}(0)]}{|\boldsymbol{V}(0)|^2} = -\frac{r_0 V^{\parallel}(0)}{|\boldsymbol{V}(0)|^2}, \tag{4.29}$$

which is positive for particles that are initially approaching. After such time t_*, the distance between particles increases and $V^{\parallel}$ becomes positive. This leads to an increase of $\langle V^{\parallel}\rangle_{r_0}$ that comes from kinematic considerations and is obviously not due to any dynamics imposed by the turbulent flow. To estimate the typical value of the minimal distance at time t_*, we have performed statistics on pair separation conditioned not only on the initial distance r_0, but also on the initial longitudinal velocity difference by binning pairs with $V^{\parallel}(0) = v_0 \pm \delta v_0$. From these statistics we have defined the averaged time $t_* = -r_0 v_0/\langle|\boldsymbol{V}(0)|^2\,|\,v_0\rangle_{r_0}$ at which trajectories, with a given initial longitudinal velocity difference v_0, are at a minimal distance. The data are shown in

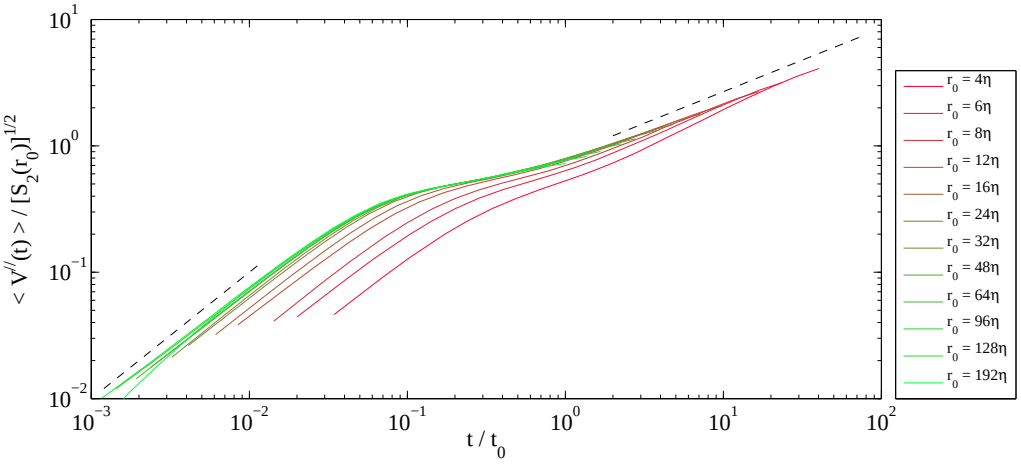

Figure 4.9: Time evolution of the averaged longitudinal velocity difference $\langle V^{\parallel}(t)\rangle_{r_0}$ for various initial separations, as labeled, and for $R_\lambda = 730$. The dashed line to the left has slope 1 and the dashed line to the right has a slope 1/2.

Fig. 4.10 for various values of r_0 and as a function of v_0. We observe that for $r_0 \gg \eta$ this time approximatively takes the form $t_* \simeq t_0\, f(v_0/\langle|\boldsymbol{V}(0)|^2\rangle_{r_0}^{1/2})$, where the function $f(x)$ attains its maximum (roughly equal to 0.05) at $x \approx 1$. This confirms the observation made in Fig. 4.9 that the initial growth of $\langle V^{\parallel}\rangle_{r_0}$ occurs on a time length of the order of a few hundredths of t_0.

In addition to the change in the mean longitudinal velocity difference discussed above, numerical measurements show that the full distribution of $V^{\parallel}$ loses its symmetry and develops fatter tails when time increases. Figures 4.11 and 4.12 represent the skewness $\mathcal{S}$ and the flatness $\mathcal{F}$ of $V^{\parallel}$ as a function of time and for the same initial separations as in Fig. 4.9. These observables are frequently used in turbulence to quantify the shape of the velocity increment distribution. For two-particle Lagrangian statistics, they are defined as

$$\mathcal{S}(t) = \frac{\left\langle [V^{\parallel}(t) - \langle V^{\parallel}(t)\rangle_{r0}]^3 \right\rangle_{r_0}}{\langle [V^{\parallel}(t) - \langle V^{\parallel}(t)\rangle_{r0}]^2\rangle_{r_0}^{3/2}} \quad \text{and} \quad \mathcal{F}(t) = \frac{\left\langle [V^{\parallel}(t) - \langle V^{\parallel}(t)\rangle_{r0}]^4 \right\rangle_{r_0}}{\langle [V^{\parallel}(t) - \langle V^{\parallel}(t)\rangle_{r0}]^2\rangle_{r_0}^{2}}. \tag{4.30}$$

As already observed for instance in [Yeung & Borgas, 2004], these quantities strongly vary as a function of time and maintain a marked dependence upon the initial separation r_0 for rather long times.

Figure 4.11 shows that the skewness of $V^{\parallel}(t)$ starts from negative values (to be in agreement with the Eulerian 4/5 law) and becomes positive at times larger than $\approx 0.01\, t_0$. This initial change of sign can also be interpreted

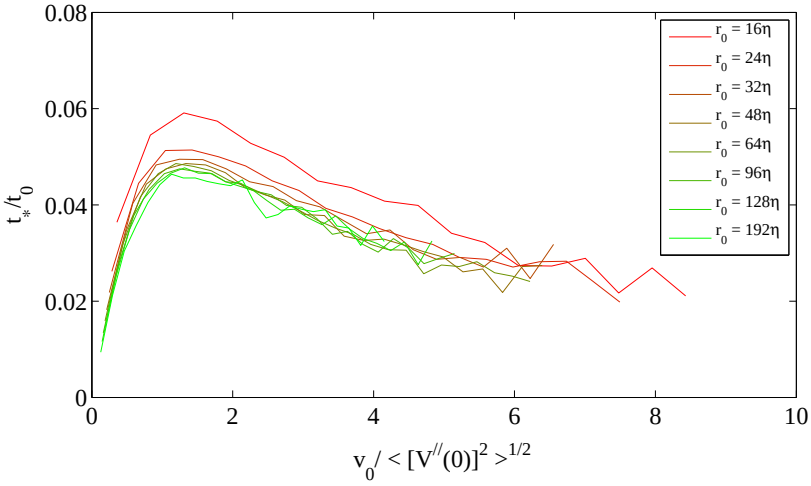

Figure 4.10: Averaged time $t_* = -r_0 v_0 / \langle |\boldsymbol{V}(0)|^2 \,|\, V^{\parallel}(0) = v_0 \rangle_{r_0}$ when trajectories with a given initial longitudinal velocity difference v_0 reach a minimal distance.

geometrically in terms of the time t_* when initially ballistically approaching pairs begin to move away. However, after this, the curves separate and each of them attains a maximum at times of the order of t_0 or slightly smaller.

This maximal value of the skewness strongly depends on the initial separation: less is r_0, higher it is. After this maximum, the skewness decreases without attaining an asymptotic regime that would be independent of r_0. This could be either due to the fact that there is a persistent memory of r_0 in such quantities or to a contamination by finite Reynolds number (and finite size) effects. The same kind of behavior is observed for the flatness $\mathcal{F}$ of the distribution of $V^{\parallel}$ as seen in Fig. 4.12. However, the increase of its maximal value when decreasing r_0 is even more pronounced. Another noticeable difference is that the initial value of $\mathcal{F}$ itself depends on r_0 and relates to the scale dependence of the Eulerian flatness.

The strong dependence on r_0 of the skewness and of the flatness can be interpreted phenomenologically in terms of the intermittent nature of velocity increments. A large positive value of $\mathcal{S}$ corresponds to a large probability of having pairs separating faster than the average. Such events will also be responsible for a large value of the flatness $\mathcal{F}$. It is clear that those particles that separate the faster are typically those which are the most separated. Also, in a turbulent flow, the typical value of the velocity increases with scale, so that the particles which get quickly separated are likely to continue separating faster than the average. This is evidenced in Fig. 4.13 and

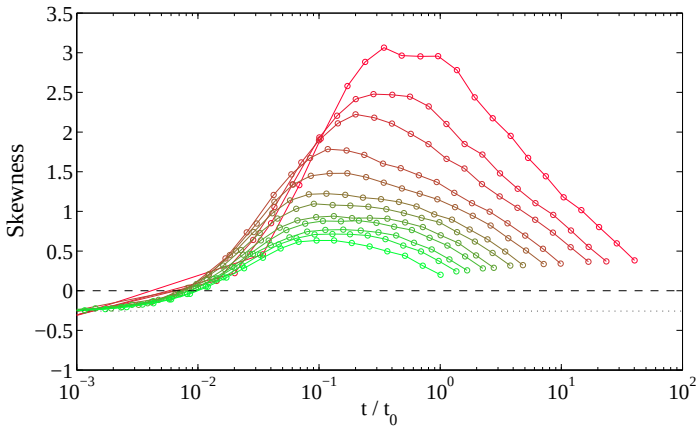

Figure 4.11: Time evolution of the skewness $\mathcal{S}(t)$ for the same initial separations r_0 as in Fig. 4.9. The dashed line is the value corresponding to a Gaussian distribution, $\mathcal{S} = 0$, and the dotted line is the initial value of the skewness obtained when assuming Kolmogorov 1941 scaling, namely $\mathcal{S} = (4/5)/C_2^{3/2}$.

4.14, which represent the mean squared distance and the averaged squared amplitude of the velocity difference conditioned on the initial value of the longitudinal velocity difference for $r_0 = 24\eta$. One observes that there is up to the latest time (of the order of $5\,t_0$), a noticeable memory on the initial value of $V^{\parallel}$. Besides this consideration, one also remarks in Fig. 4.14 that the pairs having an initially large negative longitudinal velocity difference (the blue curves) dissipate much more kinetic energy than the others. However, this does not prevent them from separating at large times faster than the pairs having initially a smaller velocity difference.

We now turn back to the explanation of the long-term dependence on r_0 of the skewness and flatness of $V^{\parallel}$. Recall that, in a turbulent flow, violent velocity differences are more probable at small scales than at larger scales. This implies that pairs with a small initial separation are more likely to experience a large (positive or negative) initial velocity difference. This will make them separate faster and thus experience even larger values of the velocity. The rapid and strong increase of fluctuations in their velocity differences is thus due to a kind of snowball effect.

4.4 "Local dissipation" and velocity diffusion

We focus in this section on providing arguments that evidence a purely diffusive behavior of velocity differences at large times. These arguments are based on two key ingredients. First, as we will see in Subsec. 4.4.1, the cube

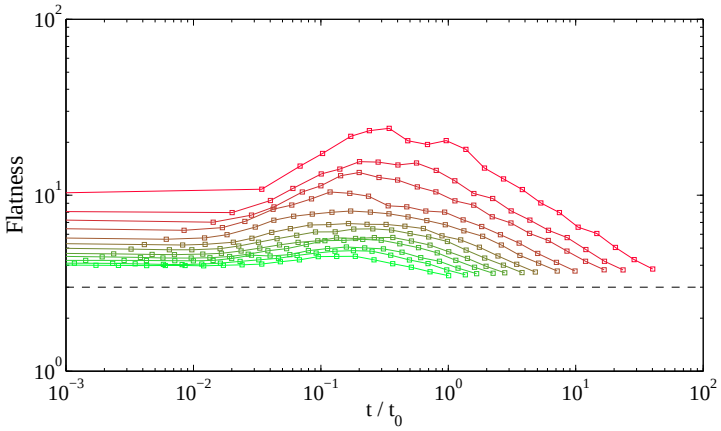

Figure 4.12: Time evolution of the flatness $\mathcal{F}(t)$ defined in Eq. (4.30) for the same initial separations r_0 as in Fig. 4.9. The dashed line is the value corresponding to a Gaussian distribution, namely $\mathcal{F} = 3$.

velocity difference rescaled by the distance between tracers, which defines a "local energy dissipation" along tracer pairs, attains on short timescales a statistically stationary regime. Second, as described in Subsec. 4.4.2, acceleration differences between tracers get uncorrelated over very-short times and data show that their variance can be related to the aforementioned "local energy dissipation". Finally, these considerations can be used to apply the central-limit theorem in order to write down in Subsec. 4.4.3 a stochastic model for the joint time evolution of separations and velocity differences.

4.4.1 Stationarity of rescaled velocity differences

We have seen in the previous sections that the velocity difference between two tracers plays a crucial role in understanding the mechanisms leading to Richardson's superdiffusive regime for separations. However, the convergence of $\langle |\boldsymbol{V}(t)|^2 \rangle_{r_0}$ to a behavior $\propto t$ is not that evident in numerical data. In addition, as we will see in the next chapter, the statistics of $\boldsymbol{V}(t)$ display very intermittent features and, as a consequence, does not converge to a behavior with temporal self-similarity, or does it only very slowly. The situation is very different when interested in mixed statistics between distances and longitudinal velocity differences. As reported in [Bitane et al., 2012b], the moment $\langle [V^{\parallel}(t)]^3 / |\boldsymbol{R}(t)| \rangle_{r_0}$, which is initially negative and equal to $-(4/5)\epsilon$, tends very quickly to a positive constant (see Fig. 4.15).

The decrease at very large times comes from the contamination of the statistics by pairs that have reached a distance of the order of the integral scale. The asymptotic value $\approx 6.2\,\epsilon$ seems to depend only weakly on the

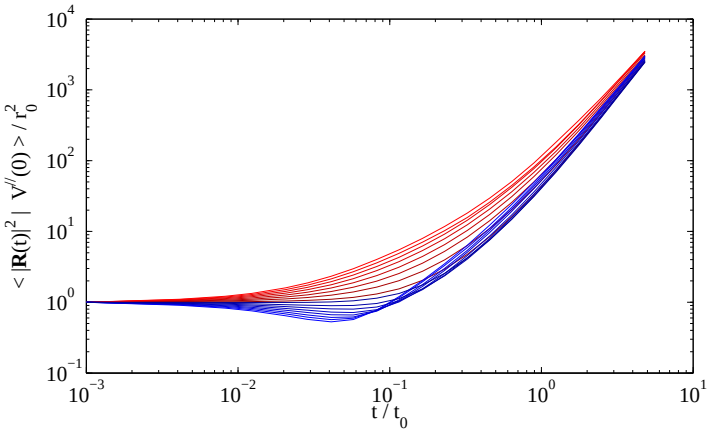

Figure 4.13: Time evolution for $r_0 = 24\eta$ of the averaged distance conditioned on $V^{\parallel}(0) = v_0$ with $|v_0|/\langle [V^{\parallel}(0)]^2 \rangle_{r_0}^{1/2} = 0.1, 0.4, 0.8, 1.2, ..., 2.8$. The red curves correspond to positive values of v_0 and the blue ones to negative values.

Reynolds number. The collapse of the curves associated to different Reynolds numbers and, for $r_0 \gg \eta$, to various initial separations indicate that the time of convergence is $\propto t_0$. Figure 4.16 shows the same moment but conditioned on the sign of the initial longitudinal velocity difference. One observes that for initially separating pairs (red curve), the convergence to the asymptotic value is on a time of the order of τ_η. Conversely for tracers that initially approach each other (blue curve), the convergence is less fast. We have seen in Sec. 4.3.2 that such pairs first attain their minimal distance at $t \approx t_* \approx 0.01\, t_0$. Then, at that time, $\langle [V^{\parallel}(t)]^3/|\boldsymbol{R}(t)| \,|\, V^{\parallel}(0) < 0 \rangle_{r_0}$ changes sign and the convergence to $\approx 6.2\epsilon$ occurs only later. Such initially approaching pairs are leading the average so that the overall convergence is on timescales of the order of t_*. The mixed moment $\langle [V^{\parallel}]^3/|\boldsymbol{R}| \rangle_{r_0}$, which is a kind of "local dissipation" along pairs of trajectories, is thus conserved by the Lagrangian flow.

Actually, it is not only the average of the "local dissipation" that converges to a constant but its full distribution seems to attain a stationary regime on times of the order of t_*. Figure 4.17 (a) shows for a given initial separation, the convergence at large times of the PDF of $[V^{\parallel}(t)]^3/|\boldsymbol{R}(t)|$. One observes that the right and left tails converge on different timescales. The tail associated to large positive values (separating pairs) occurs on timescales of the order of τ_η (which is in this case $\approx 0.07\, t_0$), while that for negative values (approaching pairs) converges slower. For the largest time ($t \approx 5\, t_0$) one observes that deviations to the asymptotic distribution occur again at

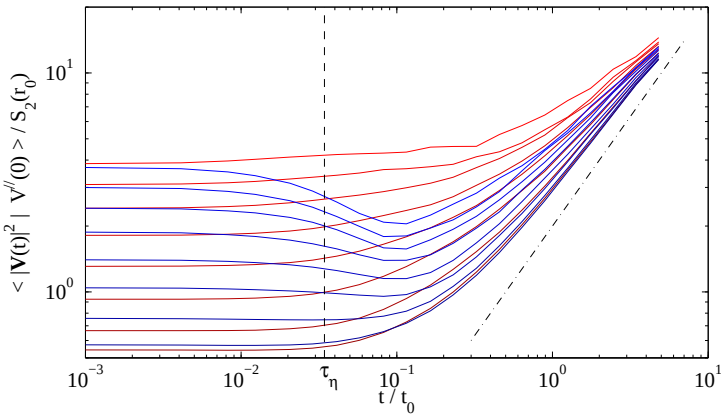

Figure 4.14: Time evolution for $r_0 = 24\eta$ of the averaged squared velocity difference conditioned on $V^{\parallel}(0) = v_0$ with $|v_0|/\langle [V^{\parallel}(0)]^2 \rangle_{r_0}^{1/2} = 0.1, 0.4, 0.8, 1.2, ..., 2.8$. The red curves correspond to positive values of v_0 and the blue ones to negative values. The dashed-dotted line is $\propto t$.

very large positive values. This is due to a contamination of such events by the large scales of the turbulent flow. This decrease is in agreement with the observed departure in Figs. 4.15 and 4.16 of the average from its asymptotic value at large times. Figure 4.17 (b) shows the PDFs of $[V^{\parallel}]^3/|\boldsymbol{R}|$ for different initial separations and at a fixed time sufficiently large to be ensured that all distributions have attained their asymptotic regime. One observes a robust collapse, much more pronounced than for both the distribution of separations and that of velocity differences. Note that in Fig. 4.17 the distributions are raw and were not rescaled by any moment of $[V^{\parallel}]^3/|\boldsymbol{R}|$. The asymptotic PDF is peaked around zero (rather than its mean value) and displays fat tails that, according to our data, are $\propto \exp(-C\,|V^{\parallel}|/|\boldsymbol{R}|^{1/3})$ on both sides.

To our knowledge, such a fast and manifest convergence of these mixed statistics has never been reported before. From a phenomenological viewpoint, one expects $[V^{\parallel}]^2 \propto t \propto |\boldsymbol{R}|^{1/3}$ in the explosive Richardson–Obukhov regime, so that the "local dissipation" $[V^{\parallel}]^3/|\boldsymbol{R}|$ should become constant at sufficiently large times. However we have observed here that the convergence of this quantity to its asymptotic value occurs much faster and in a much more definite manner than the convergence of the statistics of $|\boldsymbol{R}|$ and $|\boldsymbol{V}|$ to their respective asymptotic forms. This indicates that the statistical stationarity of the "local dissipation" is more likely to be a cause rather than a consequence of Richardson–Obukhov explosive separation. At the moment we unfortunately lack a clear understanding of the physical mechanisms that

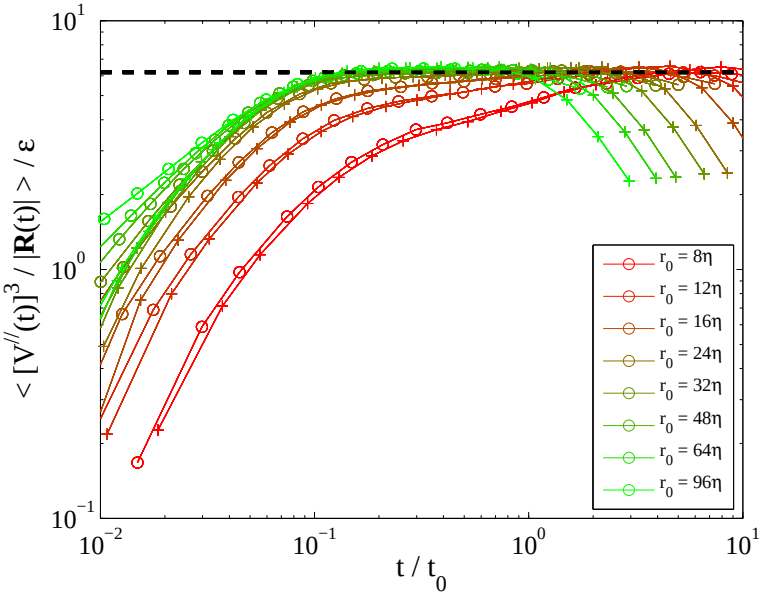

Figure 4.15: Time evolution of the mixed moment $\langle [V^{\parallel}(t)]^3/|\boldsymbol{R}(t)|\rangle_{r_0}$ for different initial separations and the two values of the Reynolds number: $R_\lambda = 730$ ($\circ$) and $R_\lambda = 460$ ($+$). The black dashed line shows the asymptotic value $\langle [V^{\parallel}(t)]^3/|\boldsymbol{R}(t)|\rangle_{r_0} \approx 6.2\,\epsilon$.

are responsible for the observed behavior of $[V^{\parallel}]^3/|\boldsymbol{R}|$ and that could shed light on its relation to explosive separation. We however present in next section its relationship to the statistics of acceleration differences between tracers.

4.4.2 Statistics of acceleration differences

We continue here our study of the timescales entering the relative dispersion process. As already stated in Subsec. 4.1.1, the velocity difference $\boldsymbol{V}$ between the two tracers stays correlated over a time of the order of the turnover time τ_r associated to the distance r between them. This time increases too fast when the separation $|\boldsymbol{R}(t)|$ increases. This result makes Richardson's diffusive approach hardly justifiable. However, it is known in turbulent flows that the acceleration, which is a small-scale quantity, is conversely correlated over times that are of the order of the Kolmogorov turnover time τ_η [Mordant et al., 2004]. Its amplitude is rather correlated on times of the order of the forcing correlation time, but this does not alter what argued so far.

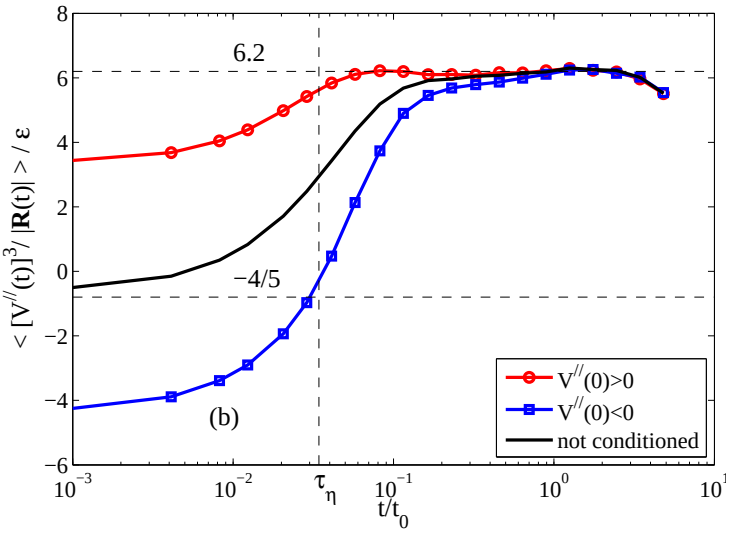

Figure 4.16: Time evolution of the mixed moment $\langle [V^{\parallel}(t)]^3/|\boldsymbol{R}(t)|\rangle_{r_0}$ for $r_0 = 24\,\eta$ and $R_\lambda = 730$ (black curve) and for the same moment but conditioned on positive (red curve) and negative (blue curve) values of the initial longitudinal velocity difference $V^{\parallel}(0)$.

We have measured the acceleration difference

$$\boldsymbol{A}(t) = (\partial_t \mathbf{u} + \mathbf{u}\cdot\nabla\mathbf{u})(\mathbf{X}_1(t),t) - (\partial_t \mathbf{u} + \mathbf{u}\cdot\nabla\mathbf{u})(\mathbf{X}_2(t),t) \tag{4.31}$$

between two tracers. Its Lagrangian autocorrelation function is represented in Fig. 4.18. We clearly see that this quantity get uncorrelated on times of the order of τ_η. This suggests that for separations in the inertial range and on timescales much longer than the Kolmogorov eddy turnover time, the difference of acceleration between two tracers can be approximated by a *delta-correlated-in-time* random process, so that

$$\boldsymbol{A} \simeq \sqrt{\tau_\eta^{\rm loc}}\,\mathbb{A}(\boldsymbol{R},\boldsymbol{V})\,\boldsymbol{\eta}(t), \tag{4.32}$$

where $\boldsymbol{\eta}(t)$ is the three-dimensional standard white noise. The matrix $\mathbb{A}$ is defined as

$$\mathbb{A}^{\mathsf{T}}\mathbb{A} = \langle \boldsymbol{A}(t)\otimes\boldsymbol{A}(t)\,|\,\boldsymbol{R},\boldsymbol{V}\rangle_{r_0}\,. \tag{4.33}$$

Here we have made use of the central-limit theorem to write Eq. (4.32). This implies that the product is there understood in the Stratonovich sense.

Dimensional arguments indicate that, as they are small-scale quantities, the "local Kolmogorov time" $\tau_\eta^{\rm loc}$ and the acceleration amplitude $A = |\boldsymbol{A}|$ depend only on the viscosity ν and on the local energy dissipation rate $\varepsilon_{\rm loc}$.

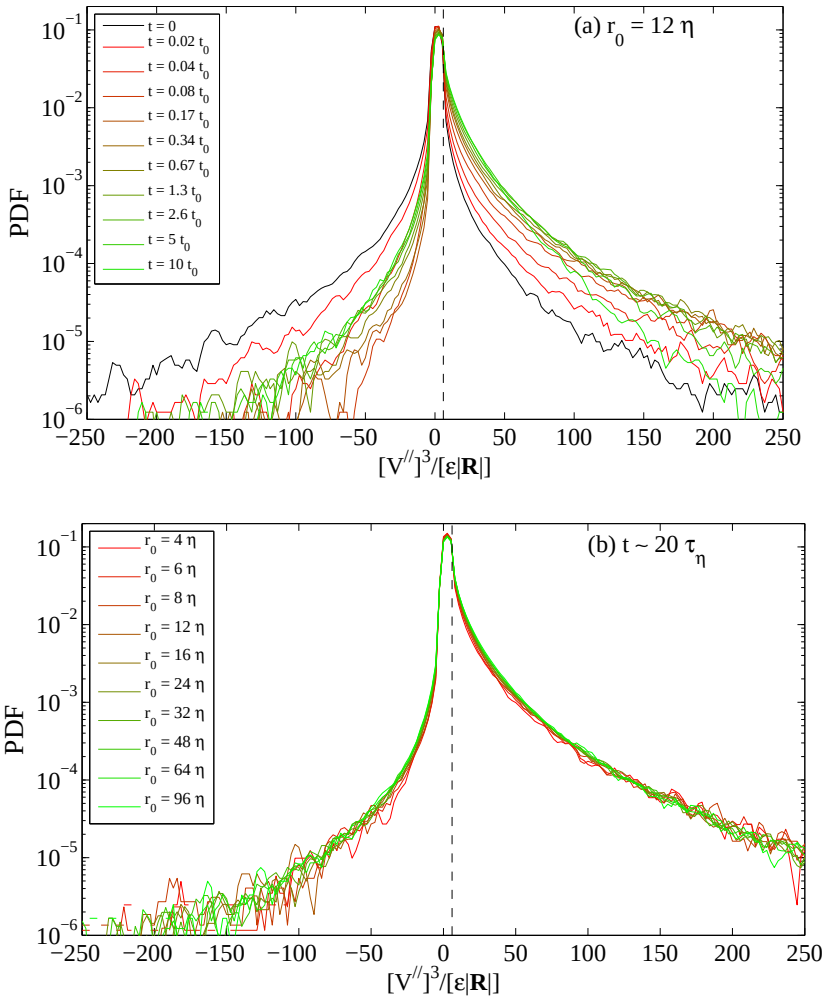

Figure 4.17: (a) PDF of the "local dissipation" $[V^{\parallel}(t)]^3/|\boldsymbol{R}(t)|$ for $r_0 = 24\,\eta$ and various times (as labeled). (b) Same for various initial separations and a time $t = 20\,\tau_\eta$ fixed. t/t_0 goes here from 0.2 to 5 so that, in all cases, the mixed quantity $[V^{\parallel}]^3/|\boldsymbol{R}|$ has reached its asymptotic regime. In both figures the vertical dashed lines show the position of the average value $\approx 6.2\epsilon$.

This rate is not only related to energy dissipation but also to energy injection from the larger structures of the flow. Approaches in terms of $\varepsilon_{\rm loc}$ are frequently used since the seminal work of Kolmogorov on refined self-similarity [Kolmogorov, 1962]. It was useful to build multifractal models based on energy dissipation (see, e.g., [Frisch, 1996] and references therein) or served for instance in the study of the statistics of acceleration conditioned on the velocity [Biferale et al., 2004]. With such an approach, the

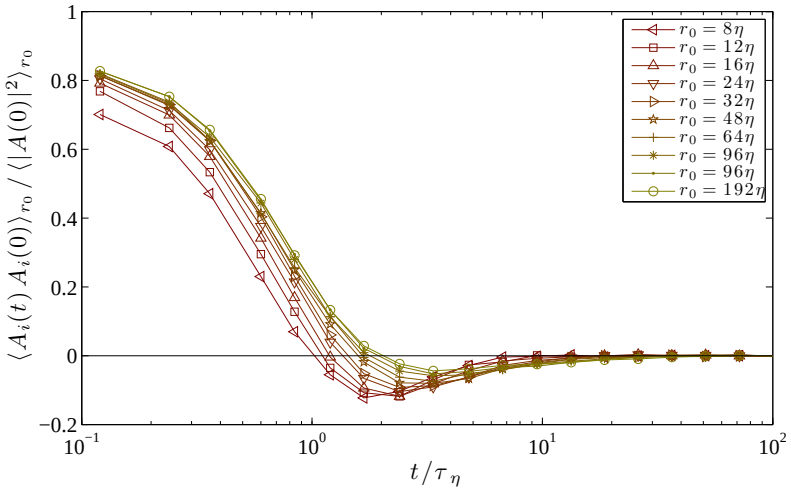

Figure 4.18: Lagrangian time autocorrelation of the acceleration difference $\langle A_i(t)A_i(0)\rangle_{r_0}$ for various r_0 and $R_\lambda = 730$.

local Kolmogorov time and the acceleration amplitude can be written as

$$\tau_\eta^{\rm loc} \sim \nu^{1/2}\,\varepsilon_{\rm loc}^{-1/2} \quad \text{and} \quad A \sim \nu^{-1/4}\,\varepsilon_{\rm loc}^{3/4}. \tag{4.34}$$

This leads to write the diffusion coefficient in Eq. (4.32) as

$$[\,\tau_\eta^{\rm loc}\,]^{1/2} A \sim \varepsilon_{\rm loc}^{1/2}. \tag{4.35}$$

It is interesting to note that this quantity is independent on ν and is thus expected to have a finite limit at infinite Reynolds numbers. The local dissipation is a function of the current values of the velocity difference $\boldsymbol{V}$ and of the separation $\boldsymbol{R}$. Dimensional arguments suggest that $\varepsilon_{\rm loc} \sim V^3/R$. However, when $V = 0$, the local dissipation is not expected to vanish and should come from an averaged contribution of larger eddies, leading to $\varepsilon_{\rm loc} \simeq \varepsilon$, the mean dissipation rate. In summary, we expect to have

$$\varepsilon_{\rm loc}(t) \sim \varepsilon + \alpha \frac{[V^\parallel(t)]^3}{|\boldsymbol{R}(t)|}, \tag{4.36}$$

where α is an adjustable parameter. We have again used here the longitudinal velocity difference between two tracers $V^\parallel = \boldsymbol{R}\cdot\boldsymbol{V}/|\boldsymbol{R}|$.

All these estimations have been tested against numerical simulations. Figure 4.19 shows the variance of the acceleration differences conditioned on the longitudinal velocity difference for various values of the initial separation r_0.

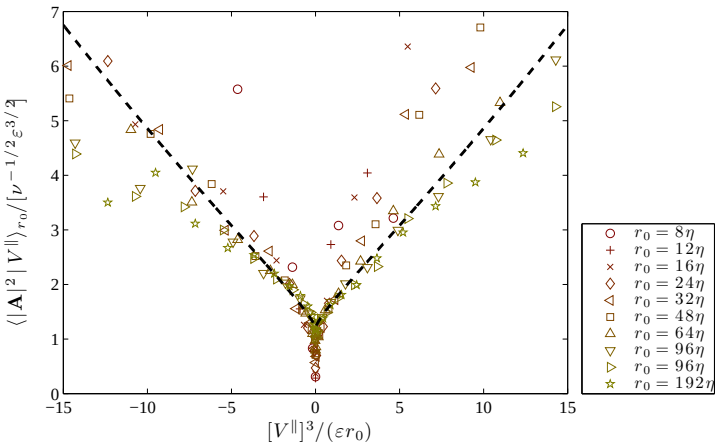

Figure 4.19: Variance of the acceleration difference amplitude conditioned on the initial longitudinal velocity difference $V^{\parallel}(0)$ as a function of the local dissipation rate $[V^{\parallel}(0)]^3/r_0$. The various symbols correspond to different values of the separation r_0, as labeled.

Up to some statistical errors, it seems that data are in rather good agreement with the phenomenological prediction given by Eqs. (4.34) and (4.36), which is represented by the dashed line for $\alpha = 0.18$.

We have here used phenomenological considerations to express the typical amplitude of the acceleration difference as a function of the distance between pairs and of the velocity difference. These phenomenological considerations are purely scalar. They give a good estimate for the variance of the acceleration difference modulus but dot not catch the full structure of the covariance tensor. Expressing it more precisely would require developing further such phenomenological arguments to account in particular for the incompressibility of the dynamics. As we will see in next subsection, we have focused for the moment on a one-dimensional version of the dynamics where such tensorial considerations are irrelevant. Extending this approach to higher dimensions goes beyond the studies reported in this thesis and is kept for future work.

4.4.3 A one-dimensional stochastic model

We have seen in previous subsection that the acceleration difference between two tracers gets uncorrelated on a very small timescale. Moreover, its variance can be related to the values of the distance and of the longitudinal velocity difference between the two tracers by dimensional arguments. In

principle, we can then apply the central-limit theorem to design a model for the joint time evolution of the separation and of the velocity difference. However, we found an expression for the amplitude of the acceleration, but not for its full tensorial structure. We thus focus here on writing a one-dimensional model that is expected to reproduce the most important features of turbulent pair dispersion.

We work here in non-dimensional units. Let us introduce the following stochastic model for the joint evolution of the separation $R(t)$ and the (longitudinal) velocity difference $V(t)$

$$\mathrm{d}R = V\,\mathrm{d}t, \qquad \mathrm{d}V = -b\,\frac{|V|}{R}V\,\mathrm{d}t + \left[1 + c\,\frac{|V|^3}{R}\right]^{1/2}\mathrm{d}W_t, \tag{4.37}$$

where $W(t)$ denotes the one-dimensional Wiener process (see Chap. 3). The multiplication by the noise is here understood in the Itō sense. This formulation can be seen as an application of the central-limit theorem to the time integral of the acceleration difference, which can be written as a sum of independent integrals over time intervals of length τ_η. The drift term is due to the change from Stratonovich's to Itō's definition of the stochastic integral. However, the constants b and c are not directly related as their ratio is supposed to come from tensorial considerations and from the prescription of incompressibility to the Lagrangian dynamics. This drift term, which is non-linear, introduces a "correlation time" equal to the turnover time $R/|V|$. Despite its dependence on V, this timescale can be seen as a "response time" of the pair dynamics which depends on both the scale and the strength of the structure under consideration.

While its form is relatively simple, the model defined by Eq. (4.37) cannot be integrated explicitly, neither under its stochastic form, nor with the help of its equivalent Fokker–Planck form. This is mainly due to the presence of non-linear terms in both the drift and the diffusion coefficient. However, we can make the following remarks. Let us write the Fokker–Planck equation for the transition probability density $p(r, v, t|r_0, v_0, 0)$ to be separated by r with a velocity difference v at time t conditioned on the initial conditions, namely

$$\partial_t p + v\partial_r p - \partial_v\left[b\,\frac{|v|\,v}{r}\,p\right] = \partial_v^2\left[\left(1 + c\,\frac{|v|^3}{r}\right)p\right]. \tag{4.38}$$

One can then easily check that Eq. (4.38) admits scaling solutions of the form $p(r, v, t) = t^\alpha \Psi(r/t^{3/2}, v/t^{1/2})$. This scaling exactly corresponds to that given by Richardson's explosive behavior (namely $r \sim t^{3/2}$ and $v \sim t^{1/2}$).

The function Ψ is a solution of

$$(\alpha+2)\,\Psi+\partial_\xi\left[\left(\mu-\frac{3}{2}\xi\right)\Psi\right]=\partial_\mu\left[\left(b\frac{|\mu|\,\mu}{\xi}+\frac{1}{2}\mu\right)\Psi+\partial_\mu\left[\left(1+c\frac{|\mu|^3}{\xi}\right)\Psi\right]\right].$$

The choice $\alpha=-2$ allows one to get ride of the term $\propto\Psi$. This equation then reduces to a stationary Fokker–Planck equation. However the traditional techniques used to solve such problems, as for instance the assumption of constant probability flux, do not work in that case and one cannot straightforwardly write a scaling solution for the transition probability density.

The difficulties encountered in solving the Fokker–Planck equation associated to the stochastic model of Eq. (4.37) led us to investigate its solutions and statistical properties by Monte–Carlo numerical simulations. We report in the rest of this subsection the results of such an approach. Let us first give some additional informations on the numerical settings. First, as the dynamics becomes stiff when $R\to 0$, we had to prescribe a cutoff at small distances. For that, a minimal scale η has been introduced and, below η, particles are evolved with a linear velocity difference that is chosen such that they separate in average (this is done in order to mimic a positive Lyapunov exponent at dissipative scales). The inverse of the rate at which the particles are separated defines a timescale τ_η. All results are reported in units of η and τ_η. Also, we have not spanned the full parameter space by varying systematically b and c. On the contrary, we have just focused on some specific values and most of the results reported here are for $b=0.1$ and $c=0.1$.

Figure 4.20 (Top) shows the evolution of the mean-squared displacement $\langle[R(t)-R(0)]^2\rangle$ as a function of time. One clearly observes for the model the two regimes that are proper to turbulent pair dispersion, namely a ballistic regime $\propto t^2$ at small times that is followed by an explosive growth of the separation where $\langle R^2(t)\rangle\propto t^3$. With our choice of units, $\varepsilon=1$ and the constant of proportionality is of the order of 0.1 for $c=b=0.1$. One also notices that this large time asymptotic regime is independent of the initial separation $R(0)$. This indicates an explosive regime, as in the case of actual turbulent pair dispersion. Also, the extension of the ballistic regime clearly depends on $R(0)$. Figure 4.20 (Bottom) shows the time evolution of the mean-squared velocity difference. The data reveal a clear diffusive behavior at large times where $\langle V^2(t)\rangle\propto t$. This law is preceded by a short increase of the pair kinetic energy and of a decrease. While the first is absent from the data corresponding to turbulent flow, the second has been observed there.

To understand better the reasons why the velocity difference becomes diffusive at large times, we have also measured the time evolution of the averaged "local dissipation" $\langle V^3(t)/R(t)\rangle$. The results are shown in Fig. 4.21.

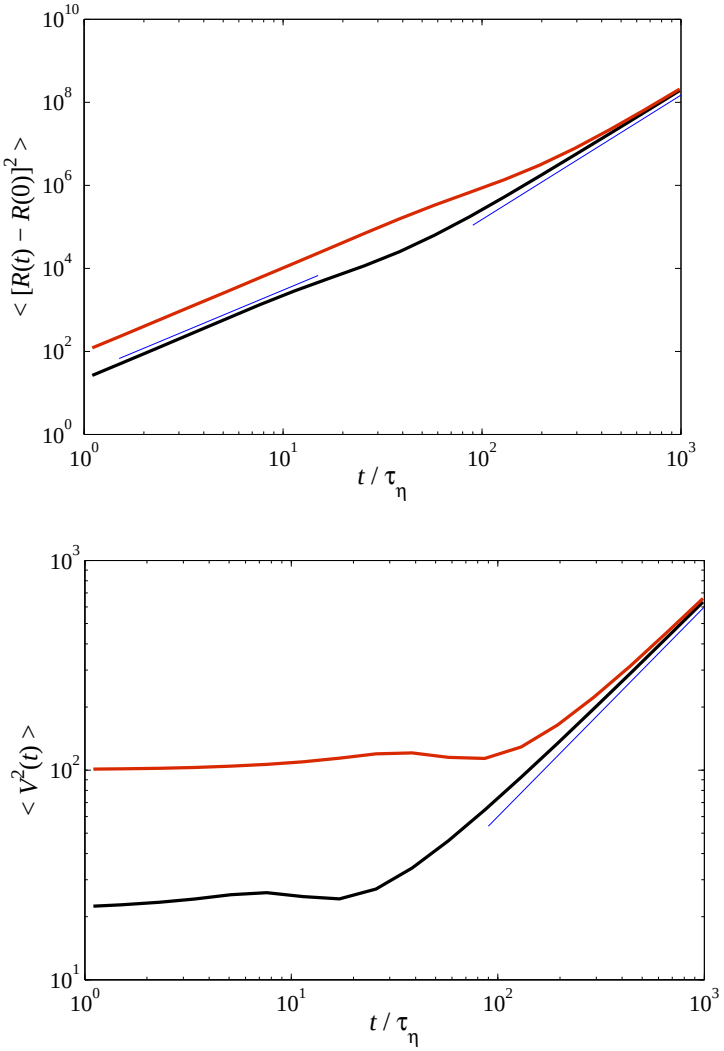

Figure 4.20: Top: time evolution of the average squared displacement for the stochastic model, Eq. (4.37), with $c = b = 0.1$ for pairs such that $R(0) = 100\eta$ (black) and $R(0) = 1000\eta$ (red). The two blue lines stand for the ballistic $\propto t^2$ regime (on the left) and the explosive $\propto t^3$ law (on the right). Bottom: Time evolution of the mean squared velocity difference for the same settings. The blue line is the diffusive behavior $\propto t$.

Contrarily to what was observed in real turbulent flows (see Subsec. 4.4.1), there is no rapid variation of this quantity on very short timescales. Surprisingly, this quantity, which is zero at small times by construction in the

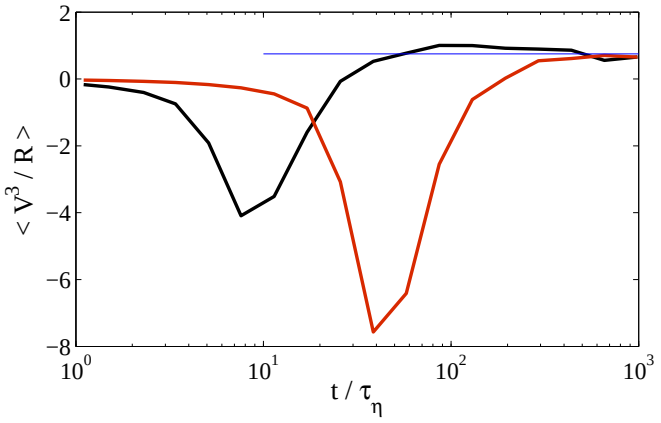

Figure 4.21: Time evolution of the mean "local dissipation" $\langle V^3(t)/R(t)\rangle$ along the solutions to the stochastic model with $c = b = 0.1$ and for pairs such that $R(0) = 100\eta$ (black) and $R(0) = 1000\eta$ (red).

stochastic case, becomes relatively quickly negative. This is related to the decrease of $\langle V^2(t)\rangle$ observed in Fig. 4.20 (Bottom). At larger times, this decrease is then followed by an increase. Later, similarly to what was observed in real flows, the average "local dissipation" stabilizes to a finite value. In the stochastic model for $c = b = 0.1$, this limit is of the order of 1. As seen in Fig. 4.21 this limit seems independent of the initial separation $R(0)$. However, conversely to what observed in real turbulent flows, the timescale of convergence to this limit depends on $R(0)$.

To complete our understanding of the behavior of the "local dissipation" along pair trajectories, we show in Fig. 4.22 their probability density functions estimated at various times. As seen in Subsec. 4.4.1 in the case of developed turbulent flow, the various curves collapse together at large times to an asymptotic distribution with fat tails. In contrast to the real-flow case, the left tails seem here less developed than the right ones. The fact that the averaged "local dissipation" $\langle V^3(t)/R(t)\rangle$ tends to a positive constant is rather due to a shift of the maximum of the distribution than to a difference in the tails. Note however that the observed fluctuations of V^3/R are anyway much larger than the measured average value. Events associated to large value of the "local dissipation" are more frequent for approaching pairs ($V < 0$) than for those that separate. This can be due to the fact that the dynamics associated to the model is compressible. However, by changing appropriately the values of the parameters b and c, one can certainly find values where this tendency is inverted. Anyway, the important suggestion

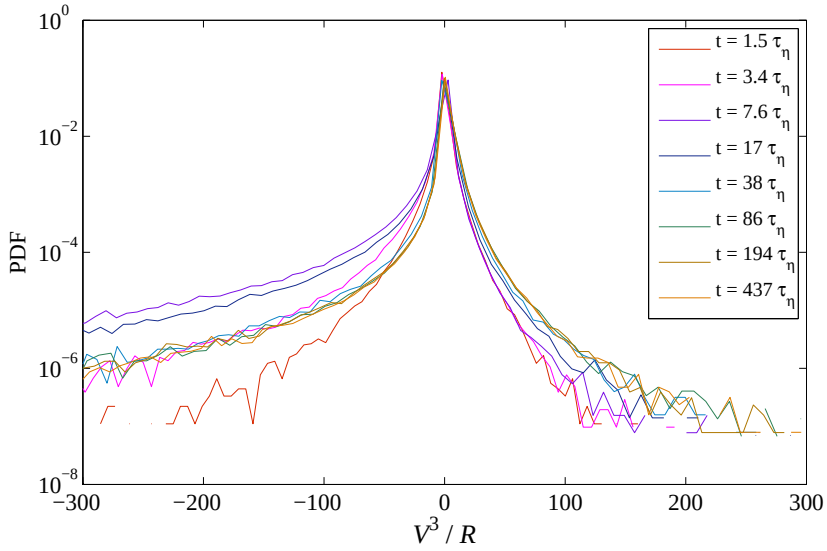

Figure 4.22: Probability density functions of the "local dissipation" $V^3(t)/R(t)$ along the solutions to the stochastic model with $c = b = 0.1$ and for pairs such that $R(0) = 100\eta$. The various colors correspond to different times, as labeled. Note that the data are not rescaled here.

made by these measurements is the apparent convergence at large times to a scaling regime of the distribution of separations and velocity differences.

This convergence of the "local dissipation", together with the long-time behaviors observed earlier in this subsection for the squared average quantities, are very similar to those obtained for tracer relative dispersion in turbulent flows. Also, they give evidence that the scaling regime discussed above in the framework of the Fokker–Planck equation could be attained by the model at large times. This asymptotic behavior is evidenced by looking at the probability distributions of the displacement and the velocity differences themselves. As seen in Fig. 4.23, once rescaled by their standard deviations, both of them converge at large times to asymptotic distributions, confirming what expected. The velocity probability density function, which was chosen Gaussian at the initial time, quickly develops fat tails. This is certainly due to the non-linear nature of the multiplicative noise in the stochastic model. The separation distribution is also developing a fat tail at large values. As seen in Fig. 4.23 (Top), these tails become more stretched than an exponential in the large-time asymptotic scaling distribution. However, we were not able to match them with Richardson's diffusive distribution discussed in Subsec. 4.1.1.

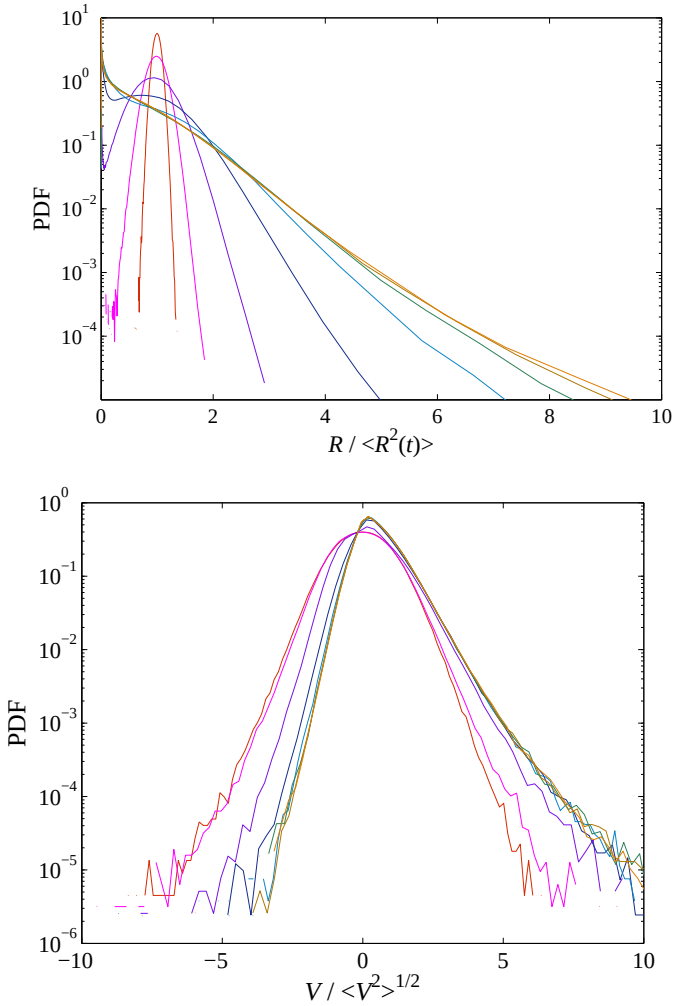

Figure 4.23: Top: probability density function of the separation R between two trajectories obtained from the stochastic model with $b = c = 0.1$ and $R(0) = 100$. The different colors correspond to the different times shown in Fig. 4.22. Bottom: same for the velocity difference V.

The probability distribution of the separation is also developing tails at small values. This is clear in Fig. 4.24 where they are represented not rescaled and in log-log coordinates. One observes there that the probability density function of the separation $p(R)$ develops at small values a power-law behavior $p(R) \propto R^{\alpha}$ where the exponent α depends on time. Initially it is equal to $+\infty$ as the distribution is centered on $R = R(0)$ and it converges to an asymptotic value ≈ -0.5 at large times. This value depends on the choice

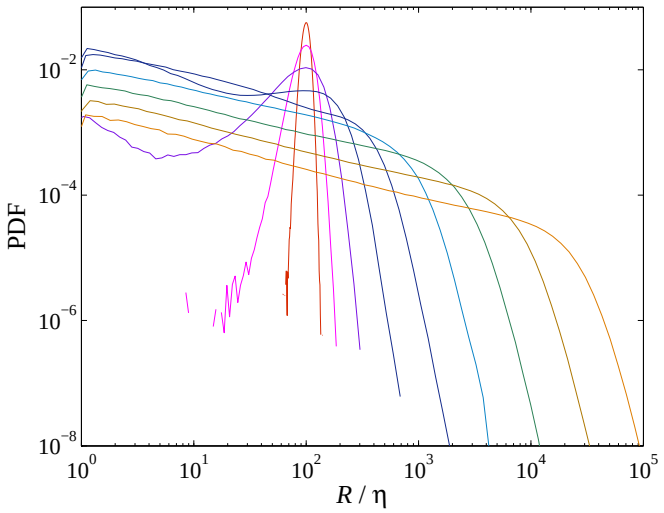

Figure 4.24: Probability density function of the separation R between two trajectories obtained from the stochastic model with $R(0) = 100\eta$. The different colors correspond to the same times as in Fig. 4.22. Note that this time the distributions are not rescales and are shown in log-log coordinates to evidence the behavior at small separations.

of the parameters b and c. The fact that it is negative is a clear signature of the compressibility of the one-dimensional stochastic model studied here. However, the intermediate time variations of α are much more relevant. Also, as seen in Fig. 4.24, one observes that at intermediate times, the exponent α is smaller than its asymptotic value, so that its behavior is non-monotonic. At such intermediate times, the pair distribution is thus more concentrated at small distances than at later times. This behavior is indicating the presence of strong fluctuations in the statistics of pair dispersion. Such extreme events are important as they relate to the probability of a slow dispersion of the transported species. As we will see in the next chapter, this behavior can also be observed for relative dispersion in actual developed turbulent flows.

To conclude, let us stress again that, so far, we have only investigated a simple one-dimensional version of the proposed model Eq. (4.37). We believe that extensions to higher dimensions will make this kind of approach more relevant to actual turbulent pair dispersion. However, the main issue will then be to account for incompressibility via the tensorial structure of the acceleration variance. This goes beyond the aim of the present study and it will be investigated in a future work.

Chapter 5

Geometry and violent events in turbulent relative motion

Here we carry on our study of the statistics of Lagrangian pair dispersion in a homogeneous isotropic flow. Again, we mostly use the results of high-resolution direct numerical simulations. In previous chapter, we have seen that the squared average quantities are well described by Richardson's eddy-diffusivity approach. An example is the t^3 behavior for the mean-squared distance between tracers, which seems rather robust. We however discussed the fact that the main assumption in this approach is hard to justify. The velocity difference is indeed correlated on times that are always longer or of the order of the considered timescales. For this reason, we have given a reinterpretation of the t^3 in terms of a diffusive behavior of the velocity differences. This hypothesis has been justified by investigating the correlation of acceleration differences.

In this chapter, the focus is again on the deviations from Richardson's eddy-diffusivity model. Our attention is on the strong fluctuations that are experienced by tracers. For that we first investigate in Sec. 5.1 the high-order moments of separation and velocity differences. Evidence is obtained that the distribution of distances attains an almost self-similar regime characterized by a very weak intermittency. The timescale of convergence to this behavior is found to be given by the kinetic energy dissipation time t_0 measured at the scale of the initial separation and which was introduced in previous chapter. Conversely the velocity differences between tracers are displaying a strongly anomalous behavior whose scaling properties are very close to that of Lagrangian structure functions. We then give a geometrical interpretation of these violent fluctuations and show that they are responsible for a long-term memory of the initial separation.

These results are then brought together to address the question of violent

events in the distribution of distances. We report in Sec. 5.2 our findings that distances much larger than the average are reached by pairs that have always separated faster since the initial time. They are responsible for the presence of a stretched exponential behavior in the tail of the inter-tracer distance probability distribution. The tail approaches a pure exponential at large times, contradicting Richardson's diffusive approach. At the same time, as we show in Sec. 5.3, the distance distribution displays a time-dependent power-law behavior at very small values, which is interpreted in terms of fractal geometry. It is argued and demonstrated numerically that the exponent converges to one at large time, again in conflict with Richardson's distribution.

5.1 High-order statistics

5.1.1 Scaling regime in the statistics of distances

We have seen in the previous chapter (Sec. 4.2) that the mean squared displacement $\langle |\boldsymbol{R}(t) - \boldsymbol{R}(0)|^2 \rangle_{r_0}$ between two tracers that were initially at a distance $|\boldsymbol{R}(0)| = r_0$, behaves ballistically as t^2 for small times and explosively as t^3 at large times. We recall that $\boldsymbol{R}(t) = \mathbf{X}_2(t) - \mathbf{X}_1(t)$ denotes the separation between two tracers. We showed that the transition between the two aforementioned regimes occurs at a time $t_0 = S_2(r_0)/(2\varepsilon)$, where $S_2(r_0)$ is the absolute-value second-order Eulerian structure function of the fluid velocity over a distance r_0 and ε is the average turbulent rate of kinetic energy dissipation. In this section, we turn to investigating the large-time behavior of higher-order moments of the separation. Figures 5.1 (a) and (b) show the time evolution of $\langle |\boldsymbol{R}(t) - \boldsymbol{R}(0)|^4 \rangle_{r_0}$ and of $\langle |\boldsymbol{R}(t) - \boldsymbol{R}(0)|^6 \rangle_{r_0}$, respectively. At times smaller than t_0 the separation grows ballistically, so that $\langle |\boldsymbol{R}(t) - \boldsymbol{R}(0)|^p \rangle_{r_0} \simeq t^p \langle |\boldsymbol{V}(0)|^p \rangle_{r_0}$ where we recall that $\boldsymbol{V}(t) = \mathbf{u}(\mathbf{X}_2, t) - \mathbf{u}(\mathbf{X}_1, t)$ denotes the velocity difference between the two tracers. The fact that we have chosen to rescale time by t_0 (which depends on second-order statistics of the initial velocity difference) implies that the moments do not collapse in this regime because of Eulerian multiscaling. However the collapse occurs for $t \gg t_0$ where these two moments grow like t^6 and t^9, respectively, with possible minute deviations. The measured power-laws give evidence that, at sufficiently long times, inter-tracer distances follow a scale-invariant law. Also the observed collapses indicate that t_0 could be again the time of convergence to such a behavior.

The presence of a scale-invariant regime is also clear when making use of ideas borrowed from extended self-similarity and representing these two mo-

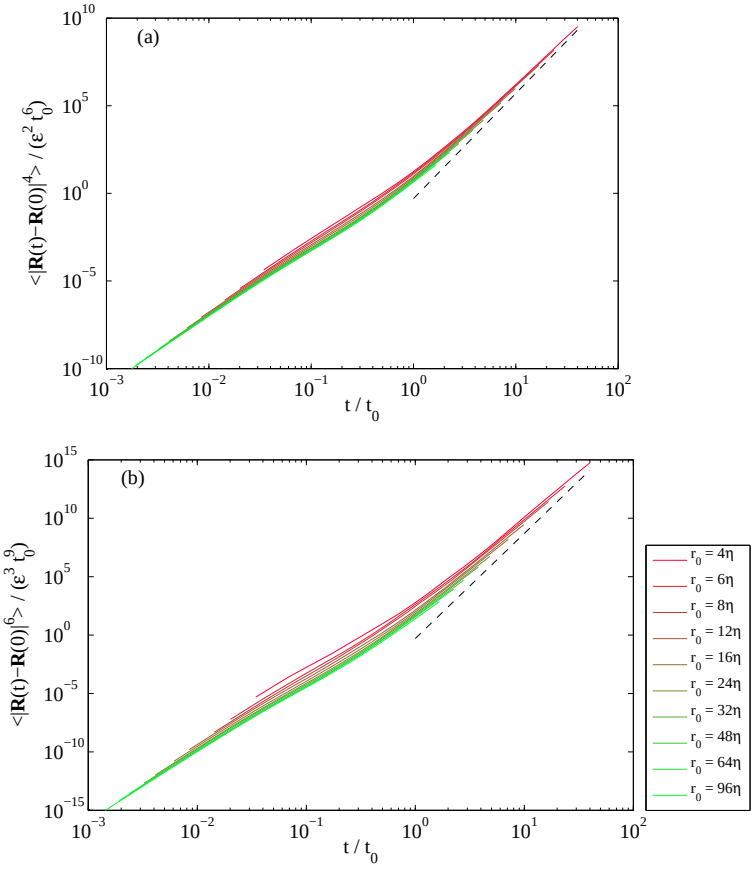

Figure 5.1: (a) Fourth-order moment $\langle|\boldsymbol{R}(t)-\boldsymbol{R}(0)|^4\rangle_{r_0}$ and (b) sixth-order moment $\langle|\boldsymbol{R}(t)-\boldsymbol{R}(0)|^6\rangle_{r_0}$ as function of t/t_0 for $R_\lambda = 730$. Both curves are normalized such that their expected long-time behavior is $\propto (t/t_0)^6$ and $\propto (t/t_0)^9$, respectively. The black dashed lines represent such behaviors.

ments as a function of $\langle|\boldsymbol{R}(t)-\boldsymbol{R}(0)|^2\rangle_{r_0}$ (see Fig. 5.2). This time, for a fixed r_0, the smallest separations correspond to the ballistic regime. There, we trivially have $\langle|\boldsymbol{R}(t)-\boldsymbol{R}(0)|^p\rangle_{r_0}/\langle|\boldsymbol{R}(t)-\boldsymbol{R}(0)|^2\rangle_{r_0}^{p/2} \simeq \langle|\boldsymbol{V}(0)|^p\rangle_{r_0}/\langle|\boldsymbol{V}(0)|^2\rangle_{r_0}^{p/2}$, which has a weak dependence on r_0, because of an intermittent distribution of Eulerian velocity increments, but does not depend on time. This normal scaling can be observed for $t \ll t_0$ in the insets of Fig. 5.2, which represent the logarithmic derivatives of the high-order moments with respect to the second order. At times of the order of t_0, noticeable deviations to normal scaling can be observed. Finally, at much larger scales, data corresponding to different values of the initial separation r_0 collapse but the curves start to bend down. One observes in the insets that the associated local slopes approach values clearly smaller than those corresponding to normal scaling.

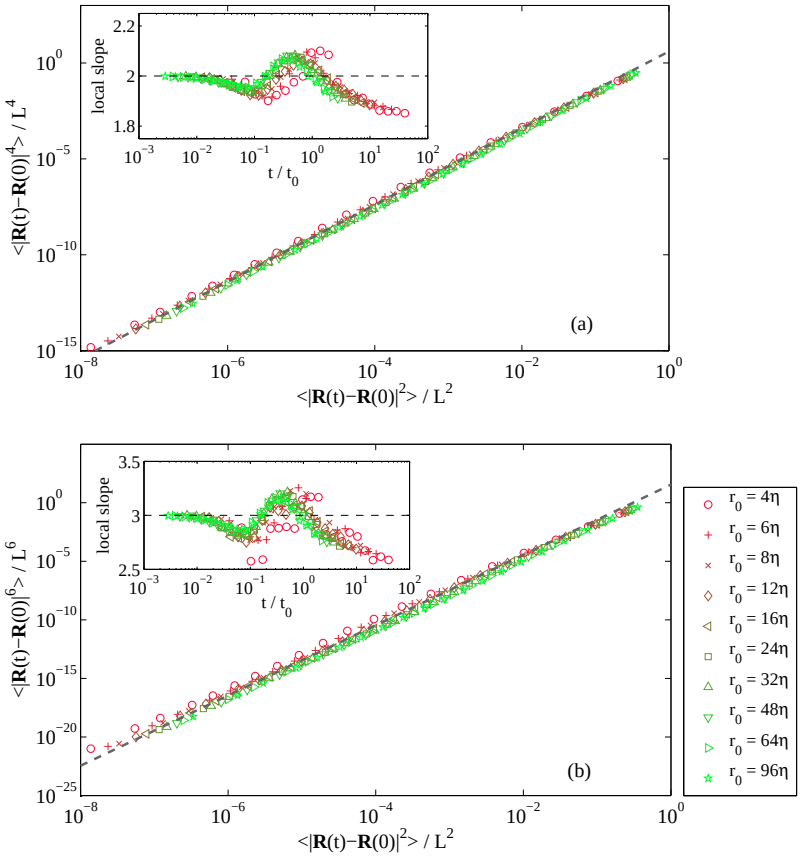

Figure 5.2: Fourth (a) and sixth (b) order moments of $|\boldsymbol{R}(t) - \boldsymbol{R}(0)|$ as a function of its second-order moment for $R_\lambda = 730$. The two gray dashed lines show a scale-invariant behavior, i.e. $\langle|\boldsymbol{R}(t)-\boldsymbol{R}(0)|^4\rangle_{r_0} \propto \langle|\boldsymbol{R}(t)-\boldsymbol{R}(0)|^2\rangle^2_{r_0}$ and $\langle|\boldsymbol{R}(t) - \boldsymbol{R}(0)|^6\rangle_{r_0} \propto \langle|\boldsymbol{R}(t) - \boldsymbol{R}(0)|^2\rangle^3_{r_0}$, respectively. The two insets show the associated local slopes, that is the logarithmic derivatives $\mathrm{d}\log\langle|\boldsymbol{R}(t)-\boldsymbol{R}(0)|^p\rangle_{r_0}/\mathrm{d}\log\langle|\boldsymbol{R}(t)-\boldsymbol{R}(0)|^2\rangle_{r_0}$, together with the normal scalings represented as dashed lines.

This gives evidence of a rather weak intermittency in the distribution of tracer separations. Note that the presented measurements were performed for $R_\lambda = 730$ but the same behavior has been observed for $R_\lambda = 460$. We refer the reader to Subsec. 4.2.1 for further details on the parameters of the numerical simulations.

To our knowledge, the most convincing observation of an intermittent behavior in pair dispersion has been based on an exit-time analysis [Boffetta & Sokolov, 2002a, Biferale et al., 2005]. However, the relation of such fixed-scale statistics to the usual fixed-time measurements we report here requires

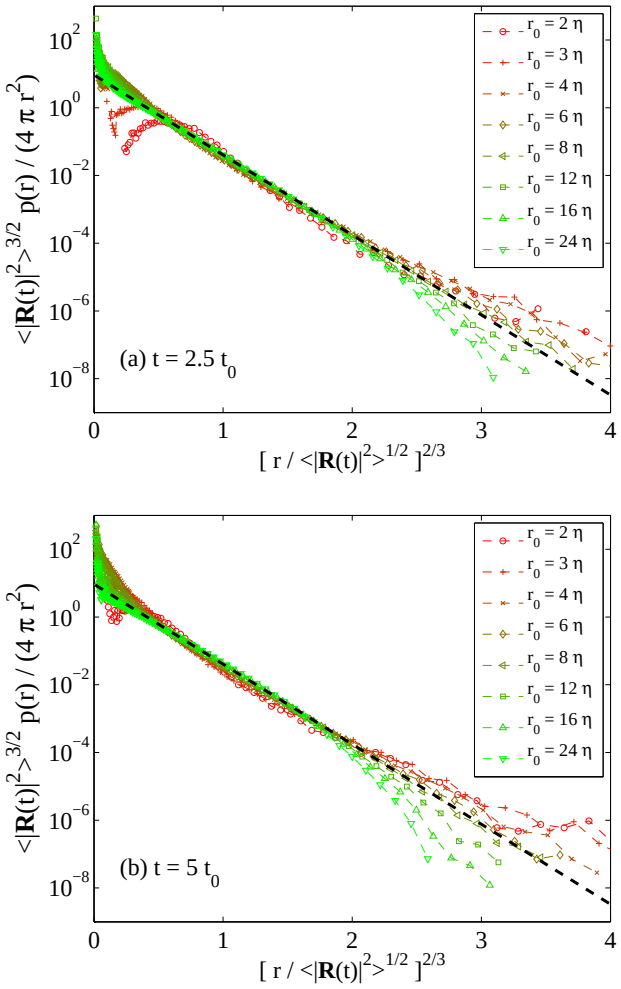

Figure 5.3: Probability density function of the distance r at time $t = 2.5\,t_0$ (a) and $t = 5\,t_0$ (b) and for various values of the initial separation. We have here normalized it by $4\pi r^2$ and represented on a $\log y$ axis as a function of $r/\langle|\boldsymbol{R}(t)|^2\rangle_{r_0}^{1/2}$. With such a choice, Richardson's diffusive density distribution (4.9) appears as a straight line (represented here as a black dashed line).

to consider pair separation velocities. As we will see in the next subsection, the velocity difference between two tracers displays statistics that are much more intermittent than those for pair separation. This implies that there is no contradiction between an almost normal scaling for distances as a function of time and an anomalous behavior of exit times as a function of distance.

To investigate further this weak intermittency in the separation distribution, we have represented in Fig. 5.3 the probability density function (PDF)

of the distance $|\boldsymbol{R}(t)|$ for various initial separation and at times where we expect to have almost converged to the explosive regime, namely at $t = 2.5\,t_0$ (a) and $t = 5\,t_0$ (b). Such measurements are compared to Richardson's diffusive law Eq. (4.9). Data suggest that a large part of the PDF's core (for $0.4 \lesssim |\boldsymbol{R}(t)|/\langle|\boldsymbol{R}(t)|^2\rangle_{r_0}^{1/2} \lesssim 4$ at time $t = 5\,t_0$) is very well described by Richardson's approach. However, deviations are observed in the far tails, at both small and large values of the separation. Such an observation is consistent with previous numerical observations [Boffetta & Sokolov, 2002a,Biferale et al., 2005, Scatamacchia et al., 2012]. Apparently, these deviations affect only weakly the moments we have considered above. We will come back to investigating and characterizing them in Sec. 5.2.

5.1.2 Intermittent distributions of velocity differences

All the considerations on the dependence of the velocity difference between tracers upon the initial separation, which were discussed in the previous chapter, are also visible in the probability distribution of the longitudinal velocity $V^{\parallel} = \boldsymbol{R} \cdot \boldsymbol{V}/|\boldsymbol{R}|$. Figure 5.4 (a) shows the centered PDF of $V^{\parallel}$ normalized to unit variance for various times and $r_0 = 12\eta$. The data clearly show that at times later than $0.01\,t_0$, there is a change in the sign of the skewness. Also, one sees that the time dependence of the skewness and of the flatness comes from the right tails associated to large velocity differences, supporting the arguments discussed above. The left tails, which correspond to approaching pairs, seem on the contrary to collapse. The right tail has a very rich behavior. It starts with broadening at times $t < t_0$, in agreement with the increase of flatness. For $t > t_0$, it then decreases and possibly goes back asymptotically to its initial form. This aspect suggests that the distribution of velocity differences will keep in memory the initial separation at any later time.

This is also evidenced from Fig. 5.4 (b), which shows the same PDFs for various separations and a time $t = 5\,t_0$ fixed. Again we observe a rather good collapse of the tails associated to negative longitudinal velocity differences, but the right tails display very strong dependence on the initial separation. Clearly, the behavior of this tail is a stretched exponential for $r_0 \lesssim 8\eta$ and is faster than exponential for larger initial separations. The actual level of statistics do not allow us to relate systematically this behavior to that of the initial velocity difference distribution.

Finally another way to address the question of intermittency of the velocity difference consists in finding how moments of its longitudinal component depend on time. For that we follow, as in the case of the moments of distances, an approach similar to that of extended self-similarity. Figures 5.5 (a)

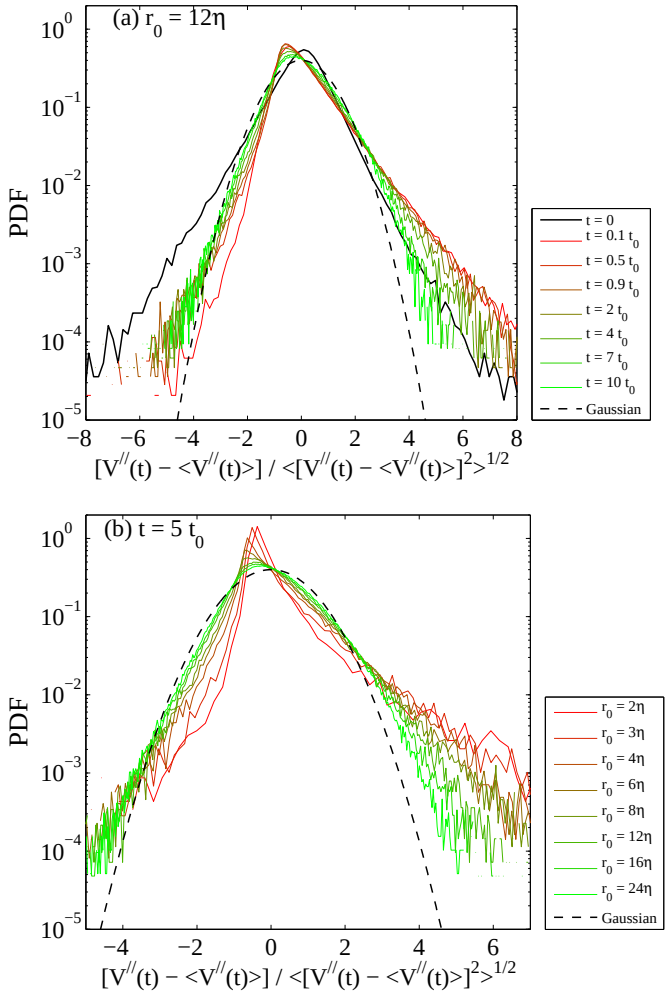

Figure 5.4: Centered and normalized probability density functions of the longitudinal velocity difference: (a) for $r_0 = 12\,\eta$ and various times and (b) for various initial separations and $t = 5\,t_0$. In both cases, the black dashed line shows a Gaussian distribution.

and (b) show the fourth and sixth-order moments of $V^{\parallel}(t)$ as a function of its second-order moment. As evidenced in the insets, they display an anomalous behavior that differs from simple scaling. However, the collapse for various r_0 is much less evident than for the moments of the distance, except perhaps at sufficiently large times. One can there guess a power-law dependence of $\langle [V^{\parallel}(t)]^p \rangle_{r_0}$ as a function of $\langle [V^{\parallel}(t)]^2 \rangle_{r_0}$. Surprisingly the power is compatible with the scaling exponent of the Lagrangian structure functions that were obtained in [Biferale et al., 2004] by relating velocity increment along tra-

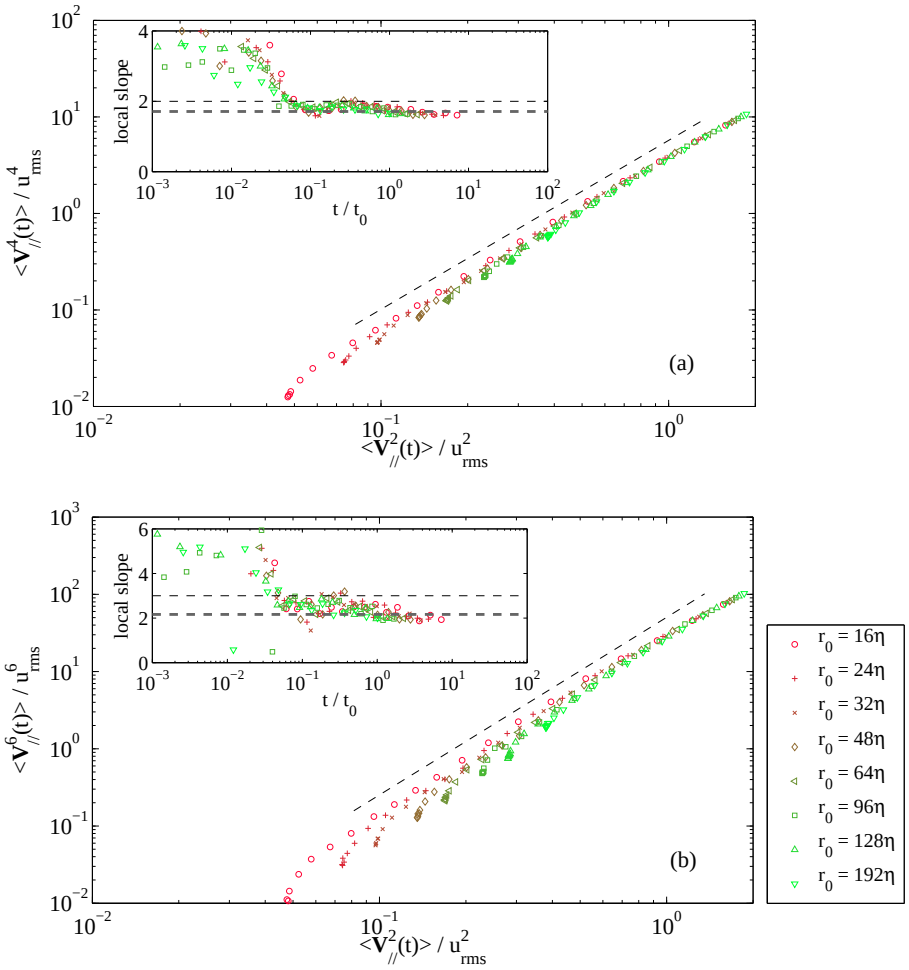

Figure 5.5: Fourth-order (a) and sixth-order (b) moments of the longitudinal velocity difference as a function of its second-order moment for various times and initial separations. The two dashed lines correspond to a scaling compatible with that of Lagrangian structure functions proposed in [Biferale et al., 2004], namely $\zeta_4^{\mathrm{L}}/\zeta_2^{\mathrm{L}} = 1.71$ and $\zeta_6^{\mathrm{L}}/\zeta_2^{\mathrm{L}} = 2.16$. The insets show the logarithmic derivative $\mathrm{d}\log\langle[V^{\parallel}(t)]^p\rangle_{r_0}/\mathrm{d}\log\langle[V^{\parallel}(t)]^2\rangle_{r_0}$ for (a) $p = 4$ and (b) $p = 6$ as a function of t/t_0; there the bold dashed lines show the Lagrangian multifractal scaling and the thin lines what is expected from a self-similar behavior.

jectories to She–Lévêque multifractal spectrum for the Eulerian field. The two dashed lines in Fig. 5.5 (a) and (b) correspond to the predicted values $\zeta_4^{\mathrm{L}}/\zeta_2^{\mathrm{L}} = 1.71$ and $\zeta_6^{\mathrm{L}}/\zeta_2^{\mathrm{L}} = 2.16$. Confirming further that this match would require much better statistics.

5.2 Memory in large-distance statistics

In this section and in the following we turn back to the statistics of the distance $|\boldsymbol{R}(t)|$ between two tracers. Our goal is to explain the mechanisms leading to very large or very small values of this distance in the light of the various observations made in previous sections and in previous chapter. Considering the relative dispersion of tracers conditioned on their initial distance r_0 can be geometrically interpreted in terms of the time evolution of an initially spherical surface of radius r_0 that is centered on a reference trajectory. The transport of this surface by a turbulent flow is generally very complex. Incompressibility implies that the volume of the sphere is conserved but the velocity field roughness will be responsible for strong distorsions of its surface. This is represented in Fig. 5.6 that shows for $R_\lambda = 460$ at three various times the shape defined by the instantaneous position of 60 trajectories that are all initially at a distance 24η from a reference tracer.

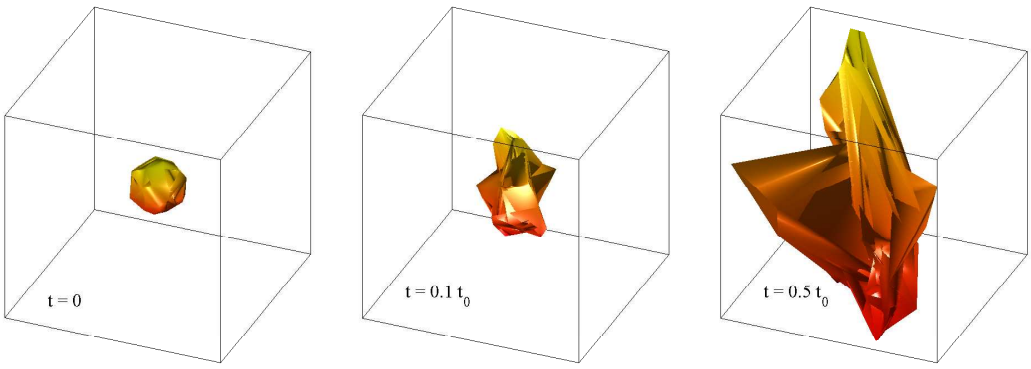

Figure 5.6: Quasi-Lagrangian evolution of the set of tracers that are initially at a distance $r_0 = 24\eta$ of a reference trajectory.

We can qualitatively deduce from these snapshots that the large excursions of the inter-trajectory distance go together with strong pinches of the surface. We also see that the intense stretchings are occurring in a time-correlated manner: the surface angles that are visible at late time have formed at very early stages. As we will now see, the most-separated pairs have been so for long times and carry a reminiscent dependence on the initial separation.

We first consider in this section the events related to distances that are much larger than their average. It was argued in Sec. 5.1.1 that the large-value tail of the separation PDF is not well described by Richardson's distribution. As seen in Fig. 5.3 (b) for $t = 5\,t_0$, the tail is indeed broader than

$\exp(-C\,|\boldsymbol{R}|^{2/3})$ for $r_0 \lesssim 8\eta$ and narrower otherwise. It seems to tend to a Gaussian when either r_0 or t are sufficiently large. We have checked that these behaviors are not due to a contamination by pairs that have reached the large scales of the turbulent flow, as the considered distances are still well below L, except maybe for the largest initial separation $r_0 = 24\eta$. These observations suggest that for such extreme events, there is a long-term memory of the initial separation.

To qualify further the history of pairs that are well separated at large times, we have performed the following analysis. Fixing a final time t_f sufficiently large to have reached the explosive Richardson–Obukhov regime, we have carried out statistics conditioned on pairs that are far separated at $t = t_\mathrm{f}$, say such that their distance is $|\boldsymbol{R}(t_\mathrm{f})| \geq 2\,\langle|\boldsymbol{R}(t_\mathrm{f})|\rangle_{r_0}$. In order to not be contaminated by finite inertial subrange effects, we have restricted this analysis to $R_\lambda = 730$ and to initial separations $2\,\eta \leq r_0 \leq 24\,\eta$, and we have chosen the largest compatible value of t_f, namely $t_\mathrm{f} = 5\,t_0$. Let us denote by $\langle\cdot\rangle_+$ the resulting conditional ensemble average, i.e. $\langle\cdot\rangle_+ = \langle\cdot \mid \{|\boldsymbol{R}(t_\mathrm{f})| \geq \langle|\boldsymbol{R}(t_\mathrm{f})|\rangle_{r_0}\}\rangle_{r_0}$. Figure 5.7 (a) represents the relative increase $\langle|\boldsymbol{R}(t)-\boldsymbol{R}(0)|^2\rangle_+/\langle|\boldsymbol{R}(t)-\boldsymbol{R}(0)|^2\rangle_{r_0}$ of the mean-squared displacement. The various curves, which are associated to different initial separations r_0, have a maximum at $t = t_\mathrm{f} = 5\,t_0$ represented by a dashed line. The value of this maximum is becoming larger when r_0 decreases and approaches the dissipative scales. This is a signature of the dependence of the large-positive value tail upon r_0. On the right-hand side of the maximum, the various curves tend back to 1. This indicates that separations that are large at a given intermediate time relax in average to an ordinary behavior at later times. This can be regarded as a consequence of the weakening of large-distance probability tails as a function of time. The situation is rather different when interested in the left-hand side of the maximum. The curves do not converge to 1, and thus to an average behavior when $t \to 0$. This means that pairs that are well separated at a given time are likely to have been so at any previous times. This asymmetry when going forward or backward in time could already be grasped in Fig. 5.6. The trajectories that are far away from the reference tracer at the latest time (as, e.g., those defining the left and top corners) are visibly also well separated at the intermediate time. Conversely the right corner at the intermediate time have later stopped separating faster than the average.

Figure 5.7 (b) shows the time evolution of the averaged longitudinal velocity difference $\langle V^\parallel(t)\rangle_+$ conditioned on having a separation twice the average at time $t_\mathrm{f} = 5\,t_0$. A first remark that cannot be seen from the log-log plot is that the initial value of this average is strictly positive. The inset represents the variation of $\langle V^\parallel(0)\rangle_+$ as a function of the initial separation. This implies

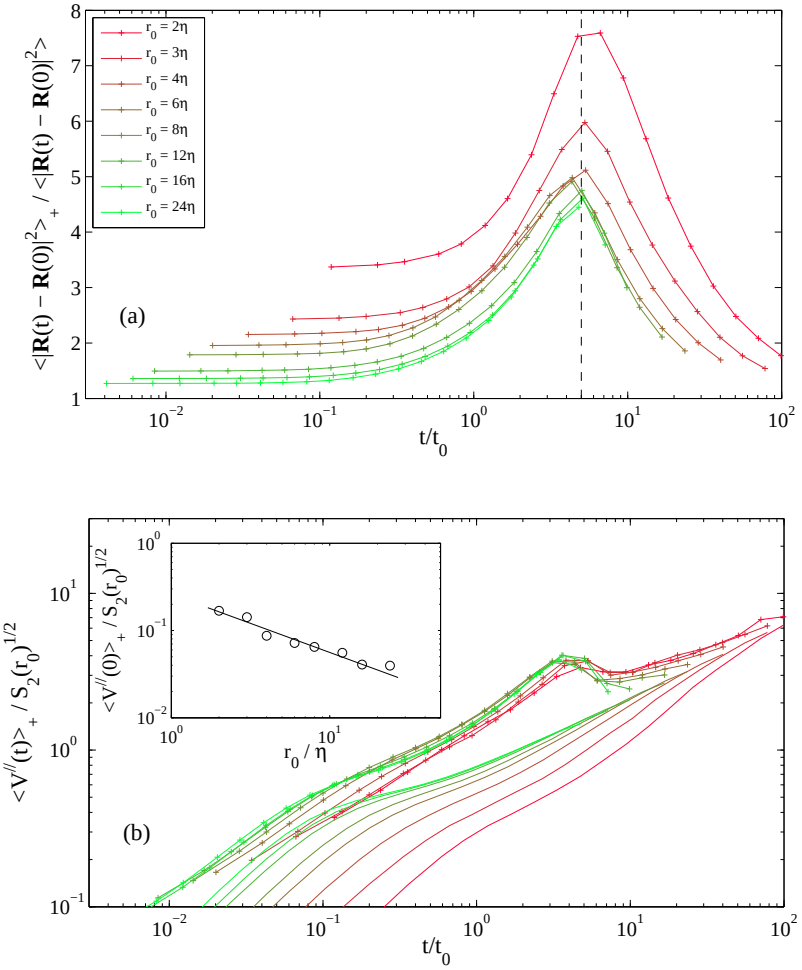

Figure 5.7: Conditional statistics over pairs that are at a distance at least twice the average at time $t_\mathrm{f} = 5t_0$ (conditional average on $|\boldsymbol{R}(5t_0)| \geq 2\,\langle|\boldsymbol{R}(5t_0)|\rangle_{r_0}$ is denoted by $\langle\cdot\rangle_+$). (a) Relative increase in the mean squared change of separation $\langle|\boldsymbol{R}(t) - \boldsymbol{R}(0)|^2\rangle_{r_0}$ as a function of time. (b) Averaged longitudinal velocity difference conditioned on the separation at time $t_\mathrm{f} = 5t_0$ (+) and without conditioning (solid line). Inset: initial value of the conditioned longitudinal velocity difference as a function of the initial separation; the solide line is $\propto r_0^{-2/3}$.

that the pairs that are well separated at a late time are preferentially separating from the very beginning. The initial longitudinal velocity fluctuation that is necessary for the pairs to be far apart at time t_f becomes weaker when r_0 increases. Data suggest that $\langle V^\parallel(0)\rangle_+/[S_2(r_0)]^{1/2} \propto r_0^{-2/3}$ as seen in

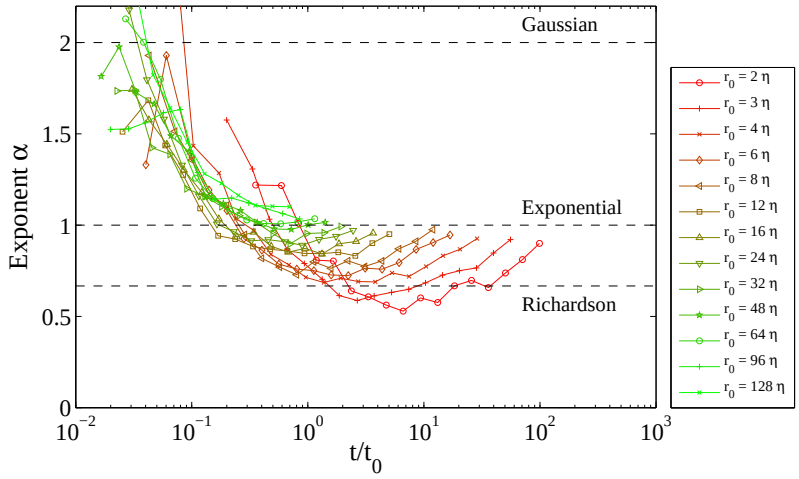

Figure 5.8: Exponent α of the right tail of the PDF of distances $|\boldsymbol{R}(t)|$ as a function of time and for various initial separations. The exponent was obtained by fitting $-\log p(|\boldsymbol{R}|)$ to a power-law for $\langle|\boldsymbol{R}(t)|\rangle_{r_0} < |\boldsymbol{R}(t)| < 0.5\,L$.

the inset. This initial separation makes the selected pairs reach an almost diffusive regime at time much shorter than the end of the average ballistic regime. For large-enough initial separations we indeed have $\langle V^{\parallel}(t)\rangle_{+} \sim t^{1/2}$ for $0.1\,t_0 \lesssim t \lesssim t_0$. The pair distance encountered a final acceleration before attaining the conditioning. After that, the longitudinal velocity difference relaxes slowly to the average regime. Again here, as in the case of the average separation, we observe that the imposing of having a large distance at a large time selects pair histories. The main contribution to statistics is indeed given by couples encountering an initially violent separation that is then followed by a rapid convergence to an explosive regime.

In order to give a more quantitative handle on the far tail of the separation PDF, we have estimated and fitted its functional shape and studied its variations. For that, following the observations made in Sec. 5.1.1, we have assumed that $p(|\boldsymbol{R}|) \propto \exp(-C\,|\boldsymbol{R}|^{\alpha})$ and measured how the exponent α depends on both time and initial separation.

Figure 5.8 shows the time behavior of the exponent α for various values of the initial separation. On the figure, the three dashed horizontal lines represent the tails of a Gaussian ($\alpha = 2$), of an exponential ($\alpha = 1$) and of Richardson's distribution ($\alpha = 2/3$). At time $t = 0$, the distribution is peaked around r_0 and compactly supported, so that $\alpha = \infty$. The exponent then decreases, crosses $\alpha = 1$ (so that the distribution becomes a stretched

exponential) for $t \approx 0.1\,t_0$, and reaches a minimal value that depends on the initial separation r_0. For the smallest r_0, this minimal value is below Richardson's prediction, as previously noticed. For larger separations, this minimum increases and when $r_0 \gg \eta$ the curves seem to saturate to the value $\alpha = 1$. Also, we cannot exclude that all curves converge to the exponential value when $t \to \infty$. The increase at the last stage can hardly be blamed on an integral-scale effect. We have indeed excluded here all pairs that are separated by a distance larger than $L/2$.

5.3 "Fractal distribution" at small distances

Much more violent and intermittent events take place for particle pairs that separate much less than the average. As already stressed and observed in Fig. 5.6, the large excursions of inter-trajectory distances go together with strong pinches of separations.

This is evidenced from Fig. 5.9 that represents the probability distribution of $|\boldsymbol{R}|$ at various times and for two inertial-range values of the initial separation. One observes that at very short times, the PDF is peaked around r_0. When time increases, its maximum, which roughly corresponds to the value of $\langle|\boldsymbol{R}(t)|\rangle_{r_0}$, shifts to larger values and the distribution broadens simultaneously at large and small values. This leads to the development for $r_0 \ll |\boldsymbol{R}| \ll \langle|\boldsymbol{R}|\rangle_{r_0}$ of an intermediate range of pairs whose separations lag behind the average evolution. In this subrange, the PDF behaves as a power law $p(|\boldsymbol{R}|) \propto |\boldsymbol{R}|^\beta$, where the exponent β evolves as a function of time and r_0. The power-law behavior is substantiated when measuring the cumulative probability $P^<(r) = \mathrm{Prob}[|\boldsymbol{R}| < r] = \int_0^r p(r')\,\mathrm{d}r' \propto r^{\beta+1}$ of inter-trajectory distances. One expects from Richardson's arguments that $\beta = 2$, so that $P^<(r) \propto r^3$. The exponent β can be interpreted in terms of fractal geometry. If all the trajectories were uniformly and independently distributed in space, the fraction of pairs at a distance less than r would be $\propto r^d$, where $d = 3$ is the space dimension. Also one would expect this fraction to be $\propto r^{d-1}$ if the trajectories were all confined on a surface, and $\propto r^{d-2}$ if they were on a curve. In general, the exponent $\beta + 1 = \lim_{r\to 0}[\log P^<(r)]/[\log r]$ measures the *correlation dimension* of a fractal set. Richardson's r^2 behavior thus corresponds to the idea that, at sufficiently long times, trajectories forget about their initial separation and distribute homogeneously in space.

As we have previously discussed, pair dispersion can be geometrically interpreted as the average Lagrangian evolution of an initially spherical surface of radius r_0 centered on a reference trajectory. At time $t = 0$, it is clear that $P^<(r)$ is a Heaviside function centered on $r = r_0$, so that $\beta = \infty$. At later

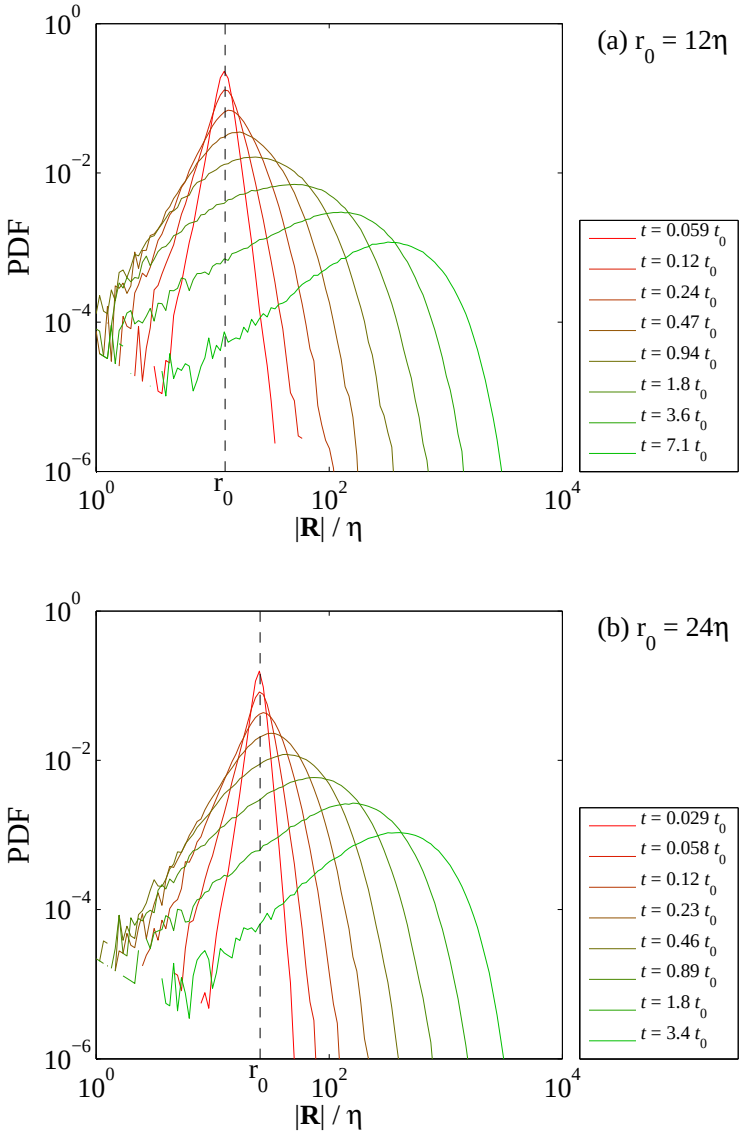

Figure 5.9: Unscaled PDFs of the absolute separation between tracers for various times and the initial separations (a) $r_0 = 12\,\eta$ and (b) $r_0 = 24\,\eta$.

times the stretching and pinching of the sphere leads to a non-trivial behavior of $P^<(r)$ for $r \ll \langle|\boldsymbol{R}|\rangle_{r_0}$. This behavior is sketched for two dimensions in Fig. 5.10. The exponent β is thus measuring the fractality of the image of the sphere by the Lagrangian flow. It relates to the fraction of this forward-in-time image that remains within a distance r of the reference trajectory. At sufficiently large times (right-most panel of Fig. 5.10), one expects the set of

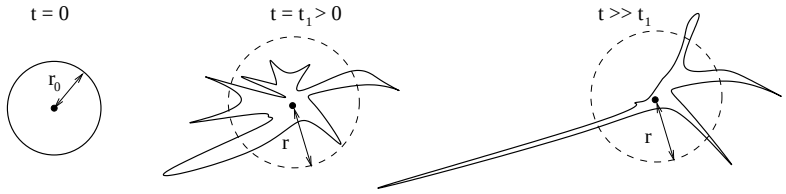

Figure 5.10: Two dimensional sketch of the time evolution of trajectories that are initially located at a distance r_0 of a reference tracer (shown as a black dot at the center of the circle) and then spread.

trajectories to be mainly stretched by the flow eddies with the most relevant correlation time, that is those of size $\langle |\boldsymbol{R}(t)| \rangle_{r_0}$, and the small scale fluctuations to become less and less important. Hence, at scales $r \ll \langle |\boldsymbol{R}(t)| \rangle_{r_0}$ and very large times, the only remaining pairs should be distributed on a surface (curve in two dimensions), so that $\beta + 1 \simeq 2$ and $p(r) \propto r$. This approach contradicts the prediction of Richardson that, somehow, postulates that the velocity difference correlation time does not depend on scale (as it is assumed to be zero).

To shed light on such ideas, we have estimated the exponent β for various r_0 and at different times. For this purpose, we have used the cumulative probability $P^<(r)$ (shown in Fig. 5.11 (a) for $r_0 = 4\eta$) to obtain $\beta + 1$ through a fit of its local slope. The resulting measurements are displayed in Fig. 5.11 (b) as a function of time. Up to the largest error bars due to a lack of statistics, one observes that the timescale t_0 is again relevant to describe both the initial dynamics and the convergence to an asymptotic regime. At small times $t \ll t_0$, the exponent β takes large positive values, which, as explained above, are due to the initial conditioning $|\boldsymbol{R}(t)| = r_0$. At time $t \approx 0.3\, t_0$, the exponent becomes smaller than 3. For $t \gg t_0$, it asymptotically approaches the value $\beta = 2$, so that data give evidence in favor of the argument exposed above. Interestingly, for small initial separations $r_0 \lesssim 16\eta$, the limit is reached from below and preceded by a minimum of β. This means that for such intermediate times, the pinching (or equivalently the stretching) of the sphere is so strong that the intersection of the latter with spheres of radius r defines a fractal object that is more concentrated than a surface. Such a temporary singular behavior is certainly related to the presence of tails fatter than exponential at very large distances.

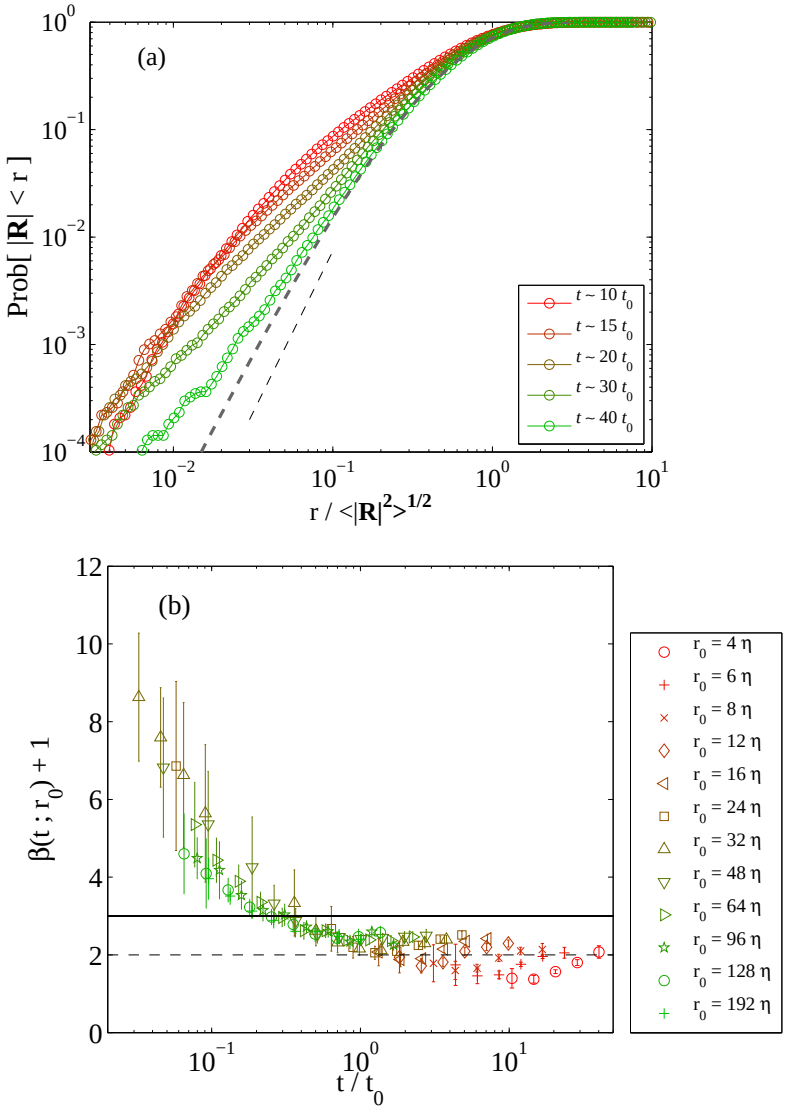

Figure 5.11: (a) Cumulative probability distribution of the distance $P^{<}(r) = \text{Prob}[|\boldsymbol{R}| < r]$ as a function of r for $r_0 = 4\eta$ and at various times; the gray dashed curve is the cumulative probability associated to Richardson's distribution that displays a behavior $\propto r^3$ at small distances. (b) Time evolution of the left-tail power-law exponent β for various values of the initial separation. The black solid line shows $\beta = 2$ corresponding to Richardson's distribution and the dashed line stands for the value $\beta = 1$ that is argued in the text.

5.4 Summary and perspectives on the problem of pair dispersion

In this section, we draw some conclusions on the work of this thesis related to turbulent pair dispersion that were reported in Chapters 4 and 5. We here focus on rather specific questions from a purely Lagrangian turbulence point of view. We believe that the problem of relative Lagrangian motion, in addition to its numerous applications to turbulent transport, can shed some new lights on basic aspects of the physics of turbulent flows.

In Chapter 4, we reported results on the timescales of convergence of turbulent pair dispersion to an asymptotic regime. We have seen that low and medium-order moments of the particle separation approach an asymptotic regime on times of the order of $t_0 = S_2(r_0)/(2\epsilon)$, where $S_2(r_0)$ denotes the (absolute value) structure function associated to the initial separation r_0 and ϵ is the mean rate of kinetic energy dissipation. This timescale has been shown to be relevant to describe also the initial kinematic change of sign of the longitudinal velocity difference $V^{\parallel}$ and the tails of the distance distribution at small values. However, we have seen that t_0 is not relevant to describe the convergence of the velocity difference statistics to an asymptotic regime. We have observed that up to the largest time, the skewness, the flatness, and more generally the shape of the velocity difference distribution still depend on the initial separation, even when time is rescaled by t_0. This leads to a behavior that is by far more intermittent than that of separations.

Also, it has been demonstrated that the Richardson explosive regime $\langle |\boldsymbol{R}|^2 \rangle \propto t^3$ for the separation between two tracers in a turbulent flow originates from a diffusive behavior of their velocity difference rather than from a scale-dependent eddy diffusivity for their distance, as commonly believed. This leads on to reinterpret the t^3 law as that of the integral of Brownian motion. Such an argument is mainly supported by two observations. First of all, the acceleration difference has a short correlation time, of the order of the Kolmogorov timescale, and this allow us to approximate it as a white noise. Second, the amplitude of this noise solely depends on the local dissipation rate $\langle [V^{\parallel}]^3/R \rangle_{r_0}$, which stabilizes to a stationary behavior with a constant mean also on short timescales. This behavior, which, to our knowledge, has never been observed before, gives very strong constraints for the development and validation of stochastic Markovian models for turbulent relative dispersion.

A central question that deserves being raised concerns the physical mechanisms leading to this fast convergence of the "local dissipation" to a statistically stationary behavior. At the moment, an even phenomenological

explanation is still missing. We have understood that kinematic considerations can be used to explain why $\langle [V^{\parallel}]^3/|\boldsymbol{R}|\rangle_{r_0}$, which is initially negative, becomes quickly positive. This is due to the fact that initially approaching trajectories will always eventually separate. However, there is no clear idea of why this average should converge to a time-independent value. Possible ideas could consist in finding other mixed moments that are strictly (and not asymptotically) conserved by the two-point turbulent Lagrangian flow. Such considerations are kept for future work.

The interpretation of Richardson's law in terms of diffusion of velocity differences strongly questions possible effects of fluid-flow intermittency on trajectory separation. Indeed, considerations on velocity scaling, which are primordial in approaches based on eddy diffusivity, are absent from the arguments leading to a diffusive behavior of $\boldsymbol{V}$. Hence, we expect the separation $\boldsymbol{R}$ to almost follow a self-similar evolution in time, independently on the order of the statistics. This has been evidenced in Chap. 5. Intermittency will however affect directly the time of convergence to such a regime. More frequent violent events, such as tracer pairs approaching or fleeing away in a strongly anomalous manner, will result in longer times for being absorbed by the average. Such arguments do not rule out the possibility of having intermittency corrections when interested in other observables than moments of the separation, as it is for instance the case for exit times [Boffetta & Sokolov, 2002a]. Such issues will certainly gain much from a systematic study of multidimensional generalizations of the stochastic model that was introduced in Chap. 4.

In Chap.5, we obtained evidence that the far tail distribution of the separation (at distances much larger than the average) is keeping a nontrivial memory on r_0 up to the largest times. Also the tail associated to small separations is keeping memory of the conditioning on the initial separation and this is reinterpreted in terms of fractal set geometry. In all these studies, we made an important use of geometrical considerations to explain phenomenologically the statistical events leading to extreme fluctuations. In particular, we argued and obtained numerical evidence that, at sufficiently large times, the probability distribution $p(r)$ of inter-tracer distances is $\propto r$ for $r \ll \langle|\boldsymbol{R}|\rangle_{r_0}$ and decays as $\exp(-C\,r)$ when $r \gg \langle|\boldsymbol{R}|\rangle_{r_0}$. These two observations strongly contradicts Richardson's eddy diffusivity approach, which seems nevertheless to give a good approximation of the core of the distribution.

Another possible extension of the current study is to apply the developed understanding of the geometry of relative dispersion to more complicated turbulent transport situations involving more than two trajectories. This is for instance the case for the forward-in-time dynamics of triangles or tetrahedrons studied in [Pumir et al., 2000]. The quality of today numerical data

would be very useful to revisit such questions with an emphasize on extreme events. Another situation that is much closer to applications is that of the transport by turbulence of pollutant patches. We have seen in this chapter that relative dispersion relates to the distorsion of a sphere by the Lagrangian flow. We related the small-scale behavior of separation statistics to the fractal dimension of this object. Such geometrical considerations could be generalized to understand and quantify the large concentration fluctuations in the dispersion of a pollutant spot. We will come back to such considerations in Chap. 7 for the general conclusion of the thesis.

Finally, the mechanisms that we have described in these two Chapters and that are responsible for large fluctuations in dispersion are purely turbulent and concern tracers. In real situations, additional effects due to the non-ideal dynamics of the transported particles can interfere with these phenomena. For instance, the turbulence of the carrier flow will tend to separate the trajectories in an explosive manner while at the same time, the particle inertia might be responsible for preferential concentration. How these two effect that are acting in reverse manner interact is still an open question. In the next chapter, we will try to shed some light on such problems by reinterpreting the dispersion of heavy inertial particles in a turbulent flow as a diffusion in a self-similar fluctuating environment.

Chapter 6

Mass fluctuations and diffusions in random environments

When interested in dissipative transport (as for instance in compressible flows or for inertial particles) the dynamics tends to create very strong spatial inhomogeneities. This is usually due to a strong correlation at small scales between the transported density and the local structure of the flow. At scales much larger than the correlation length of the flow, such inhomogeneities generally disappear as the transport becomes diffusive. However, in between these two asymptotics, fluctuations appear in the density field. They come from a mesoscopic average of the small-scale clustering mechanisms.

In nature there are many other situations where small-scale mechanisms contribute only through an averaged effect to the processes at larger scales. This is generally modeled as a fluctuating environment whose time scales of variation are much smaller than those typical of the process that we want to understand. This is for instance the case for diffusion in settings that are not at thermal equilibrium or for wave propagation in non-uniform media. In statistical physics, such phenomena are considered as systems with the presence of a disordered state that is not in thermodynamical equilibrium and is called *quenched disorder*. This name is due to the fact that the behavior of these systems is defined by random and time invariant variables. Classical cases of quenched disorders are the directed polymers [Imbrie & Spencer, 1988, Halpin-Healy & Zhang, 1995], the wave propagation in random media [Howe, 1971], the heat transport in open-cell foams [Wang & Pan, 2008], and the viscous permeability in porous materials [Sahimi, 2011]. The main goal is usually to derive an effective diffusivity, conductivity, or permeability of the medium [Dean et al., 2007]. In order to describe these kind of environments, several models introducing some random disorder have been developed to derive the effective properties of the medium. Among all we recall, for in-

stance, the Kraichnan velocity ensemble for turbulent transport [Kraichnan, 1968] and the Sherrington–Kirkpatrick model for spin-glasses (i.e. magnetic disorder) [Parisi, 1979, Mezard et al., 1987, Sherrington & Kirkpatrick, 1975].

In this chapter we motivate the study of fluctuations in the transport of heavy particles in terms of mass ejection models. We will then consider one-dimensional diffusive processes in quenched random media. In particular we are interested in discrete versions, better known as *random walks in random environment*. For the sake of simplicity from now on, it will referred to as RWRE. The work reported here is the subject of a publication in the *New Journal of Physics* [Krstulovic et al., 2012].

6.1 Fluctuations in heavy particle density as an ejection process

In this section, we give some motivations for studying the fluctuations in the spatial distribution of heavy particles in terms of certain types of random walks in random environments. Let us first recall what we intend as "heavy inertial particle". We have seen in Sec. 3.2.2 that particles whose size is much smaller than the Kolmogorov scale, with a Reynolds number (defined with their slip velocity) much less than unity, and a mass density much larger than the carrier fluid have a dynamics given by

$$\frac{d\mathbf{x}}{dt} = \mathbf{v}, \quad \frac{d\mathbf{v}}{dt} = -\frac{1}{\tau_s}[\mathbf{v} - \mathbf{u}(\mathbf{x}, t)], \tag{6.1}$$

where the response time τ_s depends on the particle size and density. In the limit $\tau_s \to 0$, the particles respond instantaneously to the flow and one recovers the dynamics of tracers. It is known since the work of Maxey [Maxey, 1987] that such heavy particles tend to be ejected from the rotating structures of the flow and to concentrate in the straining regions. This is evidenced in Fig. 6.1 (Left) which shows a snapshot of the distribution of heavy particles, together with the underlying structures of the fluid flow. What is shown is the result of a small numerical simulation of the two-dimensional Navier–Stokes equation.

To understand this ejection phenomenon, let us consider a linear rotating flow in two dimensions, namely

$$\mathbf{u}(\mathbf{x}, t) = \Omega \begin{bmatrix} x_2 \\ -x_1 \end{bmatrix} = \Omega \begin{bmatrix} 0 & 1 \\ -1 & 0 \end{bmatrix} \mathbf{x}, \tag{6.2}$$

where Ω is the vorticity that measures the strength of the vortex. The particle

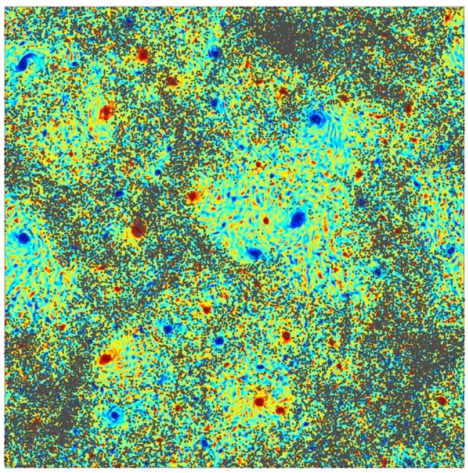

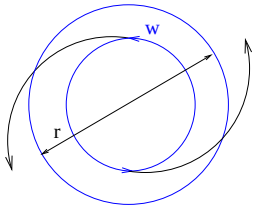

Figure 6.1: Left: snapshot of the positions of heavy particles (gray dots) and of the vorticity field (curl of velocity) of a two-dimensional turbulent flow (colored background). Blue and red structures are flow vortices. Note the strong anti-correlation between the spatial distribution of particles and that of eddies (courtesy of J. Bec). Right: sketch of the centrifugal ejection process for heavy particles (black trajectories) in a rotating flow (in blue).

dynamics is then linear and can be integrated. In the position-velocity phase-space, the four eigenvalues are then

$$\lambda_{\pm,\pm} = \frac{-1 \pm \sqrt{1 \pm 4\mathrm{i}\tau_s\Omega}}{2\tau_s}. \tag{6.3}$$

Two of them ($\lambda_{+,-}$ and $\lambda_{+,+}$) always have a positive real part. This implies that particle trajectories are always moving away from the origin exponentially in time. If we now assume that the rotating structure of strength Ω has a finite size r (see Fig. 6.1 Right), it is clear that the amount of particles within a distance r from the origin will decrease exponentially in time.

Indeed, one can easily check that the number of particles at a distance r from the origin will be given by

$$\begin{aligned} N(t) &= N(0)\,(1-\gamma) \\ &\text{with } \gamma = 1 - \exp\left[-\frac{t}{\tau_s}\left(-1 + \frac{1}{2}\sqrt{2\sqrt{1+16\tau_s^2\Omega^2}+2}\right)\right], \end{aligned} \tag{6.4}$$

which explains ejection from the rotating structures of the flow.

One observes in Fig. 6.1 (Left), that the fluctuations in the distribution of particles extend to scales much larger than the typical size of eddies. Despite the fact that rotating or straining regions are differenced only at

small spatial scales, their averaged collective effect can lead to the formation of clusters and voids on much larger scales. The mechanisms explaining this are due to the fluctuations of the vorticity field itself. Such idea led Bec and Chétrite [Bec & Chétrite, 2007] to introduce a mass ejection model to describe the meso-scale fluctuations of the density of inertial particles. Here it is given a generalization of this model that justifies the study made in the following Chapter.

Consider that the two-dimensional domain is divided in regular square cells of size $\Delta x = r$ (indexed by (i,j)), each of them containing between time t_n and time $t_{n+1} = t_n + \Delta t$ a given ejecting structure of strength $\Omega_{i,j}(n)$. The particles in each cell will then be ejected to the four direct neighbors with a rate $\gamma_{i,j}(n)$ given by replacing Ω by $\Omega_{i,j}(n)$ and t by Δt in Eq. (6.4). The density $\rho_{i,j}$ of particles in the cell (i,j) then evolves according to

$$\begin{aligned}\rho_{i,j}(n+1) &= [1-\gamma_{i,j}(n)]\,\rho_{i,j}(n) + [\gamma_{i-1,j}(n)\,\rho_{i-1,j}(n) + \gamma_{i+1,j}(n)\,\rho_{i+1,j}(n) \\ &\quad +\gamma_{i,j-1}(n)\,\rho_{i,j-1}(n) + \gamma_{i,j+1}(n)\,\rho_{i,j+1}(n)]/4. \qquad (6.5)\end{aligned}$$

As argued in Sec. 6.3, one recognizes in the right-hand side the two-dimensional discrete Laplacian of $\gamma_{i,j}(n)\rho_{i,j}(n)$. This means that the continous limit (when $\Delta_x \to 0$ and $\Delta t \to 0$ with $\Delta x^2/\Delta t$ constant) of Eq. (6.5) is

$$\partial_t \rho = \frac{1}{4}\nabla^2(\bar{\gamma}(\mathbf{x},t)\,\rho), \qquad (6.6)$$

where $\bar{\gamma}(i\Delta x, j\Delta x, n\Delta t) = \gamma_{i,j}(n)$. As we can see from this model, the fluctuations of the small-scale processes are now encoded in the spatial and time dependence of the continuous ejection rate $\bar{\gamma}$. Its statistical properties are in principle prescribed by those of the fluid velocity gradients. This approach hence justifies the use of a mass ejection model with a random rate to describe the meso-scale distribution of heavy particles in an incompressible flow.

6.2 Generality on random walks

Random walks, whose name has been introducted by the British mathematician K. Pearson [Pearson, 1905], have been studied and used to explain the behavior of stochastic processes in various fields of science as well as in economy and other domains. The environment in which a random walk evolves is characterized by the transition law that says how the *walker* steps from the current position to the next one. Clearly the environment can be given by any law. As already seen in Sec. 3.1.2, there are different types of random walks and their level of complexity makes them more suitable to describe a

process rathen than another. In case of diffusive processes in quenched random media, one usually applies RWRE techniques. Many mathematicians and physicists have largely investigated RWRE in their discrete version for simple reasons of handability in theoretical studies [Hughes, 1996].

Generally one considers a lattice with a fixed random probability of transition from a site to another and on this setting the behavior of a random walk is studied. A classic reference for random walks on the integer lattice is the book [Spitzer, 1976]. Much work has been dedicated to a delicate point, that is to determine the assumptions under which RWRE are transient or recurrent. In other words, to establish whether they escape to infinity or indefinitely come back to their starting position. For a time-independent random environment with no space correlations, it has been shown that the randomization of the environment slowdowns the diffusive properties of the random walk [Solomon, 1975]. Furthermore, under some precise assumptions, Y. G. Sinai [Sinai, 1982] proved that one-dimensional nearest-neighbor symmetric random walks (which consist in walkers that can only step between the current position and a point in its neighbors, with a symmetric transition probability, i.e. $p(x, y) = p(y, x)$, where x and y are two different positions) in an uncorrelated environment are sub-diffusive and that, at very large time, the position goes like

$$X_t \sim \log^2 t, \quad \text{for } t \to \infty, \tag{6.7}$$

where X_t denotes the position of the walker at time t. In the same year B, Derrida and Y. Pomeau have demonstrated that when the assumption of symmetry is relaxed, the evolution of the position for a random walk follows a power law in time [Derrida & Pomeau, 1982]

$$X_t \sim t^{\alpha}, \tag{6.8}$$

where the exponent α is greater than zero and smaller than one. More recently it was showed that the upper critical dimension for random walks in a time-independent random environment is equal to 2. Namely, in dimensions greater than 2, RWRE are always purely diffusive [Bricmont & Kupiainen, 1991]. In the last decade important efforts have been also devoted to prove central-limit theorems or large-deviations principles for quenched disorders [Sznitman, 2004, Zeitouni, 2004, Varadhan, 2004]. Generally, it is assumed that the environment is independent of time and uncorrelated in space, or at least with very short spatial correlations.

On the contrary, much less is known in case of time-dependent environments. One then deals with annealed statistics (that is a disordered system described by random time-dependent variables) where the averages must be

performed over the fluctuations of the random medium. In such settings and under some rather general assumptions, it was shown that random walks are always diffusive and that central limit theorems generally hold [Bérard, 2004, Dolgopyat et al., 2008].

In this part of my thesis the interest is focused on situations where both temporal and spatial scales of diffusion are comparable, or longer, than those at which the environment fluctuates. This is equivalent to have a time-dependent random medium whose temporal and spatial correlations cannot be neglected. An instance where such settings are relevant is turbulent transport. As we have seen in previous section, the fluctuations of the density in heavy inertial particle suspensions can be captured, at least qualitatively, by diffusions in a time-varying random environment. However, also in the case of simple tracers, such an approach can be relevant. In that case, most of the models that are classically used, for example in meteorology and engineering, are based on an *eddy-diffusivity* approach [Frisch, 1996], which in general requires a large time-scale separation between the turbulent fluctuations and the large-scale variations of the averaged velocity field. Advanced homogenization techniques can be applied to show that the mean concentration field satisfies an effective advection-diffusion equation, with an advecting velocity and a diffusion coefficient tensor that are dependent on the slow variables describing the evolution in time and space of the average velocity field [Goudon & Poupaud, 2004]. The mixing at large scale, originating from fluctuations at small scales, acts only through the diffusive term. At the same time, as the solutions to a diffusion equation obey a maximum principle, the diffusive term cannot be responsible for the creation of large concentrations. Therefore the concentrations observed in compressible flows can only come from the effective advection term. As we have seen in Sec. 6.1 and as we will further discuss in this chapter, the situation can be somewhat different when interested in other types of compressible transport, as for instance for inertial particles.

6.3 Description of the model

We consider the dynamics described by the Itō stochastic differential equation, defined by

$$\mathrm{d}\mathbf{X}_t = \sqrt{2\Gamma}\,\sigma(\mathbf{X}_t, t)\,\mathrm{d}\mathbf{W}_t, \tag{6.9}$$

where $\mathbf{W}_t$ is the classical d-dimensional Wiener process, already discussed in Sec. 3.1.2. We suppose here that the diffusion coefficient $\sigma(\mathbf{X}_t, t)$ is a random, space-time dependent field, whose statistics are independent of $\mathbf{W}_t$

as we will see afterwards. Before specifying the settings considered, it might be useful to motivate such model by considering, for instance, two interesting physical problems where Eq. (6.9) arises as a limiting process.

As a first example let us consider particles whose dynamics is dissipative in the entire phase space and assume that their trajectories obey the Newton equation

$$\dot{X}_t = V_t, \qquad \dot{V}_t = -\mu V_t + \frac{1}{\sqrt{\varepsilon}} f\left(X_t, t, \frac{t}{\varepsilon}\right), \tag{6.10}$$

where μ is the Stokes viscous damping coefficient and ε is a small parameter. Here the vectorial notation is neglected but still all considerations in what follows can be easily generalized to any dimension. Equation (6.11) describes, for instance, the dynamics of a heavy inertial particles in a velocity field that varies over two different time scales that are separated by a factor ε. In this equation the forces acting on the particle are the viscous drag and the external force f, which depends on space and on two different time scales (t and t/ϵ). If we imagine to have a large particle embedded in a time and space dependent thermal bath, the fast timescale ε can be interpreted as the typical time of momentum exchange between the particle and its environment. As in the Einstein original work on Brownian motion, the timescale ε is much smaller than the viscous damping time $1/\mu$. In the limit when $\varepsilon\mu$ vanishes, the force f can be considered as a Gaussian noise with correlation

$$\begin{aligned} C(t,t') &= \left(\frac{1}{\varepsilon}\right) \left\langle f\left(X_t, t, \frac{t}{\varepsilon}\right) f\left(X_{t'}, t', \frac{t'}{\varepsilon}\right) \right\rangle_\varepsilon \\ &\simeq 2\Gamma\mu^2\sigma^2(X_t,t)\delta(t-t'), \end{aligned}$$

where the average $\langle\cdot\rangle_\varepsilon$ is done with respect to the fast time variable. The space-time variations of σ^2 can be interpreted as a non-homogenous temperature field in the thermal bath associated to the δ-correlation in time. The resulting dynamics is thus

$$\dot{X}_t = V_t, \qquad \dot{V}_t = -\mu\left[V_t - \sqrt{2\Gamma}\,\sigma(X_t,t)\,\eta(t)\right], \tag{6.11}$$

where η is the standard white noise.

We next consider the limit when the response time $1/\mu$ is much shorter than the slow time scale. This introduces a new fast time scale $\mathrm{O}(1/\mu)$ over which the particle velocity fluctuates. The velocity correlation is then given by

$$\langle V_t\, V_{t'}\rangle_\varepsilon = \int_{-\infty}^{t}\int_{-\infty}^{t'} C(s,s')\mathrm{e}^{\mu(s+s'-t-t')}\mathrm{d}s\,\mathrm{d}s' = \int_{-\infty}^{\min\{t,t'\}} 2\Gamma\mu^2\sigma^2(X_s,s)\mathrm{e}^{\mu(2s-t-t')}\mathrm{d}s$$

Therefore, integrating by parts and neglecting exponentially small terms, we obtain

$$\langle V_t\, V_{t'}\rangle_\varepsilon \approx \Gamma\,\mu\,\sigma^2(X_{\min\{t,t'\}}, \min\{t,t'\})\,\mathrm{e}^{-\mu|t-t'|}. \tag{6.12}$$

Finally, taking the limit $\mu \to \infty$ in Eq. (6.12) we have

$$\langle V_t\, V_{t'}\rangle = 2\Gamma\,\sigma^2(X_t,t)\delta(t-t'). \tag{6.13}$$

The particle position thus satisfies the stochastic equation (6.9). The model that we are considering is thus relevant in studying of Langevin dynamics in a fluctuating environment.

The second situation where Eq. (6.9) appears is in the continuous limit of a mass-ejection model, as we have already forseen in Sec. 6.1. To address this issue let us consider a d-dimensional periodic lattice of internode length Δx and period $L = N\Delta x$. Naturally, also the time is discrete and it is expressed in units of Δt. Such a lattice defines a tiling on which our discrete-time dynamics is considered. Basically, the generic cell indexed by $\mathbf{i}$ (with $\mathbf{i} = 1, 2, \ldots, N$) contains at time $n\Delta t$ a given mass $\rho_{\mathbf{i}}(n)$. Between two consecutive times $n\Delta t$ and $(n+1)\Delta t$, a fraction $\gamma_{\mathbf{i}}(n)$ (ranging from 0 to $1/(2d)$) of such mass is ejected from the cell $\mathbf{i}$ to one of its $2d$ neighbors. Clearly the periodic boundary conditions ensure that the total mass $M = \sum_{\mathbf{i}=\mathbf{1}}^{N} \rho_{\mathbf{i}}$ is conserved. For a given set of ejection rates $\{\gamma_{\mathbf{i}}(n)\}_{\mathbf{i}\in\{1,\ldots,N\}^d}$ the variables $\{\rho_{\mathbf{i}}(n)\}_{\mathbf{i}\in\{1,\ldots,N\}^d}$ define a Markov chain whose master equation is given by

$$\rho_{\mathbf{i}}(n+1) = [1 - 2d\,\gamma_{\mathbf{i}}(n)]\,\rho_{\mathbf{i}}(n) + \sum_{\mathbf{j}\in\mathcal{N}_{\mathbf{i}}} \gamma_{\mathbf{j}}(n)\rho_{\mathbf{j}}(n), \tag{6.14}$$

where $\mathcal{N}_{\mathbf{i}}$ is the number of the neighboring cells of $\mathbf{i}$-th cell and d is a generic dimension. Equation (6.14) describes a mass-ejection process in a time-dependent and non-homogeneous environment determined by the ejection rates $\gamma_{\mathbf{i}}(n)$. It states that the amount of mass contained in the $\mathbf{i}$-th cell is given by the sum of the mass contained at the previous time, the fraction $\gamma_{\mathbf{i}}(n)$ of mass ejected and the fraction of mass coming from the neighboring cells. As already mentioned, a similar model has been studied by [Bec & Chétrite, 2007] in the particular case where the environment $\gamma_{\mathbf{i}}(n)$ takes only two values, γ or 0, uncorrelated in both space and time.

We now take the ejection model in Eq. (6.14) and switch from the discrete to the continuous case considerin the limits $\Delta x \to 0$ and $\Delta t \to 0$ and, doing this, we suppose that the ratio $\Delta x^2/\Delta t = c$ is kept fixed. We denote the continous limit of the ejection rate by

$$\Gamma\sigma^2(\mathbf{x},t) = \lim_{\Delta x\to 0} c\,\gamma_{\mathbf{x}/\Delta x}(c\,t/\Delta x^2).$$

We choose here σ of the order of unity, so that the coefficient Γ denotes the typical amplitude of the ejection rate. The dimensionless function $\sigma(\mathbf{x}, t)$ is assumed to be time and space continuous. In this limit, Eq. (6.14) becomes

$$\frac{\partial \rho(\mathbf{x}, t)}{\partial t} = \Gamma \nabla^2 \left[\sigma^2(\mathbf{x}, t)\rho(\mathbf{x}, t)\right]. \tag{6.15}$$

This is the Fokker-Planck equation associated to the Itō stochastic differential Eq. (6.9). For a time $t > s$, we define the forward transition probability density

$$p(\mathbf{x}, t \,|\, \mathbf{y}, s) = \langle \delta(\mathbf{X_t} - \mathbf{x}) \,|\, \mathbf{X_s} = \mathbf{y} \rangle, \tag{6.16}$$

where $\langle \cdot \rangle$ designates averages with respect to the realizations of the Wiener process $\mathbf{W}_t$. Then the solutions to Eq. (6.15), for all times t greater than s, trivially satisfy

$$\rho(\mathbf{x}, t) = \int p(\mathbf{x}, t \,|\, \mathbf{y}, s)\, \rho(\mathbf{y}, s) \mathrm{d}\mathbf{y}. \tag{6.17}$$

The model described by the diffusion equation Eq. (6.15) can thus be reinterpreted in terms of a RWRE. Indeed, the discrete version of the process defined by Eq. (6.9) corresponds to a random walk on a d-dimensional lattice, with a probability equal to $2d\,\gamma_{\mathbf{i}}(n)$ to hop from the $\mathbf{i}$-th site to one of its neighbors.

6.4 Statistical properties of the random environment

6.4.1 Definition of the random ejection rate

In the following we specify the statistical properties of the random environment σ that is used in our model. We consider d-dimensional periodic settings in a domain of size $L = 2\pi$. The environment $\sigma(\mathbf{x}, t)$ is then entirely determined in terms of its Fourier series, which can be written as

$$\sigma(\mathbf{x}, t) = \sum_{|\mathbf{k}|} a_{\mathbf{k}}\, \chi_{\mathbf{k}} \left(\frac{t}{\tau_{\mathbf{k}}}\right) \mathrm{e}^{i\mathbf{k}\cdot\mathbf{x}}, \tag{6.18}$$

where the $a_{\mathbf{k}}$'s are positive real amplitudes and the $\tau_{\mathbf{k}}$'s are scale-dependent characteristic times. The Fourier modes $\chi_{\mathbf{k}}$ are such that

$$\chi_{-\mathbf{k}}(t) = \overline{\chi}_{\mathbf{k}}(t) \quad \text{and} \quad \chi_{\mathbf{0}} \equiv 0.$$

They are independent Gaussian processes with unit variance and unit correlation time. The modes $\chi_{\mathbf{k}}$ are chosen as complex Ornstein–Uhlenbeck

processes that solve the stochastic differential equation [Uhlenbeck & Ornstein, 1930]

$$\mathrm{d}\chi_{\mathbf{k}}(s) = -\chi_{\mathbf{k}}\mathrm{d}s + \sqrt{2}\,\mathrm{d}B_{\mathbf{k}}(s), \tag{6.19}$$

where the $B_{\mathbf{k}}$'s are independent, one-dimensional complex Wiener processes.

We now prescribe some scale-invariance properties for the random medium. Our interest is in environments that satisfy, in a given statistical sense,

$$|\sigma(\mathbf{x}+\mathbf{r},t) - \sigma(\mathbf{x},t)| \sim |\mathbf{r}|^h, \tag{6.20}$$

where h is the *local Hölder exponent* of σ and controls, in our case, the regularity of the ejection rate. In general h can take any values but it is equal to 0 at points of discontinuity, 1 at differentiable points where $\sigma' \neq 0$ and it is non-negative only if the function is bounded around x. This exponent can be also seen as a sort of "local scale" in the sense of fractal geometry (see [Mandelbrot, 1983]). Some other considerations on the Hölder exponent are reported at the end of this paragraph. We request that the exponent h being positive and less than 1. We assume that the Fourier mode amplitudes behave as

$$a_{\mathbf{k}} = \frac{1}{2}\,|\mathbf{k}|^{-\frac{1}{2}-h}. \tag{6.21}$$

This corresponds to prescribing that (6.20) is satisfied for the second-order moment of the environment increments.

The temporal scale invariance is setted by taking $\tau_{\mathbf{k}} = |\mathbf{k}|^{-\beta}$ with $\beta > 0$. This latter exponent β relates the time dependence to the spatial scale invariance; in particular when $\beta = 0$ the function σ has a single correlation-time, while when $\beta \to \infty$ one has a white-noise. As we shall see below, when $h < 1$ dimensional analysis will lead to choose $\beta = 2 - 2h$.

6.4.2 Numerical methods

In the numerical results that are presented hereafter, the averages are performed by summing over several realizations of the environment. These realizations are obtained by integrating the stochastic equation (6.19) for the evolution of the mode amplitudes by a standard stochastic Euler scheme. The time evolution of the mass distribution is obtained in two different manners, depending on the nature of the question we want to address. A first approach consists in using an Eulerian scheme that integrates the partial differential equation (6.15) for the time evolution of the density field ρ. For that we implemented a second-order finite-difference discretization for the Laplacian operator and a semi-implicit Euler temporal scheme. This numerical scheme ensures the conservation of the total mass with a high accuracy.

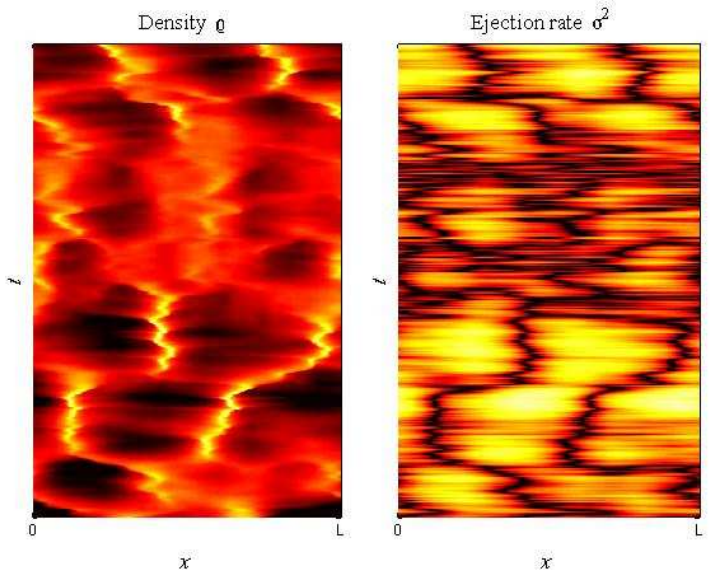

Figure 6.2: Left: space-time plot of the density $\rho(x,t)$ in one dimension for $h = 1$. Colors yellow and black correspond to highest and lowest values of density, respectively. Right: evolution of the ejection rate $\sigma^2(x,t)$. Same code color as before. Both left and right pannels refer to the same realization.

The numerical resolutions vary in one dimension from $N = 512$ to $N = 8192$ collocation points and the time-step is chosen small enough to resolve with precision the fastest time scale occurring in the problem. The second method we use is a Lagrangian Monte–Carlo approach, which consists in integrating the stochastic differential equation (6.9) for different realizations of the noise, and using again a standard stochastic Euler scheme. In both cases, we expect the error made on the solution to act as a numerical diffusion with a constant diffusivity proportional to the time step.

Figure 6.2 represents the temporal evolution of the density $\rho(x,t)$ (left panel) and of the ejection rate $\sigma^2(x,t)$ (right panel) for a typical realization in one dimension. One observes strong correlations between the maxima of density (yellow curves on the left panel) and the zeros of the environment (black curves on the right panel). Figure 6.3 shows simultaneously a snapshot of the random environment σ and the position of a set of diffusive particles. The particle positions are given by the stochastic equation (6.9) in two dimension. As seen in Fig. 6.3, the high density zones of particles are located in the vicinity of the zeros of the environment.

The zeros of the random ejection rate play an important role on the statis-

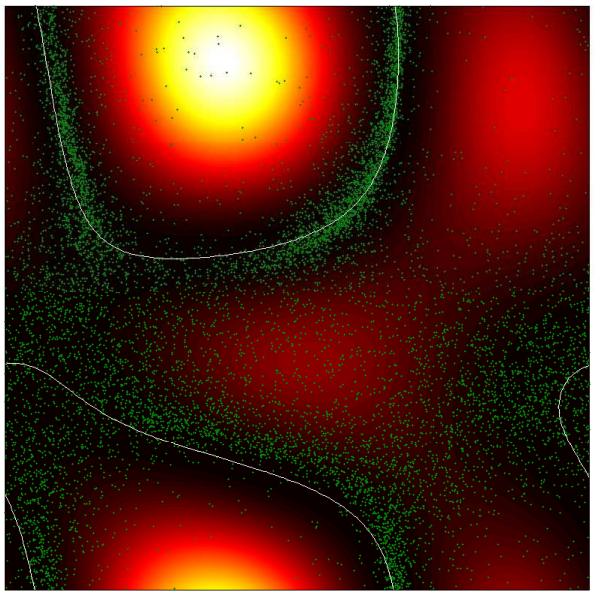

Figure 6.3: Snapshot of $\sigma^2(x,t)$ in two dimension and of the particle positions (green dots) that obey Eq. (6.9). Colors yellow and black correspond to highest and lowest values of σ, respectively; thin white lines represent the contour corrisponding to $\sigma = 0$.

tical properties of the mass density and on the particles diffusion properties; this will be further discussed throughout this chapter.

6.4.3 Phenomenology and dimensionless parameters

The important role of zeros can be heuristically understood in the following way. In contrast with the standard diffusion equation coming from Fick's first law, the differential operator $\nabla^2[\sigma^2(\mathbf{x},t)\,\cdot]$, appearing in the right-hand side of Eq. (6.15), is not positive definite. In such a case the maximum principle is not valid and the solution is expected to behave very differently from those of classical diffusion equations. Indeed, the mass gradually accumulates on the zeros of σ. Suppose that in one dimension $\sigma(x,t) \simeq Cx$ in the vicinity of $x = 0$, where C is a given constant. At leading order, the flux then reads

$$J = -\Gamma\partial_x(\sigma^2\rho) \simeq -2\Gamma C^2 x\rho,$$

which is positive for $x < 0$ and negative for $x > 0$. Thus, there is a permanent flux of mass towards the point $x = 0$. This justifies the importance of characterizing the zeros, their densities and their lifetimes.

The distribution and time-evolution of the zeros of σ strongly depend on the dimensionality and on the parameter h. It is clear from the right panel of Fig. 6.2 that the zeros follow random paths in dimension one. We can also observe that for such a large value of h, that is for a smooth environment, the zeros typically appear in pairs and then diffuse and separate until they merge together or with another zero. The diffusive behavior of the zeros in one dimension can be explained heuristically. For this, let us assume without loss of generality that the ejection rate has only two modes and takes the simple form

$$\sigma(x,t) = \sigma_r(t)\,\cos x - \sigma_i(t)\,\sin x, \tag{6.22}$$

with $\sigma_r + \mathrm{i}\,\sigma_i = 2\chi_1$ (where χ_1 denotes the first Fourier mode). Using the Itō formula it is possible to show that σ can be equivalently rewritten as

$$\sigma(x,t) = A_t\,\sin\left(x - \Phi_t\right), \tag{6.23}$$

where the processes A_t and Φ_t satisfy the stochastic equations

$$\mathrm{d}A_t \;=\; -\left(A_t - \frac{1}{A_t}\right)\mathrm{d}t + \sqrt{2}\,\mathrm{d}B_t^A\,, \qquad \mathrm{d}\Phi_t = \frac{\sqrt{2}}{A_t}\mathrm{d}B_t^\Phi. \tag{6.24}$$

Here B_t^A and B_t^Φ are uncorrelated Wiener processes. It is clear that the amplitude A_t fluctuates around the value $A = 1$ and that its correlation time is of order one. From Eq. (6.24) it follows that, for typical values of A_t, the phase Φ_t and the position of the zeros of σ diffuse on a timescale of the order of unity. This aspect will be used later to quantify the mass distribution.

As mentioned before, in the particular case in which $h < 1$, the random environment presents scaling properties and thus one expects a very different behavior. Indeed, we have that the second-order structure function of σ, by construction, behaves as

$$\delta\sigma_\ell^2 = \overline{|\sigma(x,t) - \sigma(x+\ell,t)|^2} \sim \left(\frac{\ell}{L}\right)^{2h}. \tag{6.25}$$

The over-line stands for the ensemble average with respect to the fluctuations of the environment, i.e. with respect to the Ornstein–Uhlenbeck processes $\chi_{\mathbf{k}}$. In this study it has been choosen to relate the space and time correlations through a dimensional argument. The characteristic time τ_k introduced in Eq. (6.18), behaves as a power law, so that the correlation time of σ at scale ℓ is

$$\tau_{\mathrm{c}}(\ell) = \left(\frac{\ell}{L}\right)^{\beta}.$$

According to Eq. (6.25) the diffusion timescale associated to such spatial scale ℓ behaves as

$$\tau_{\rm d}(\ell) = \frac{\ell^2}{\Gamma \delta\sigma_\ell^2} \sim \Gamma^{-1} L^{2h} \ell^{2-2h}.$$

The ratio between these two times defines a dimensionless space-dependent parameter that is usually called the Kubo number

$$\mathrm{Ku}(\ell) = \frac{\tau_{\rm C}(\ell)}{\tau_{\rm D}(\ell)} \simeq \Gamma L^{-(2h+\beta)} \ell^{\beta+2h-2}. \tag{6.26}$$

When $\mathrm{Ku}(\ell) \gg 1$, the environment can be considered as "frozen" whilst for $\mathrm{Ku}(\ell) \ll 1$ it fluctuates in an almost time-uncorrelated manner. In the case in which $\beta \neq 2-2h$, the Kubo number depends on the scale ℓ and this breaks any possibility of scale invariance of the mass distribution. Only when $\beta = 2-2h$ one has that $\mathrm{Ku}(\ell) = \mathrm{Ku} = \Gamma/L^2$ and hence the scale invariance is possible. Here, the focus is on this latter case and we will see the mass concentration properties in terms of the dimensionless parameter $\mathrm{Ku} \propto \Gamma$. Note that the choice of having a scale-independent Kubo number is common in the framework of turbulence and is expected to be relevant to problems of inertial particle diffusion in turbulent flows.

Before moving to next section on the diffusion properties, let us do some other remarks on the dependence upon the Hölder exponent h of the environment. Using Parseval's theorem, it is possible to show that

$$\overline{\|\sigma\|_{L^2}^2} = \zeta(1+2h) \text{ and } \overline{\|\partial_x \sigma\|_{L^2}^2} = \zeta(-1+2h), \tag{6.27}$$

where $\zeta(s)$ is the Riemann zeta function. Thus one has that $\overline{\|\sigma\|_{L^2}} < \infty$ when $h > 0$ and that $\overline{\|\partial_x\sigma\|_{L^2}} < \infty$ when $h > 1$. Note that at each fixed time, $\sigma(x,t)$ is a Gaussian field whose increments have a variance given by Eq. (6.25). Therefore $\sigma(\cdot,t)$ is a *fractional Brownian motion* of exponent h [Mandelbrot & Ness, 1968]. For $h = 1/2$ it corresponds to the standard Brownian motion. For $h > 1/2$ the increments of σ are not independent, their covariance is positive and the zeros of σ are finite and isolated. On the contrary, when $h < 1/2$ the covariance of the increments is negative, therefore we expect that the number of zeros become infinite and that they accumulate. As we will see in the next sections, these different behaviors of the random environment will affect the general properties of the diffusion.

Finally, as the Ornstein–Uhlenbeck processes $\chi_{\mathbf{k}}$ are stationary, the fluctuations of the ejection rate σ^2 are a stationary and homogeneous random field. Hence one expects that, at sufficiently large times, the density distribution reaches a statistically stationary state and indeed numerical simulations indicate that this is the case. The results reported here (most of which are in

one dimension) mainly concern the statistical properties of the density field in this large-time asymptotics.

6.5 Diffusive properties

From now on we will consider a one-dimensional situation. This section concerns the study of the individual trajectories of the Itō stochastic diffusion equation (6.9) in the cases of smooth and non-smooth environments. As we will see, when the environment σ has a finite correlation length, particles are found to have standard diffusion properties at large times with a displacement distribution that approaches that Gaussian.

By solving implicitly Eq. (6.9) one obtains

$$X(t) = X(0) + \sqrt{2\Gamma} \int_0^t \sigma(X(s), s)\, \mathrm{d}W_s, \tag{6.28}$$

so that

$$\left\langle [X(t) - X(0)]^2 \right\rangle = 2\Gamma \int_0^t \left\langle \sigma^2(X(s), s) \right\rangle \mathrm{d}s, \tag{6.29}$$

where the angular brackets denote average over all trajectories (that are realizations of the Wiener process). At times much larger than the correlation time of σ^2 along particle trajectories, the integral becomes a sum of independent random variables, so that the law of large numbers can be applied. If the stochastic flow defined by Eq. (6.9) is ergodic, one then has

$$\langle [X(t) - X(0)]^2 \rangle \sim 2D(\Gamma, h)\, t,$$

with

$$D(\Gamma, h) = \Gamma \overline{\langle \sigma^2(X(t), t) \rangle} = \frac{\Gamma}{L} \int_0^L \overline{\sigma^2(x, t) \rho(x, t)}\, \mathrm{d}x. \tag{6.30}$$

The over-line denotes here the average with respect to the environment. The effective diffusion constant $D(\Gamma, h)$ involves an average of the environment along particle trajectories, which is equivalent in the case of an ergodic dynamics to a spatial average weighted by the density ρ. As we have anticipated, the trajectories might spend a long time near the zeros of σ. We thus expect the Lagrangian average of σ^2 to be less than the full Eulerian spatial average.

The displacement fluctuations of order less than $\sqrt{t}$ are expected to be given by the central-limit theorem. However, larger fluctuations should obey a large-deviation principle with a rate function that might not be purely quadratic as it is non-trivially related to the Lagrangian properties of the environment. To study these fluctuations, a Monte-Carlo simulations of Eq. (6.9) is performed.

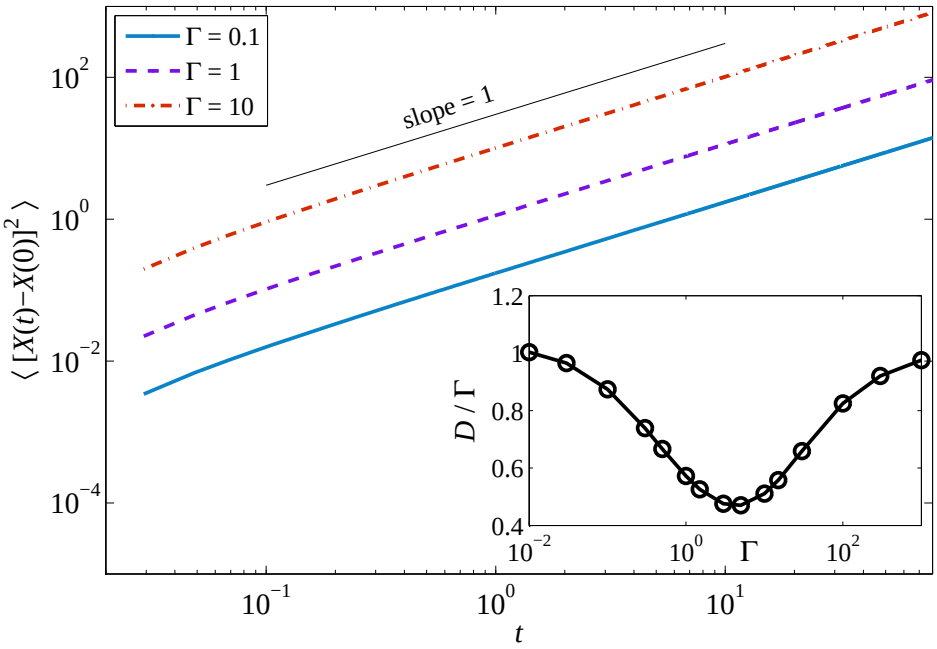

Figure 6.4: Mean-square displacement $\overline{\langle (X(t) - X(0))^2 \rangle}$ as a function of time for different values of Γ, as reported in the legend. Inset: Dependence on Γ for a smooth environment ($h = 2$) of the effective diffusion constant D defined in Eq. (6.30).

6.5.1 Diffusion coefficient

We first consider the case where the ejection rate σ^2 is a smooth function of space, namely when the Hölder exponent is greater that 1. In this configuration there is a finite and small number of isolated zeros of σ separated by a distance of the order of $L/2 = \pi$. A number of simulations of Eq. (6.9) has been performed (using 32 modes) for different values of the amplitude Γ and $h = 2$. Figure 6.4 shows the mean-square displacement of particles averaged over 1000 realizations of the diffusion and 20 000 realizations of the environment.

As expected from Eq. (6.30), a linear growth is observed at large times in Fig. 6.4. Moreover, as we can see in the inset of Fig. 6.4, the diffusion coefficient depends in a non-trivial way on Γ. Such a non-monotonic behavior of $D(\Gamma)/\Gamma$ can be explained by two competing phenomena. From one hand, in the limit of $\Gamma \to 0$ (or equivalently $\mathrm{Ku} \to 0$) the environment changes fairly fast compared to the characteristic time of diffusion given by $1/\Gamma$. There-

fore we can imagine that the particle trajectories sample homogeneously the environment, so that the Lagrangian average can be replaced by the spatial Eulerian average. This leads to

$$D(\Gamma, h) \simeq \frac{\Gamma}{L} \int \overline{\sigma(x,t)^2}\, \mathrm{d}x = \Gamma\zeta(1+2h) \quad \text{when} \quad \Gamma \to 0. \tag{6.31}$$

For the case $h = 2$, we obtain $D(\Gamma, 2)/\Gamma \simeq 1.03$ at small values of Γ, which is in agreement with the value observed in the inset of Fig. 6.4. As Γ increases, the trajectories spend a longer time at the zeros of σ decreasing the value of $D(\Gamma)/\Gamma$. From the other hand, in the limit of $\Gamma \to \infty$ (or equivalently $\mathrm{Ku} \to \infty$), the environment can be considered completely frozen so that the mass density, solving Eq. (6.15), is expected to be approximately given by $\rho(x,t) \sim 1/\sigma^2(x,t)$. From Eq. (6.30) one finds that

$$D(\Gamma, h) = \frac{\Gamma}{L} \int \overline{\sigma^2 \rho}\, \mathrm{d}x \;\approx\; \frac{\Gamma}{L} \int \mathrm{d}x = \Gamma, \tag{6.32}$$

which explains why $D(\Gamma)/\Gamma = 1$ at $\Gamma \to \infty$ (see inset of Fig. 6.4). For such asymptotic values of Γ the mass is completely concentrated at the zeros of the ejection rate and the diffusion is carried out by the diffusive motions of the latter. We have indeed seen earlier that in one dimension the zeros diffuse on timescales of the order of unit since their dynamics is similar to Eq (6.24).

6.5.2 PDF of displacement

To complete this description on the diffusive properties in the case $h = 2$, let us consider the normalized probability distribution functions (PDFs) of the displacements. They are shown in Fig. 6.5. The three panels refer to different values of Γ (0.1, 1, and 10) and for each of them the PDFs for different times are plotted.

At early times and for low values of Γ (panel (a)), the PDF's present exponential tails. The same observation can be done at intermediate times, for larger values of Γ (blue curves in panels (b) and (c)). In all cases, it is clear that the PDFs approach the Gaussian distribution at the largest times. Note that for sufficiently large values of Γ, some oscillations can be observed in the PDF tails at intermediate times. As we shall see, this is due to a "trapping effect" rising in the zeros of $\sigma(x,t)$. To clarify this point, it is useful to compare the PDF of the displacement for different values of Γ chosen at the time t^* such that

$$\overline{\langle (X(t^*) - X(0))^2 \rangle} = (L/2)^2 = \pi^2.$$

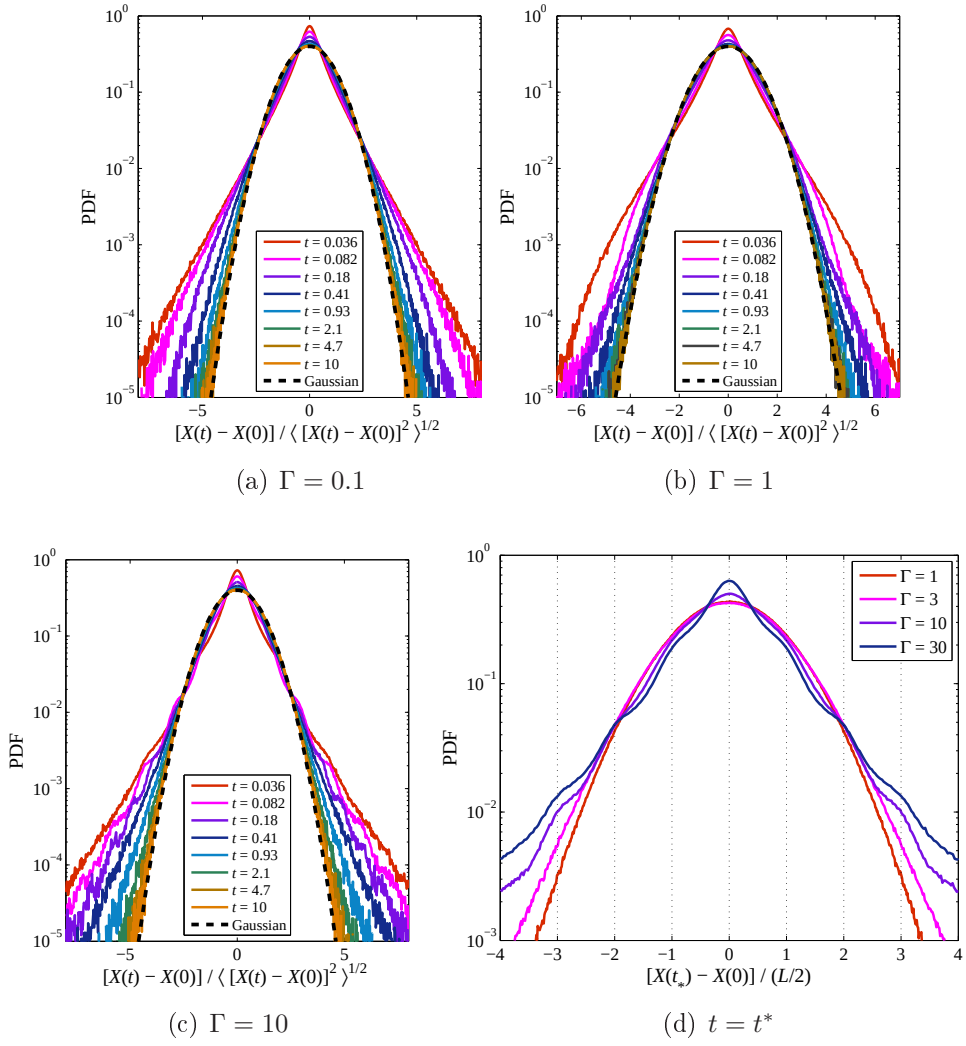

(a) $\Gamma = 0.1$ (b) $\Gamma = 1$

(c) $\Gamma = 10$ (d) $t = t^*$

Figure 6.5: Rescaled PDFs of the displacement $X(t) - X(0)$ in the case $h = 2$. Panels (a), (b) and (c) refer to $\Gamma = 0.1, 1$ and 10 respectively. For each panel, colors correspond to PDFs at different times (as labeled) and the dashed line is the Gaussian PDF of reference. The initial condition was chosen in the statistically stationary regime. (d) Same for $t = t^*$ for different values of Γ. t^* is defined as the time needed for particles to travel a distance comparable to the separation between two zeros of σ, which is of the order of $L/2 = \pi$.

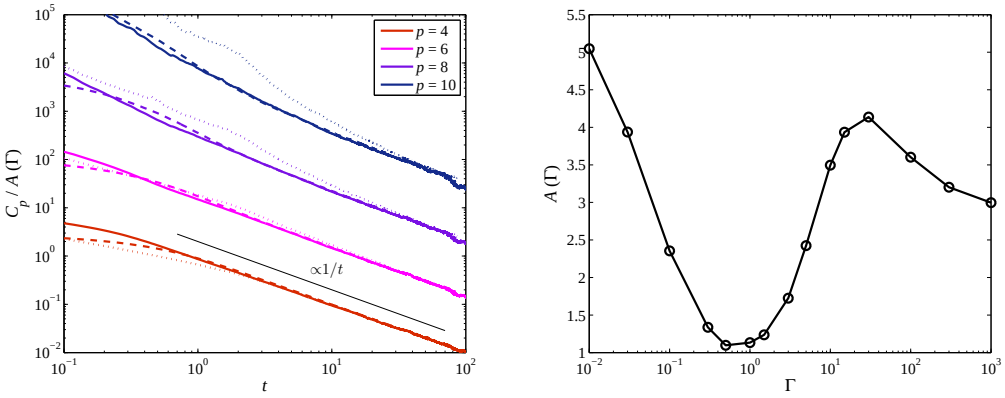

(a) (b)

Figure 6.6: (a) Time evolution of the normalized moments C_p, defined in Eq. (6.33), for different values of p. For each order the cases $\Gamma = 0.1$ (solid lines), $\Gamma = 1$ (dashed lines), and $\Gamma = 10$ (dotted lines) are shown. (b) Behavior of the function $A(\Gamma)$, which gives the dependence of C_p on Γ and which is defined in Eq. (6.34).

t^* is the time that particles need to travel a distance approximately equal to the distance that separes two zeros, which is around $L/2$ for smooth environments. The probability density function of the displacement $(X(t^*) - X(0))/(L/2)$ at that time is displayed in Fig. 6.5 (d) for various values of Γ. One clearly observes that, for large Γ's, the bumps appear at values that are multiple of $L/2$. A possible explanation is that particles are close to some zero of σ with a high probability. If they travel away, there is still a high probability that they are trapped by another zero, and so on. This picture might thus explain the multimodal distribution in Fig. 6.5 (d).

To better quantify the large-time behavior of the displacement, the corresponding higher-order moments are computed and compared to those typical of a Gaussian distribution. For even orders p, we can thus define a p-th order deviation from a Gaussian distribution C_p as

$$C_p = \frac{\langle (X(t) - X(0))^p \rangle}{\langle (X(t) - X(0))^2 \rangle^{p/2}} - \frac{2^{p/2}}{\sqrt{\pi}} \Gamma\left[\frac{p+1}{2}\right]. \tag{6.33}$$

Here $\Gamma[z]$ denotes the Gamma function (which is the factorial function whose argument is generalized to non-integer values and shifted down by 1, i.e. $\Gamma[z] = (z-1)!$ [Davis, 1959]). If the quantity $[X(t) - X(0)]$ is a Gaussian variable then for all $p \geq 2$ we have $C_p = 0$. More generally, the moment C_p is by construction equal to zero for $p = 2$, while in the case $p = 4$ it

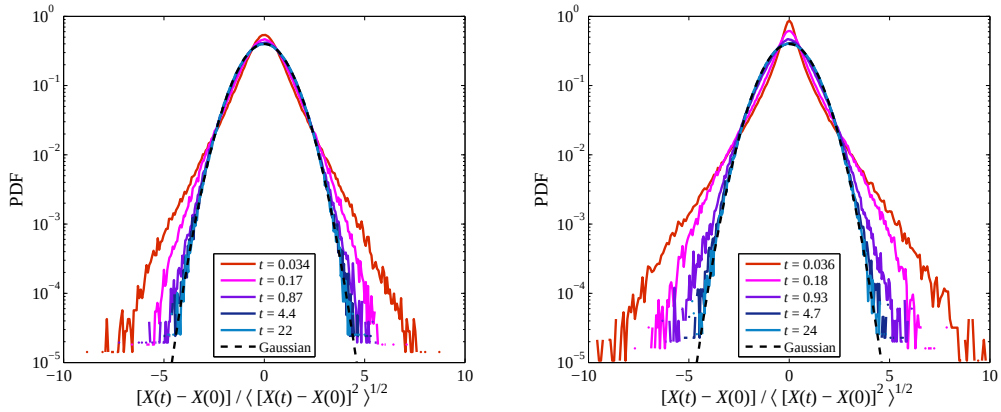

(a) (b)

Figure 6.7: Rescaled probability density function of $[X(t)-X(0)]$ at different times for $h = 0.2$ (a) and $h = 0.6$ (b). In both cases $\Gamma = 1$. Black dashed lines correspond to the Gaussian distribution.

corresponds to the Kurtosis. As seen from Fig. 6.6(a), data suggest that all the C_p's display a $1/t$ behavior at large times. The constant in front of this behavior depends of course on the amplitude Γ and on the order p. However, the behavior at large times is well fitted by a function of the form

$$C_p \simeq \frac{A(\Gamma)\lambda^{p/2}}{t}, \tag{6.34}$$

where λ is a positive constant. The temporal evolution of $C_p/A(\Gamma)$ for different values of Γ and p, and the function $A(\Gamma)$ are displayed in Fig. 6.6(a) and 6.6(b), respectively. As seen in Fig. 6.6(a), the data for different Γ and for p fixed collapse at large times. The limiting lines associated with different orders are equally spaced, confirming the dependence in $\lambda^{p/2}$ of the constant. The value of λ was found to be $\lambda \approx 15$.

Different simulations have been performed for various values of the exponent h and a behavior similar to the smooth case was found. For instance, the particles diffuse at large times and their statistics become Gaussian. This is evident from the rescaled PDFs of the displacement shown in Fig. 6.7, for $h = 0.2$ (a) and $h = 0.6$ (b), which both correspond to $\Gamma = 1$. Also, it has been found that the averaged squared displacement $\overline{\langle (X(t) - X(0))^2 \rangle}$ presents a linear growth consistent with Eq. (6.30) (the data is not shown here). Finally, the diffusion coefficient $D(\Gamma, h)$ was measured as a function of the exponent h and the result is reported in Fig. 6.8. In this plot, which refers to the case $\Gamma = 1$, the divergent behavior of $D(\Gamma, h)$ at small h is due

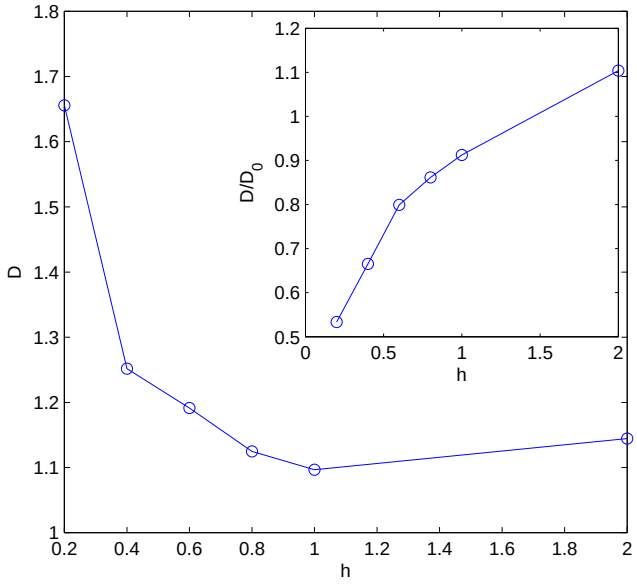

Figure 6.8: Behavior of the diffusion coefficient $D(\Gamma, h)$ as a function of the exponent h, for $\Gamma = 1$. The inset shows the same data normalized by $D_0 = \overline{\|\sigma\|^2_{L^2}}$.

to the divergence of the $L^2 - norm$ of $\sigma(x,t)$ when $h \to 0$. The inset of Fig. 6.8 shows the trend of the diffusion coefficient normalized by the square $L^2 - norm$ of the environment σ

$$D_0 = \Gamma\, \overline{\|\sigma\|^2_{L^2}} = \Gamma\, \zeta(1+2h).$$

$D(\Gamma, h)/D_0$ measures the deviations of the diffusion coefficient with respect to uniformly distributed particles. The case $D(\Gamma, h)/D_0 \ll 1$ corresponds to an important contribution from the zeros of σ^2 in the integration along the particle paths. As seen from the inset of Fig. 6.8, for a fixed value of Γ, the influence of the zeros increases when h decreases.

6.6 Density fluctuations

As previously observed, the spatial fluctuations of mass density are correlated to the distribution of the zeros of the random environment $\sigma(x,t)$. More precisely, from the diffusion-like equation (6.15) (which describes the evolution of ρ) we observe that the flux of mass is

$$J(x,t) = \Gamma\, \sigma(x,t)\left[2\partial_x\sigma(x,t)\rho(x,t) + \sigma(x,t)\partial_x\rho(x,t)\right]. \tag{6.35}$$

This means that the flux of mass vanishes at the zeros of σ, and hence that such zeros would act like sinks concentrating all of the mass if they were not moving. However, since the zeros undergo diffusion, they are not able to indefinitely concentrate mass and the density saturates in their neighborhood. At the same time, as the total mass is conserved, this concentration process causes the creation of voids in the regions where σ is of the order of 1.

Under some homogeneity and ergodicity assumptions for the dynamics, the probability density function of the mass density can be written as

$$\begin{aligned} P(\bar{\rho}) &= \frac{\mathrm{d}}{\mathrm{d}\bar{\rho}} \left(\text{measure}(\{(x,t) \,|\, \rho(x,t) \leq \bar{\rho}\})\right) \\ &= \lim_{T\to\infty} \frac{1}{2\pi T} \int_0^T \int_0^{2\pi} \delta\left(\rho(x,t) - \bar{\rho}\right) \mathrm{d}x \, \mathrm{d}t \equiv \lim_{T\to\infty} P_T(\bar{\rho}), \end{aligned} \tag{6.36}$$

where $P_T(\rho)$ indicates the time-averaged distribution of ρ over a time interval of length T. Understanding this quantity will be the main subject of next sections. As we will see, it strongly depends on the parameters Γ and h. The PDF of density defined in Eq. (6.36) in terms of a space-time average will be a precious tool to examine first the stationary case and later to propose a phenomenological approach to treat the non-stationary case.

6.6.1 Smooth random environments

We consider first the limit when the Kubo number Ku goes to infinity, which corresponds to an ejection rate amplitude Γ infinitely larger than the inverse of the diffusion time of the zeros of σ. This also corresponds to the diffusion in a time-stationary environment because the fastest timescale is that of the motion of mass. Note that, in the limit of a time-independent environment, no stationary state can be achieved. Mass will then concentrate in the zeros and at $t = \infty$ the density will become atomic, in the sense that it will be concentrated in points that are exactly the zeros of $\sigma(x)$. For sufficiently large but finite times, as almost all the mass is concentrated around the zeros of σ, the ejection rate can be rewritten through a Taylor expansion in the vicinity of these points.

Without loss of generality, let us assume that a zero appears at the origin $x = 0$ at the initial time $t = 0$ and does not move. In this limit Eq. (6.15) reduces to

$$\partial_t \rho = \Gamma C^2 \partial_x^2 (x^2 \rho), \tag{6.37}$$

where $C = \mathrm{d}\sigma/\mathrm{d}x|_{x=0}$. The change of time scales $t \mapsto s = t\Gamma C^2$ allows us to set $\Gamma\, C^2 = 1$. Moreover we consider an infinite domain and an initial

condition which is bounded in space.

$$\rho(x,0) = \begin{cases} 1 & \text{for } |x| \leq 1 \\ 0 & \text{elsewhere} \end{cases} .$$

Equation (6.37) can be integrated analytically using the method of characteristics. For $x > 0$ the change of variable $u(y,t) = e^{2t}\rho(x = e^{y-3t}, t)$ leads to the homogeneous heat equation that can be easily solved by using the corresponding Green function (the solution for $x < 0$ is obtained by symmetry). One then has

$$\begin{aligned} \rho(x,t) &= \frac{\mathrm{e}^{2t}}{\sqrt{4\pi t}} \int_0^\infty \exp\left[-\frac{(z - \log|x| - 3t)^2}{4t}\right] \mathrm{d}z \\ &= \frac{1}{2}\,\mathrm{e}^{2t}\,\mathrm{erfc}\left[\frac{\ln|x| + 3t}{2\sqrt{t}}\right], \end{aligned} \tag{6.38}$$

where $\mathrm{erfc}(z) = 2/\sqrt{\pi}\int_z^\infty \mathrm{e}^{-s^2}\mathrm{d}s$ is the complementary error function.

The time-averaged distribution $P_T(\bar{\rho})$ defined in Eq. (6.36) can then be calculated. One has

$$P_T(\bar{\rho}) = \frac{1}{2\pi T}\int_0^T\int_0^{2\pi} \frac{\delta(x - x_{\bar{\rho}}(t))}{|\partial_x \rho(x(t),t)|}\,\mathrm{d}x\,\mathrm{d}t, \tag{6.39}$$

where $x_{\bar{\rho}}(t)$ is the space-time contour line of the density corresponding to $\rho(x_{\bar{\rho}}(t),t) = \bar{\rho}$. As the complementary error function is bounded, it is clear from Eq. (6.38) that this line exists only for $t > \ln\bar{\rho}/2$. The contour lines of $\rho(x,t)$ are displayed on Fig. 6.9. One observes that, after transients, all the mass is concentrated around the point $x = 0$.

The high-density areas are concentrated in a narrow region of space. This will justify the saddle-point approximation used below. Changing variable $t \mapsto \lambda = 2t/\ln\bar{\rho}$ and introducing $\mu(\lambda;\bar{\rho}) = -\ln x_{\bar{\rho}}(t)/\ln\bar{\rho}$, after some algebra, Eq. (6.39) becomes

$$P_T(\bar{\rho}) = \frac{1}{T}\sqrt{\frac{\ln^3\bar{\rho}}{4\pi}}\int_1^{\frac{2T}{\ln\bar{\rho}}} \sqrt{\lambda}\,\mathrm{e}^{-\ln\bar{\rho}F(\lambda;\bar{\rho})}\mathrm{d}\lambda, \tag{6.40}$$

where

$$F(\lambda;\bar{\rho}) = \lambda + \mu(\lambda;\bar{\rho}) - \frac{1}{2\lambda}\left(\frac{3}{2}\lambda - \mu(\lambda;\bar{\rho})\right)^2$$

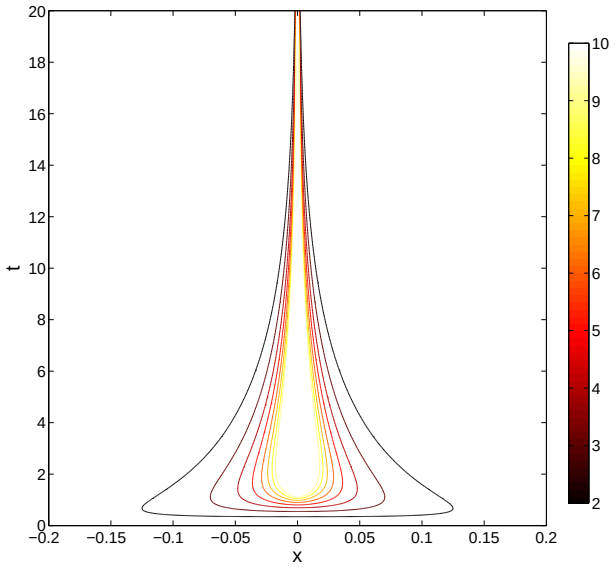

Figure 6.9: Graphic representation of the contour lines of the solution for the density $\rho(x,t)$. Its analytic solution is reported in Eq. (6.38).

and

$$\mu(\lambda;\bar{\rho}) = \frac{3}{2}\lambda - \sqrt{\frac{2\lambda}{\ln\bar{\rho}}}\mathrm{erfc}^{-1}\left(\frac{2}{\bar{\rho}^{\lambda-1}}\right) \approx \frac{3}{2}\lambda - \sqrt{2\lambda(\lambda-1)}.$$

In the last equation the asymptotic of $\mathrm{erfc}^{-1}(z) \approx \sqrt{\log(1/z)}$ for $z \approx 0$ has been used to obtain the right-most term (recall that we are considering $\lambda > 1$). By applying the saddle-point approximation for $\ln\bar{\rho} \gg 1$ to the integral in Eq. (6.40), one obtains to leading order (for simplicity, hereafter the bar over ρ is omitted)

$$P_T(\rho) \sim \frac{1}{\rho^\alpha} = \frac{1}{\rho^2}, \quad \text{since} \quad \alpha = \inf_\lambda F(\lambda) = 2\,. \tag{6.41}$$

Such a scaling is in perfect agreement with what is observed in Fig. 6.10. In that figure, the data correspond to solutions to Eq. (6.15) integrated with the stationary environment $\sigma(x,t) = \sin x$.

We also observe in the same figure that another clear power-law scaling is present for small values of the mass density. To explain this second scaling we consider a cell of length Δx, located at x_0, far away from a zero of $\sigma(x)$, and where the density reaches its minimum value. At leading order the mass ejected from this cell between the time t and $t + dt$ is proportional to

$$J \simeq \rho(x,t)\,\Gamma\,\partial_x\sigma^2(x)|_{x=x_0}$$

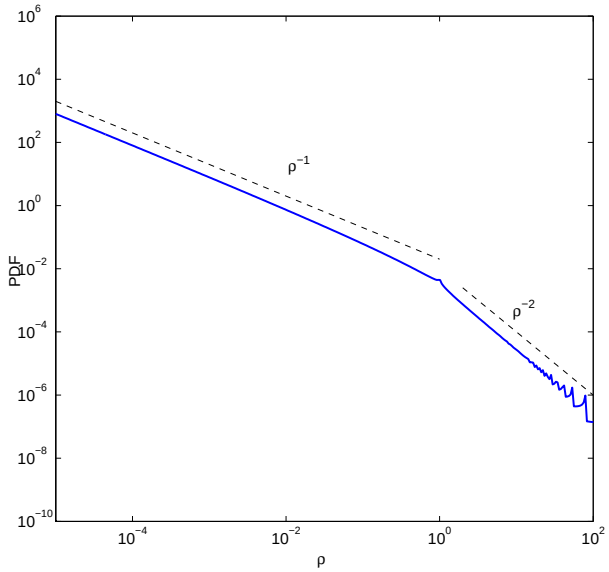

Figure 6.10: Probability distribution function of the density ρ given in Eq. (6.36). The PDF seems to display two different scaling for large and small values of ρ that are in agreement with Eqs. (6.41) and (6.42), respectively. Dashed lines highlight these scalings.

as $\partial_x \rho \approx 0$ at the point $x = x_0$. Considering that $\partial_x \sigma^2(x)$ is constant near x_0 yields an exponential decay of the mass in the cell. Introducing in Eq. (6.36) a density of mass of the form $\rho(x,t) \sim \rho_0 \, \mathrm{e}^{-\sigma_0^2 t}$ (where σ_0^2 would be an effective ejection rate) leads to

$$P_T(\rho) \sim \frac{1}{\rho}, \tag{6.42}$$

which is in agreement with the left-hand scaling in Fig. 6.10.

The situation is rather different in the non-stationary case in which the motion of the zeros of the ejection rate limits the process of mass concentration. As already seen in Sec. 6.4, the coefficients $\sigma_r(t)$ and $\sigma_i(t)$ of Eq. (6.22) are the Ornstein–Uhlenbeck processes defined in Eqs. (6.18) and (6.19). The probability density function of ρ in the non-stationary case, for an environment with a single mode $K = 1$ and different values of Γ, is displayed in Fig. 6.11.

The time needed for the density to accumulate near the zero of the ejection rate σ^2 is of the order of Γ^{-1}. Hence, for small values of Γ (i.e. $\mathrm{Ku} \ll 1$) the temporal variations of $\sigma(x,t)$ are very rapid and, as a consequence, the system does not have much time to cumulate mass. In this case it is apparent that most of the mass is distributed around the mean value $\langle \rho \rangle = 1$ (see

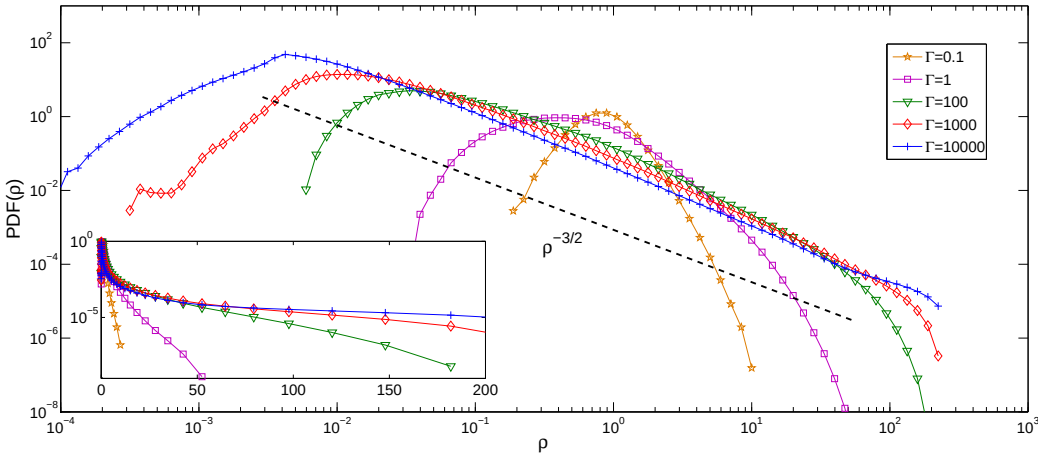

Figure 6.11: Log-log plot of the probability density function of the density ρ in the non-stationary case for $K = 1$. Different colors refer to different values of Γ. The inset displays the same figure but on a log-lin scale.

orange curve for $\Gamma = 0.1$ in Fig. 6.11). However, for large but finite values of the Kubo number Ku, the accumulation process is fast enough and the resulting $\rho^{-3/2}$ scaling is observed. This scaling can be derived by considering that for large Kubo numbers the system quickly relaxes to a quasi-stationary solution, in a time of the order of Γ^{-1}, and stays in such a state for a time comparable to the correlation time of σ.

Depending on how distant we are from a zero, we can have two cases. Far from a zero, the environment behaves as $\sigma(x) \simeq C\,x$, therefore we can overlook its temporal evolution. In this region, the density converges to a quasi-stationary solution. The time derivative of ρ is there negligible, so that, to leading order, $\partial_x^2(\sigma^2\rho) \approx 0$. Hence one has $\rho \approx \sigma^{-2} \propto 1/x^2$. In another region, closer to the zero, the time variations of its location become faster than the concentration of mass and the density saturates to a finite value $\rho_{\max}$ (see the sketch in Fig. 6.12(Left)). The transition between these two regimes occurs at a distance Δx from the zero that, by continuity, satisfies the relation

$$\Delta x \sim \rho_{\max}^{-1/2}.$$

The length Δx is of the order of the distance travelled by the zero during a timescale equal to that of mass concentration. Hence, if we assume that the zero diffuses, we have that $\Delta x \sim \Gamma^{-1/2}$ and the typical value of $\rho_{\max}$ is of the order of Γ. The distribution of the density has thus a crossover at $\rho \sim \Gamma$. In the case $\rho \ll \Gamma$, which occurs for values much below the plateau at $\rho \approx \rho_{\max}$, the behavior is dominated by the divergence of the quasi-stationary density

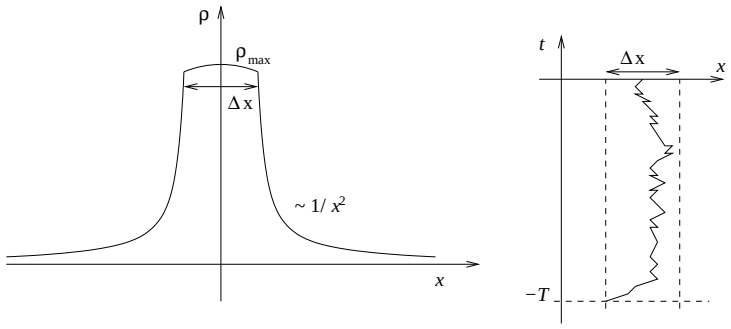

Figure 6.12: Left: sketch of the density field in the vicinity of a zero of the ejection rate σ^2 at $x = 0$. The density grows as x^{-2} and, at a distance $\Delta x \sim \rho_{\max}^{-1/2}$ of the zero, it reaches its saturation value $\rho_{\max}$. Right: sketch of the diffusive time evolution of the position of a zero of σ^2. Looking backward before the reference time $t = 0$, the zero stays at a distance less than Δx for a lapse of time T.

profile. Replacing $\rho(x) \sim 1/x^2$ in Eq. (6.36) one finally obtains

$$P(\rho) \sim \rho^{-3/2} \quad \text{for} \quad 1 \ll \rho \ll \Gamma. \tag{6.43}$$

Remarkably, this value of the exponent of the power-law in the intermediate large density tail is very robust. It is not shown here but the same behavior has also been observed for a larger number of modes and with a different environment, that is of the form $\sigma(x,t) = \sqrt{\Gamma}\cos(x - ct)$.

The behavior of the PDF of density when $\rho \gg \Gamma$ is related to the large fluctuations of $\rho_{\max}$ and thus to the events when the zero does not move much for a lapse of time larger than Γ^{-1}. More precisely, if at a fixed time we observe a large value of $\rho_{\max}$, it means that the zero has not moved by a distance larger than $\rho_{\max}^{-1/2}$ during an interval of time T; the latter is larger than Γ^{-1} as illustrated by the sketch in Fig. 6.12(Right). When the zeros diffuse, this probability is equal to the probability of the first exit time of a diffusive process. The time T is indeed defined as the first time when the Brownian motion (representing the displacement of the zero) touches a barrier situated at a distance Δx from its initial location. The probability density of the first time T at which the Wiener process exits the interval $|x| < \Delta x$ is $\sim \exp(-CT/\Delta x^2)$ (see, e.g., [Feller, 1971]). We thus obtain

$$\text{Prob}\,(\rho_{\max} > \rho) \sim \int_{\Gamma^{-1}}^{\infty} \mathrm{e}^{-C\,T\,\rho}\,\mathrm{d}T. \tag{6.44}$$

For $\rho \gg \Gamma$ the leading-order behavior is given by $T = \Gamma^{-1}$. This leads to the

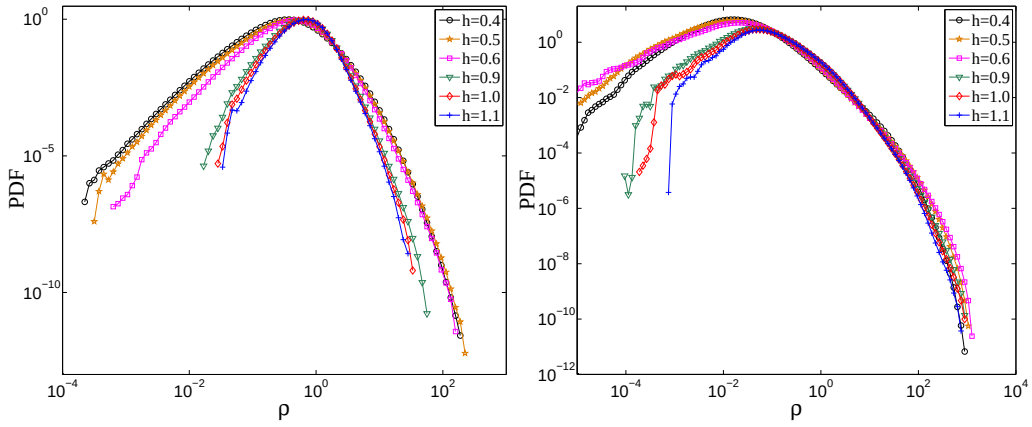

(a) (b)

Figure 6.13: Log-log plot of the PDF of the density ρ in the case of non-smoooth environment, for $\Gamma = 0.1$ (a) and $\Gamma = 10$ (b) and different values of h.

following exponential cutoff for the PDF of mass density

$$P(\rho) \sim \mathrm{e}^{-C\,\Gamma^{-1}\,\rho} \text{ for } \rho \gg \Gamma. \tag{6.45}$$

This exponential behavior is confirmed numerically as can been seen in the inset of Fig. 6.11.

6.6.2 Non-smooth random environment

We continue here to analyse the probability density function of the density but in the case of a time-dependent non-smooth ejection rate σ. Figure 6.13 shows the PDF of ρ for different values of the exponent h and two values of Γ, 0.1 and 10. Remark that for large Γ a power-law behavior is observed at small masses. The behavior of these tails can be interpreted on the basis of phenomenological arguments similar to those used in [Bec & Chétrite, 2007]. In this regard, let us consider an extreme event causing a very low density in a cell. We assume that for a long time, mass has only been ejected from this cell. The quantity of matter ejected per unit time is proportional to the mass. This implies that the density is expected to display an exponential decay and thus to take smal value in a time of the order of $T \propto -\Gamma^{-1} \ln \rho$. Now, let $p < 1$ be the probability of having such a configuration, with p that depends only on the properties of the environment. As the environment σ de-correlates in a time of the order of 1, the number n of independent

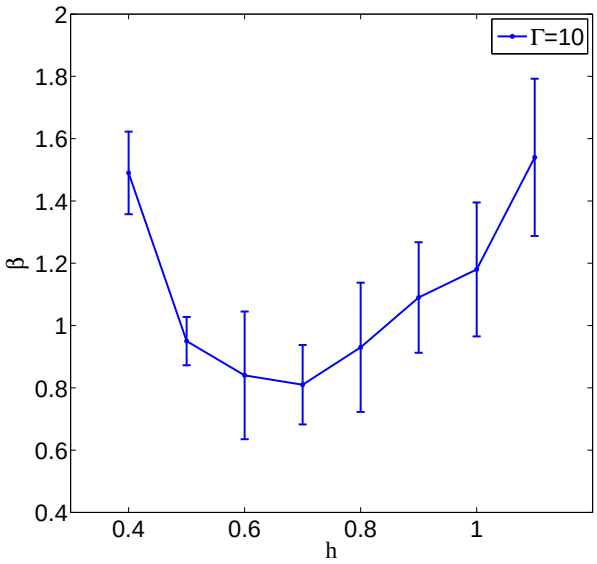

Figure 6.14: Fit of the exponent β of the power-law left tails of the PDFs shown in Fig.6.13(b), which corresponds to the case $\Gamma = 10$.

realizations of σ required for the full process to take place during a time T is proportional to T itself. Hence one has $n \simeq -C\,\Gamma^{-1}\ln\rho$, where C is a constant that depends on h. Therefore, the probability of this complete event is

$$p^{-C\,\Gamma^{-1}\ln\rho} = \left(\mathrm{e}^{\ln p}\right)^{-C\,\Gamma^{-1}\ln\rho} = \mathrm{e}^{-\ln p\,C\,\Gamma^{-1}\ln\rho} = \rho^{-C\,\Gamma^{-1}\ln p},$$

and we obtain that the probability of such an extreme event is ρ^{β}, with $\beta = -C\ln p/\Gamma > 0$. Note that this is actually a lower bound to the small mass tail that is valid as long as $p \neq 0$ and $C \neq 0$. Having an analytic expression of the exponent β is a challenging problem that goes beyond the aim of this study. The exponent β can be achieved by fitting the left tails of the mass density PDFs within the range where the power-law is observed. These fits are presented in dashed lines in the inset of Fig. 6.13(b) and the dependence of β on the Hölder exponent h is displayed in Fig. 6.14 for the value $\Gamma = 10$.

Note that the breadths of the PDFs in Fig. 6.13 clearly depend on the value of the Hölder exponent h as it is apparent on Fig. 6.15 that represents the variance of the density $\delta\rho^2 = \langle(\rho - \langle\rho\rangle)^2\rangle$. The fact that both the exponent β and the standard deviation $\delta\rho$ do not have a monotonic behavior as a function of h, can be qualitatively explained in the following way. When the value of h decreases, the number of zeros of $\sigma(x,t)$ increases. However

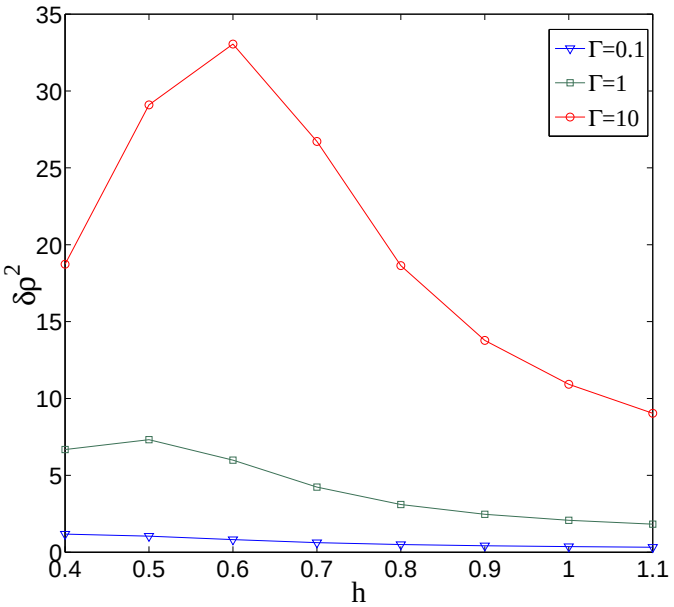

Figure 6.15: Variance of the density $\delta\rho^2 = \langle(\rho - \langle\rho\rangle)^2\rangle$ as a function of the exponent h for $\Gamma = 0.1$, 1 and 10.

the spatial distribution of the zeros also depends on the Hölder exponent h. On the one hand, for $h > 1/2$ the space increments of σ are positively correlated. This implies that there is no accumulation of zeros and the mass is transported from the zones with non-vanishing values of $\sigma(x,t)$ to the nearest zeros. Therefore decreasing h from 1 to $1/2$, more and more zeros appear creating zones with high mass concentration and, at the same time, void regions. This increases the density fluctuations. On the other hand, for $h < 1/2$ the covariance of increments is negative and some finite-size regions with a large number of zeros appear. In such zones $\sigma(x,t)$ vanishes many times and thus the diffusion is very weak. The mass is trapped and its transfer becomes inefficient, reducing thus the probability to have extremely large or low mass concentrations. In other words, a large number of zeros increases the density fluctuations as long as these zeros are not too dense. The expected transition between these two behaviors happens near $h = 1/2$. This is in agreement with the observed variations of β and $\delta\rho^2$ shown in Figs. 6.14 and 6.15. This behavior is especially evident for the largest value of Γ where the properties of the system are supposed to depend more strongly on the distribution of zeros of the ejection rate.

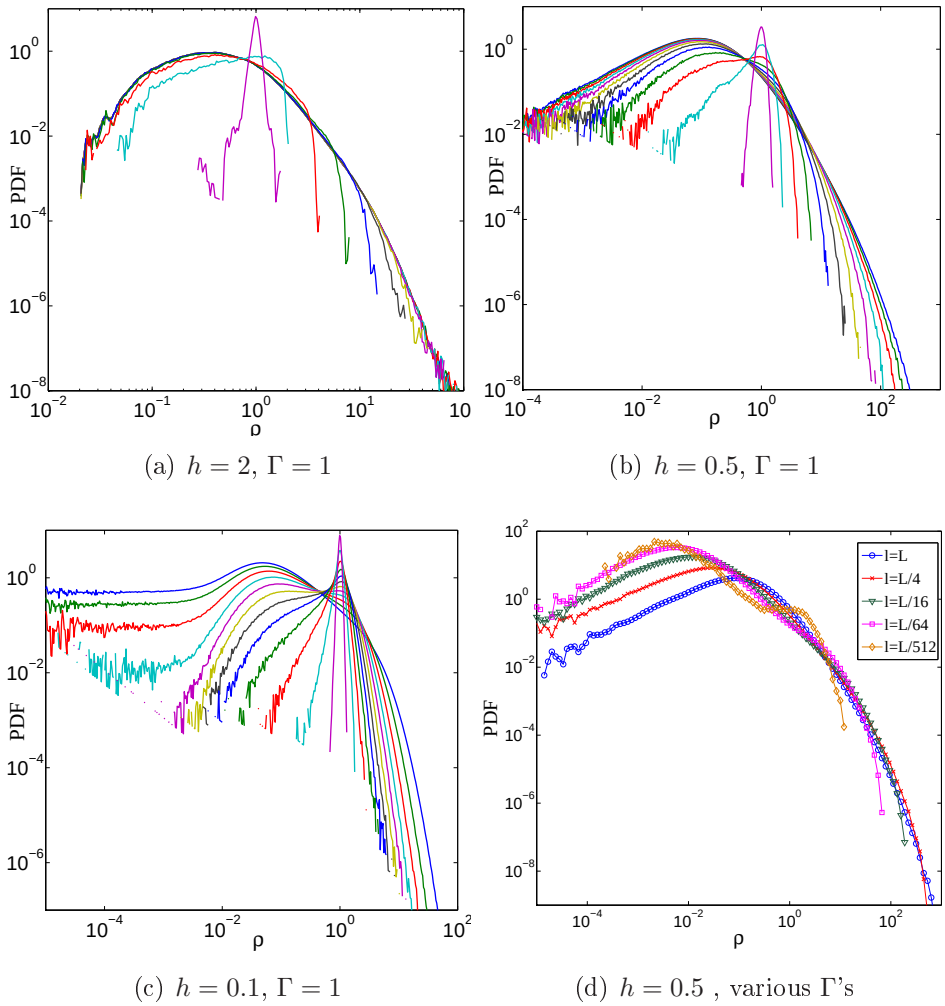

(a) $h = 2$, $\Gamma = 1$

(b) $h = 0.5$, $\Gamma = 1$

(c) $h = 0.1$, $\Gamma = 1$

(d) $h = 0.5$, various Γ's

Figure 6.16: (a) (b) and (c) PDFs of the coarse-grained density ρ_ℓ for $\Gamma = 1$ and three values of the exponent h. Colors correspond to different coarse-graining scales ℓ chosen of the form $\ell = L/2^k$ with $k = 1, \dots 13$. In each panel, the narrowest curve corresponds to the largest scale $L/2$ and the widest curve corresponds to the smallest $L/2^{13}$. The width of the PDF increases monotonically when the scale decreases. (d) PDF of the coarse-grained density ρ_ℓ for $h = 1/2$ and different combinations of Γ and ℓ chosen such that the effective rate defined in Eq. (6.48) is constant.

6.7 Scale invariance of the mass density field

We finally study the scaling properties of the density field. In Sec. 6.4, we have prescribed some scale invariance properties of the ejection rate σ.

The question we want to adress is whether or not and to which extent such properties translate to the distribution of mass.

For that we consider the coarse-grained mass density, which is defined as

$$\rho_\ell(x,t) = \frac{1}{\ell}\int_{x-\ell/2}^{x+\ell/2} \rho(y,t)\,\mathrm{d}y. \tag{6.46}$$

By homogeneity we have that $\langle\rho\rangle = \langle\rho_\ell\rangle$. The probability density function of the coarse-grained density ρ_ℓ, computed using the definition in Eq. (6.36), is displayed in Fig. 6.16 for different values of h and for $\Gamma = 1$. In each panel the PDFs monotonically increase their width when the scale decreases. The narrowest PDF and the widest PDF correspond to the largest scale $L/2$ and the smallest $L/2^{13}$, respectively.

Comparing the panels, we can see that in cases of spatially smooth environments, the coarse-grained PDF of mass density becomes gradually invariant with respect to the scale when h increases and this is particularly evident in Fig. 6.16(a) for $h = 2$. This indicates that the density field is spatially smooth and that the zeros are isolated. Moreover the collapse is faster for small densities because the accumulation of mass is weak and occurs only on few small clusters while the rest of the domain mainly consists of large void zones. These large voids dominate the coarse-grained density statistics up to their typical size, which is $\ell \simeq L/8$, as seen in Fig. 6.16(a). Indeed all curves corresponding to $\ell < L/8$ collapse in the left-hand side of this figure. On the contrary, the typical size of mass clusters ℓ_{clust} is rather small. Averaging over scales larger than ℓ_{clust} implies the reduction of the largest mass fluctuations. Indeed, the coarse-grained density cannot exceed m_{clust}/ℓ, where m_{clust} is the mass captured by the cluster. This cutoff decreases with ℓ, as can be seen in Fig. 6.16(a), allowing less and less fluctuations of the coarse-grained density.

Such arguments cannot be applied for non-smooth environments where the distribution of zeros is more complicated. The scale invariance is then broken, as shown in Figs. 6.16(b) and 6.16(c). This is what can also be seen in Fig. 6.17, which displays the variance of the coarse-grained density $\delta\rho_\ell^2 = \langle(\rho_\ell - \langle\rho\rangle)^2\rangle$ as a function of the scale ℓ for different values of h. For $h > 1$ and $\ell \ll L$ the variance $\delta\rho_\ell^2$ does not depend on the scale ℓ. However, one observes that for $h < 1$ and $\ell \ll L$ the variance presents a power-law scaling $\delta\rho_\ell^2 \sim \ell^{-\zeta}$ that suggests a self-similar behavior of the density. The trend of the power-law exponent $\zeta(h;\Gamma)$ is displayed in the inset of Fig. 6.16(c).

To understand the scaling invariance of the density field we should look closely to what happens in the neighborhood of the zeros of σ. If we assume that the ejection rate vanishes at $x = x_0$, then in the neighborhood of x_0, we

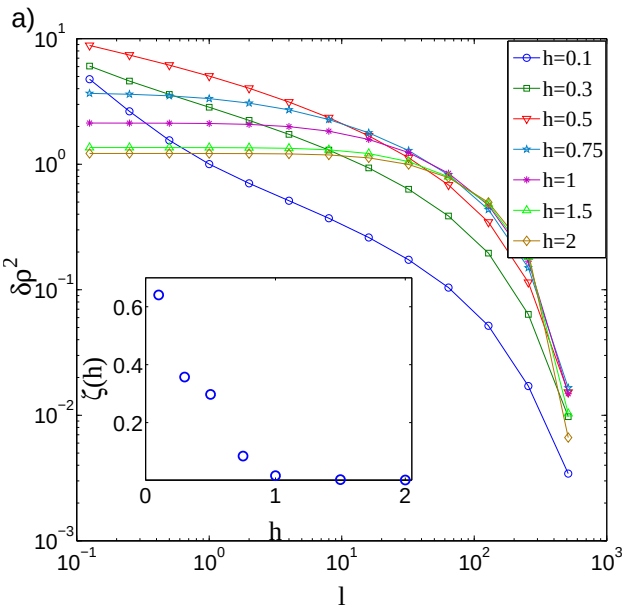

Figure 6.17: Variance of the coarse-grained density $\langle \delta\rho_\ell^2 \rangle = \langle (\rho_\ell - \langle \rho \rangle)^2 \rangle$ as a function of ℓ for different values of h, as labeled. Inset: exponent $\zeta(h;\Gamma)$ of the power-law of the variance $\langle \delta\rho_\ell^2 \rangle \sim \ell^{-\zeta(h;\Gamma)}$ for $\Gamma = 1$.

have $\sigma(x,t)^2 = |\sigma(x_0+x,t)|^2 \sim x^{2h}$. Supposing now that the density behaves as a power law in the vicinity of x_0 and rescaling the space as $\tilde{x} = \lambda x$, one can easily see that the rescaled density $\tilde{\rho} = \rho(\tilde{x})$ is a solution of

$$\partial_t \tilde{\rho}(\tilde{x},t) = \Gamma \lambda^{2-2h} \partial_{\tilde{x}}^2 \left[\sigma^2(\tilde{x},t) \tilde{\rho}(\tilde{x},t) \right]. \tag{6.47}$$

Hence, we expect that if the coarse-grained density ρ_ℓ presents a self-similar property then the PDF of ρ_ℓ, for a fixed value of Γ, will coincide at large values with the PDF of $\rho_{\lambda\ell}$, which corresponds to an effective ejection rate of amplitude

$$\Gamma_{\text{eff}} = \Gamma \lambda^{2-2h}. \tag{6.48}$$

This scale invariance is in agremeent with the collapse at large values of the density seen in Fig. 6.16(d), where different PDF's of ρ_ℓ, with ℓ such that $\Gamma_{\text{eff}} = \text{const}$ (for different values of Γ), are confronted for $h = 1/2$.

6.8 Brief summary and conclusions

We give here a short outline of the results obtained in this Chapter. We have introduced a diffusion model that can be either derived from asymptotic

considerations or obtained as the hydrodynamical limit of a simple discrete mass ejection process where the ejection rates are random variables with temporal and spatial correlations. The model can be interpreted in terms of random walks in a time-dependent random environment. However the settings are such that, while the mass is conserved, it does obey a maximum principle and the density can become arbitrarily large. We have motivated this model to study fluctuations in turbulent transport.

We have considered space-periodic environments where the temporal dependence of each Fourier mode is given by independent Ornstein–Uhlenbeck processes and both the amplitude of the modes and their correlation times present some prescribed spatial scaling properties. This allowed us to consider smooth and non-smooth environments with fast and slow temporal dependence. No other assumptions were made on the environments and we expect them to display generic properties and to be representative of sufficiently general situations.

The model was studied analytically and numerically. The corresponding particle dynamics is given by an Itō differential equation with a multiplicative noise and no drift. We observed that random trajectories diffuse at large times. Also, the probability distribution of their displacements tends to a Gaussian at large times and the deviations to this asymptotic behavior decrease as t^{-1}. To take into account the fluctuations of mass due to the randomness of the environment we have introduced and studied the probability distribution of the density. We obtained some analytical results on it in the case of a stationary environment and we showed that it displays a power-law tail at large masses with exponent -2. In the general case, we observed a competition between a trapping effect due to vanishing ejection rates of the random environment and the mixing due to its temporal dependence that leads to large fluctuations of the density of mass. These fluctuations were studied for both smooth and non-smooth random environment. In the smooth case, we showed that the PDF has an intermediate power-law behavior, like in the stationary case but with an exponent $-3/2$ followed by an exponential cutoff. Finally, we studied the spatial scaling properties of the mass distribution by introducing a coarse-grained density field. For smooth random environments the coarse-grained density was found to be scale invariant. We showed that at large masses, it possesses some scaling properties that depend on the coarse-graining size, the ejection rate typical amplitude, and the Hölder exponent of the environment.

The overall dynamics of the model proposed in this chapter contains several space and time scales. Mass rapidly accumulates near the regions with a vanishing ejection rate and slowly moves following the diffusion of the zeros. Depending on the properties of the environment, there is also a clear

separation of length scales: small mass fluctuations at small scales and large mass at the scale between the distance of two vanishing ejection rates. This scale separation strongly suggests trying to determine, by standard homogenization techniques, a large-scale effective diffusion tensor and eventually an effective transport term. This issue is kept for future work.

Extending our approach to dimensions higher than one is another possible direction for future. The ejection rate will then vanish on complicated sets that, depending on its regularity, might display fractal properties. Varying the Hölder exponent of the random environment, its amplitude and the observation scales could then lead to a rather rich collection of different regimes. For instance, a particular attention should be paid to understand whether or not a power-law is still present in the mass density probability distribution.

To conclude, let us stress again that the zeros of the environment play a crucial role on both the diffusive properties and the mass density statistics. They are responsible for mass accumulation but, at the same time, constitute barriers to transport. This duality implies that the fine statistical details of such systems crucially depend on the features of the zeros and specially on the local structure of the ejection rate in their vicinity. In particular the presence of an extra drift in the dynamics would completely alter the role of the zeros and would prevent mass accumulation. In this thesis work, we have decided to focus on ejection rates that can be written as the square of a generic Gaussian random function. However this choice cannot be always relevant and, for instance, it might be sometimes more appropriate to write the ejection rate rather as the exponential of a random function. This would change drastically most of the results showed.

Chapter 7

Conclusions and perspectives

In this chapter we shortly come back to the main results obtained during this thesis and place them in the prospect of applying them to concrete problems of atmospheric transport. We naturally distinguish between questions related to tracer and passive scalar dynamics and issues where particle inertia plays a role.

Fluctuations of an advected concentration
We have related in Chap. 4 the statistics of a passive scalar, and in particular its spatial correlations, to the study of the two-point motion of Lagrangian tracers. Several questions remain open on the work that was presented on this topic.

Firstly, we have studied in Sec. 4.4.1 what we called the "local dissipation", which is defined as the ratio $[V^{\parallel}]^3/R$ between the cube of the longitudinal velocity difference and the distance between two tracers. We have obtained unexpected evidence that this quantity attains a scaling regime after a short time: its statistical properties become quickly independent of both time and initial separations. This suggests that the "local dissipation" is, to leading order, statistically conserved by the Lagrangian two-point dynamics. However, we have not been able to understand the physical mechanisms leading to this behavior. Its average $\langle [V^{\parallel}]^3/R \rangle_{r_0}$ over all pairs that are initially at a distance r_0 is initially negative because of Kolmogorov's 4/5 law. We found geometrical arguments that explain why during Batchelor's ballistic regime, this average rapidly changes sign and becomes positive. Its convergence to a constant positive value remains unexplained. Identifying the reasons for such a behavior will have important impacts on the phenomenon of relative dispersion and in particular on a possible reinterpretation of Richardson's explosive separation in terms of a purely diffusive behavior of velocity differences.

Other works concerned the deduction of a model for relative dispersion

from the observation that acceleration differences are correlated over short time scales. As explained in Subsec. 4.4.3, the main tool used in this derivation is the central limit theorem that allowed us to write the time derivative of velocity differences as a stochastic process with multiplicative noise. Interestingly and despite its non-linearity, we argued that the model reaches at large times a self-similar behavior compatible with Richardson's scaling. However, one of the main shortcomings of this approach is the fact that it mixes phenomenological and rigorous arguments in such a way that the tensorial structure of acceleration correlations is not taken into consideration and, for the moment, the model is still purely one-dimensional. Extending it to higher dimensions represents a real challenge. This would allow us validating it more systematically against numerical data and comparing this approach with other realistic stochastic models. Also, we expect such developments to give an alternative way to understand the mechanisms leading to a statistically stationary behavior of the "local dissipation".

We now turn to the applications of pair dispersion to the study of fluctuations in turbulent transport. The results obtained in Secs. 5.2 and 5.3 give some geometrical interpretations of the extreme events that can be observed in the statistics of distances between two tracers. Such approaches can be extended to the relative motion of more than two trajectories and in particular to the time evolution of a blob of Lagrangian tracers. This would have be of straightforward relevance to characterize the dispersion by turbulence of a spot of pollutants. We used in Sec. 5.3 fractal geometry considerations to quantify the probability that a couple of tracers remain at small distances. One of the plans is to extend this approach to blobs. This would allow one to quantify better the probability that a blob keeps a small size or folds to create concentrations that are much higher than those predicted by eddy-diffusivity approaches. On the contrary, extremely large separations relate to low concentrations. As we have stressed in Sec. 5.2, a violent growth of the inter-particle distance is explained by a long-time memory of the initial separation. An extension of these results to the case of blobs of tracers is again of interest. We indeed expect that such a study will give clues on how to characterize the dispersion properties as a function of the initial local fluctuations of the turbulent flow. A certainly too-optimistic objective could be to design a control process for instantaneous pollutant emissions that would choose release times as a function of flow structures in order to optimize dispersion.

Finally, let us discuss to what extent our work applies to pollutant dispersion in situations that are more generic than the forward-in-time evolution of pollutant spots. In many interesting cases one is concerned with time-continuous sources. In principle, because of the linearity of the advection-

diffusion equation, such settings can equivalently be treated as the sum of several instantaneous releases. This superposition principle can be used to determine the evolution of average concentrations from the dynamics of a single blob. However, when interested in fluctuations, that is statistics with a non-linear dependence on the concentration (as, e.g., its variance), these ideas cannot be applied. Quantifying fluctuations then requires a knowledge of multi-scale multi-time correlations. As a consequence, the problem of turbulent relative dispersion has to be in principle generalized to the full study of the Lagrangian flow. However, depending on the question of interest, the required information can be more tractable. For instance, let us consider tracers that are emitted from a point source with a constant rate. When interested in the second-order statistics of the concentration field, one can easily see that they relate to the probability that a particle emitted at a time $t_1 < t$ is at time t nearby another particle, which was emitted at a time $t_2 < t$. This probability is different from the transition density used for relative dispersion, as it requires that the two particles were at the same location but at different times in the past. Clearly, some of the notions that were developed and used in this thesis for the classical situation of relative dispersion have their equivalent in this analogous problem. However such extensions would require some efforts.

Universality of heavy particle concentrations

A natural question that arises on the extensions of this thesis work on relative dispersion concerns its validity in the case of non-ideal particles. When the transported species have inertia, preferential concentration will compete with Richardson's dispersion. Previous experimental and numerical work suggests that in that case the explosive law for separation is recovered at sufficiently large times [Bec et al., 2010, Gibert et al., 2010]. However, little is known about the effect of inertia on the extreme events of the inter-particle distance. Clearly, the small-scale clustering of heavy particles will enhance the probability that particles remain close together and will strongly affect the fractality observed for small separations between tracers. For large separations, we have seen that for tracers, a large initial velocity difference is required for them to separate at all times faster than the average. It is known that such large velocity differences are even more probable for heavy particles. This is due to the "sling effect" that they are experiencing when ejected from vortices [Falkovich & Pumir, 2007]. One expects fluctuations to be again enhanced by inertia, as these large velocity differences will trigger particle separation. However, this effect might be very sensitive to the value of the Stokes number as the dissipative dynamics of particles will introduce a decorrelation of their velocities on times larger than their response time.

All these extensions of relative dispersion to the case of inertial particles require analyzing the data of numerical simulations varying the particle Stokes number and the initial separation in the inertial range.

We now give some ideas on the implication of the results of Chap. 6 on the concentration properties of heavy particles. We have motivated the introduction of a random mass ejection model to describe the statistical properties of the distribution of particles inside the inertial range. We have shown that for such models the high concentrations are strongly affected by the zeros of the ejection rate. In particular, the latter are responsible for the presence of a power-law range in the probability distribution of the density. Such a regime has not been observed in direct numerical simulations of heavy particles in turbulent flows [Bec et al., 2007a]. This can be explained by the following shortcoming of the settings in Sec. 6.4. Indeed, we have seen in Sec. 6.1 that a phenomenological estimation of the ejection rate involves exponentials that never vanish. In the model studied later, we have rather written the positive ejection rate as the square of a function that generically has zeros. It would thus be worth extending the results on density fluctuations that are reported in Sec. 6.6 to different kinds of ejection rates. This would be particularly useful to assess whether or not mass ejection models (or equivalently random walks in fluctuating random environments) can be divided in different universality classes and, if this is the case, to understand to which of them inertial particle dynamics belongs. To finish, it is important to stress that mass ejection models can provide a new framework to characterize particle concentration in the inertial range of turbulent flows. Classically, clustering properties are quantified in terms of deviations from the Poisson distribution that uniformly spread particles would follow. These deviations, which are very useful in estimating how wrong it is to neglect preferential concentration, do not give much information on the nature of the inertial-range particle distribution. Designing new observables from simple statistical physics models might be helpful. Also, it would be of interest to apply to such models the approach in terms of a analysis of the Voronoï mesh that was developed in [Obligado et al., 2011]. This could be useful to understand whether for such observables, heavy particles belong or not to the same universality class as random diffusions in random environments.

Bibliography

[Acheson, 1990] Acheson, D. (1990). *Elementary Fluid Dynamics*. Oxford: Clarendon Press.

[Anselmet et al., 1984] Anselmet, F., Gagne, Y., Hopfinger, E., & Antonia, R. (1984). High-order velocity structure functions in turbulent shear flows. *Journal of Fluid Mechanics*, 140, 63–89.

[Arnéodo et al., 2008] Arnéodo, A., Benzi, R., Berg, J., Biferale, L., Bodenschatz, E., Busse, A., Calzavarini, E., Castaing, B., Cencini, M., Chevillard, L., et al. (2008). Universal intermittent properties of particle trajectories in highly turbulent flows. *Physical review letters*, 100(25).

[Arya, 1999] Arya, S. (1999). *Air pollution meteorology and dispersion*. New York: Oxford University Press.

[Basset, 1888] Basset, A. (1888). *A treatise on hydrodynamics: with numerous examples*, volume 2. Deighton, Bell and Co.

[Batchelor, 1950] Batchelor, G. (1950). The application of the similarity theory of turbulence to atmospheric diffusion. *Quarterly Journal of the Royal Meteorological Society*, 76, 133–146.

[Batchelor, 1952] Batchelor, G. (1952). Diffusion in a field of homogeneous turbulence. ii. the relative motion of particle. *Mathematical Proceedings of the Cambridge Philosophical Society*, 48(02), 345–362.

[Battaner, 1996] Battaner, E. (1996). *Astrophysical fluid dynamics*. Cambridge: Cambridge University Press.

[Bec, 2003] Bec, J. (2003). Fractal clustering of inertial particles in random flows. *Physics of Fluids*, 15, L81.

[Bec et al., 2007a] Bec, J., Biferale, L., Cencini, M., Lanotte, A., Musacchio, S., & Toschi, F. (2007a). Heavy particle concentration in turbulence at dissipative and inertial scales. *Physical review letters*, 98(8), 84502.

[Bec et al., 2010] Bec, J., Biferale, L., Lanotte, A., Scagliarini, A., Toschi, F., et al. (2010). Turbulent pair dispersion of inertial particles. *Journal of Fluid Mechanics*, 645, 497–528.

[Bec et al., 2007b] Bec, J., Cencini, M., & Hillerbrand, R. (2007b). Clustering of heavy particles in random self-similar flow. *Physical Review E*, 75, 025301.

[Bec & Chétrite, 2007] Bec, J. & Chétrite, R. (2007). Toward a phenomenological approach to the clustering of heavy particles in turbulent flows. *New Journal of Physics*, 9(3), 77.

[Bérard, 2004] Bérard, J. (2004). The almost sure central limit theorem for one-dimensional nearest-neighbour random walks in a space-time random environment. *Journal of applied probability*, 41(1), 83–92.

[Bernard et al., 2006] Bernard, D., Boffetta, G., Celani, A., & Falkovich, G. (2006). Conformal invariance in two-dimensional turbulence. *Nature Physics*, 2(2), 124–128.

[Bernard et al., 1996] Bernard, D., Gawedzki, K., & Kupiainen, A. (1996). Anomalous scaling in the n-point functions of a passive scalar. *Physical Review E*, 54, 2564.

[Biferale et al., 2004] Biferale, L., Boffetta, G., Celani, A., Devenish, B., Lanotte, A., & Toschi, F. (2004). Multifractal statistics of lagrangian velocity and acceleration in turbulence. *Physical Review Letters.*, 93, 064502.

[Biferale et al., 2005] Biferale, L., Boffetta, G., Celani, A., Devenish, B., Lanotte, A., & Toschi, F. (2005). Lagrangian statistics of particle pairs in homogeneous isotropic turbulence. *Physics of Fluids*, 17, 115101.

[Biferale & Procaccia, 2005] Biferale, L. & Procaccia, I. (2005). Anisotropy in turbulent flows and in turbulent transport. *Physics Reports*, 414, 43–164.

[Bitane et al., 2012a] Bitane, R., Bec, J., & Homann, H. (2012a). Geometry and violent events in turbulent pair dispersion. *(submitted to Journal of Turbulence)*, arXiv:1209.2296.

[Bitane et al., 2012b] Bitane, R., Bec, J., & Homann, H. (2012b). Time scales of turbulent relative dispersion. *Physical Review E*, 86(4), 045302.

[Boffetta & Ecke, 2012] Boffetta, G. & Ecke, R. (2012). Two-dimensional turbulence. *Annual Review of Fluid Mechanics*, 44.

[Boffetta & Musacchio, 2010] Boffetta, G. & Musacchio, S. (2010). Evidence for the double cascade scenario in two-dimensional turbulence. *Physical Review E*, 82, 016307.

[Boffetta & Sokolov, 2002a] Boffetta, G. & Sokolov, I. (2002a). Relative dispersion in fully developed turbulence: The richardson's law and intermittency corrections. *Physics Review Letters*, 88, 094501.

[Boffetta & Sokolov, 2002b] Boffetta, G. & Sokolov, I. (2002b). Statistics of two-particle dispersion in two-dimensional turbulence. *Physics of Fluids*, 14, 3224.

[Borgas & Yeung, 2004] Borgas, M. & Yeung, P. (2004). Relative dispersion in isotropic turbulence. part 2. a new stochastic model with reynolds-number dependence. *Journal of Fluid Mechanics.*, 503, 125–160.

[Bourgoin et al., 2006] Bourgoin, M., Ouellette, N., Xu, H., Berg, J., & Bodenschatz, E. (2006). The role of pair dispersion in turbulent flow. *Science*, 311(5762), 835.

[Boussinesq, 1885] Boussinesq, V. (1885). Sur la résistance qu'oppose un liquide indéfini en repos. In *Acad Sci*, volume 100 (pp. 935–7).

[Bricmont & Kupiainen, 1991] Bricmont, J. & Kupiainen, A. (1991). Random walks in asymmetric random environments. *Communications in mathematical physics*, 142(2), 345–420.

[Busse & Müller, 2008] Busse, A. & Müller, W. (2008). Diffusion and dispersion in magnetohydrodynamic turbulence: The influence of mean magnetic fields. *Astronomische Nachrichten*, 329, 714–716.

[Cardy et al., 2008] Cardy, J., Falkovich, G., & Gawedzki, K. (2008). *Non-equilibrium statistical mechanics and turbulence*, volume 355. Cambridge University Press.

[Castaing et al., 1990] Castaing, B., Gagne, Y., & Hopfinger, E. (1990). Velocity probability density functions of high reynolds number turbulence. *Physica D*, 46, 177–200.

[Celani et al., 2000] Celani, A., Lanotte, A., Mazzino, A., & Vergassola, M. (2000). Universality and saturation of intermittency in passive scalar turbulence. *Physical Review Letters*, 84(11), 2385–2388.

[Charnoz et al., 2011] Charnoz, S., Fouchet, L., Aleon, J., & Moreira, M. (2011). Three-dimensional lagrangian turbulent diffusion of dust grains in a protoplanetary disk: Method and first applications. *The Astrophysical Journal*, 737(1), 33.

[Cooper & Alley, 2002] Cooper, C. & Alley, F. (2002). *Air pollution control: A design approach*, volume 3rd edition. Waveland Press (Prospect Heights, IL.).

[Csanady, 1973] Csanady, G. (1973). *Turbulent diffusion in the environment*, volume 3. Springer.

[Davis, 1959] Davis, P. (1959). Leonhard euler's integral: A historical profile of the gamma function. *The American Mathematical Monthly*, 66(10), 849–869.

[De Pater & Lissauer, 2001] De Pater, I. & Lissauer, J. (2001). *Planetary science*. Cambridge University Press.

[Dean et al., 2007] Dean, D., Drummond, I., & Horgan, R. (2007). Effective transport properties for diffusion in random media. *Journal of Statistical Mechanics: Theory and Experiment*, 2007(7), P07013.

[Derrida & Pomeau, 1982] Derrida, B. & Pomeau, Y. (1982). Classical diffusion on a random chain. *Physical Review Letters*, 48(9), 627–630.

[Dimotakis, 2005] Dimotakis, P. (2005). Turbulent mixing. *Annual Review of Fluid Mechanics*, 37, 329–356.

[Dolgopyat et al., 2008] Dolgopyat, D., Keller, G., & Liverani, C. (2008). Random walk in markovian environment. *Annals of Probability*, 36(5), 1676–1710.

[Douady et al., 1991] Douady, S., Couder, Y., & Brachet, M. (1991). Direct observation of the intermittency of intense vorticity filaments in turbulence. *Physical review letters*, 67(8), 983–986.

[Eckart, 1948] Eckart, C. (1948). An analysis of the stirring and mixing processes in incompressible fluids. *Journal of Marine Research*, 7, 265–275.

[Eyink, 2011] Eyink, G. (2011). Stochastic flux freezing and magnetic dynamo. *Physics Review E*, 83, 056405.

[Falkovich et al., 2002] Falkovich, G., Fouxon, A., & Stepanov, M. (2002). Acceleration of rain initiation by cloud turbulence. *Nature*, 419(6903), 151–154.

[Falkovich et al., 2001] Falkovich, G., Gawęedzki, K., & Vergassola, M. (2001). Particles and fields in fluid turbulence. *Reviews of Modern Physics*, 73(4), 913–975.

[Falkovich & Pumir, 2007] Falkovich, G. & Pumir, A. (2007). Sling effect in collisions of water droplets in turbulent clouds. *Journal of the Atmospheric Sciences*, 64, 4497–4505.

[Faxén, 1922] Faxén, H. (1922). Der widerstand gegen die bewegung einer starren kugel in einer zähen flüssigkeit, die zwischen zwei parallelen ebenen wänden eingeschlossen ist. *Annalen der Physik*, 373(10), 89–119.

[Feller, 1971] Feller, W. (1971). *An introduction to Probability Theory*, volume 1 and 2. New York: Wiley.

[Frisch, 1996] Frisch, U. (1996). *Turbulence*. Cambridge University Press.

[Gagne et al., 1990] Gagne, Y., Hopfinger, E., & Frisch, U. (1990). A new universal scaling for fully developed turbulence: the distribution of velocity increments. *New trends in nonlinear dynamics and pattern-forming phenomena. NATO ASI*, 237, 315–319.

[Gardiner, 1985] Gardiner, C. (1985). *Handbook of stochastic methods for physics, chemistry and the natural sciences*, volume 42. Springer.

[Gatignol, 1983] Gatignol, R. (1983). Faxen formulae for a rigid particle in an unsteady non-uniform flow. *Journal de Mécanique théorique et appliquée*, 1(2), 143–160.

[Gibert et al., 2010] Gibert, M., Xu, H., & Bodenschatz, E. (2010). Inertial effects on two-particle relative dispersion in turbulent flows. *Europhysics Letters*, 90, 64005.

[Gillespie, 1992] Gillespie, D. (1992). *Markov processes: an introduction for physical scientists*. Academic Pr.

[Gollub et al., 1991] Gollub, J., Clarke, J., Gharib, M., Lane, B., & Mesquita, O. (1991). Fluctuations and transport in a stirred fluid with a mean gradient. *Physical Review Letters*, 67, 3507–3510.

[Goudon & Poupaud, 2004] Goudon, T. & Poupaud, F. (2004). Homogenization of transport equations: weak mean field approximation. *SIAM Journal on Mathematical Analysis*, 36, 856–881.

[Grauer et al., 2012] Grauer, R., Homann, H., & Pinton, J.-F. (2012). Longitudinal and transverse structure functions in high Reynolds-number turbulence. *New Journal of Physics*, 14, 063016.

[Halpin-Healy & Zhang, 1995] Halpin-Healy, T. & Zhang, Y. (1995). Kinetic roughening phenomena, stochastic growth, directed polymers and all that. aspects of multidisciplinary statistical mechanics. *Physics Reports*, 254, 215–414.

[Harrison & Perry, 1986] Harrison, R. & Perry, R. (1986). *Handbook of air pollution analysis*, volume 2nd edition. Chapman and Hall, New York.

[Homann et al., 2009] Homann, H., Bec, J., Fichtner, H., & Grauer, R. (2009). Clustering of passive impurities in magnetohydrodynamic turbulence. *Physics of Plasmas*, 16, 082308.

[Homann et al., 2007] Homann, H., Dreher, J., & Grauer, R. (2007). Impact of the floating-point precision and interpolation scheme on the results of dns of turbulence by pseudo-spectral codes. *Computer Physics Communications*, 177(7), 560–565.

[Howe, 1971] Howe, M. (1971). Wave propagation in random media. *Journal of Fluid Mechanics*, 45(04), 769–783.

[Hughes, 1996] Hughes, B. (1996). *Random Walks and Random Environments: Random Environments (Vol. 2)*. Oxford University Press.

[Ilyin et al., 2010] Ilyin, V., Procaccia, I., & Zagorodny, A. (2010). Stochastic processes crossing from ballistic to fractional diffusion with memory: Exact results. *Physical Review E*, 81, 030105.

[Imbrie & Spencer, 1988] Imbrie, J. & Spencer, T. (1988). Diffusion of directed polymers in a random environment. *Journal of Statistical Physics*, 52, 609–626.

[Ishihara et al., 2009] Ishihara, T., Gotoh, T., & Kaneda, Y. (2009). Study of high-reynolds number isotropic turbulence by direct numerical simulation. *Annual Review of Fluid Mechanics*, 41, 165–180.

[Jayesh & Warhaft, 1991] Jayesh, J. & Warhaft, Z. (1991). Probability distribution of a passive scalar in grid-generated turbulence. *Physical Review Letters*, 67, 3503–3506.

[Jullien et al., 1999] Jullien, M., Paret, J., & Tabeling, P. (1999). Richardson pair dispersion in two-dimensional turbulence. *Physical Review Letter*, 82, 2872–2875.

[Kolmogorov, 1941a] Kolmogorov, A. (1941a). Dissipation of energy in locally isotropic turbulence. *Dokl. Akad. Nauk SSSR*, 32, 16–18.

[Kolmogorov, 1941b] Kolmogorov, A. (1941b). The local structure of turbulence in incompressible viscous fluid for very large reynolds numbers. *Dokl. Akad. Nauk SSSR*, 30, 9–13.

[Kolmogorov, 1941c] Kolmogorov, A. (1941c). On generation (decay) of isotropic turbulence in an incompressible viscous liquid. *Dokl. Akad. Nauk SSSR*, 31, 538–540.

[Kolmogorov, 1962] Kolmogorov, A. (1962). A refinement of previous hypotheses concerning the local structure of turbulence in a viscous incompressible fluid at high reynolds number. *Journal of Fluid Mechanics*, 13, 82–85.

[Koochesfahani & Dimotakis, 1986] Koochesfahani, M. & Dimotakis, P. (1986). Mixing and chemical reactions in a turbulent liquid mixing layer. *Journal of Fluid Mechanics*, 170, 83–112.

[Kraichnan, 1966] Kraichnan, R. (1966). Dispersion of particle pairs in homogeneous turbulence. *Physics of Fluids*, 9, 1937–1943.

[Kraichnan, 1968] Kraichnan, R. (1968). Small-scale structure of a scalar field convected by turbulence. *Physics of fluids*, 11, 945–953.

[Kraichnan, 1971] Kraichnan, R. (1971). Inertial-range transfer in two- and three-dimensional turbulence. *Journal of Fluid Mechanics*, 47(03), 525–535.

[Krstulovic et al., 2012] Krstulovic, G., Bitane, R., & Bec, J. (2012). Diffusions in time-dependent random environments: mass fluctuations and scaling properties. *New Journal of Physics*, 14(7), 073053.

[Kurbanmuradov, 1997] Kurbanmuradov, O. (1997). Stochastic lagrangian models for two-particle trelative turbulent dispersion in high-reynolds number turbulence. *Monte Carlo Methods and Application*, 3, 37–52.

[La Porta et al., 2001] La Porta, A., Voth, G., Crawford, A., Alexander, J., & Bodenschatz, E. (2001). Fluid particle accelerations in fully developed turbulence. *Nature*, 409, 1017–1019.

[Lewis & Bala, 2006] Lewis, D. & Bala, S. (2006). Plankton predation rates in turbulence: A study of the limitations imposed on a predator with a non-spherical field of sensory perception. *Journal of Theoretical Biology*, 242(44).

[Majda & Kramer, 1999] Majda, A. & Kramer, P. (1999). Simplified models for turbulent diffusion: theory, numerical modelling, and physical phenomena. *Physics Reports*, 314, 237–574.

[Mandelbrot, 1983] Mandelbrot, B. (1983). *The fractal geometry of nature*. Wh Freeman.

[Mandelbrot & Ness, 1968] Mandelbrot, B. & Ness, J. V. (1968). Fractional brownian motions, fractional noises and applications. *SIAM Review*, 10(4), 422–437.

[Maxey, 1987] Maxey, M. (1987). The gravitational settling of aerosol particles in homogeneous turbulence and random flow fields. *Journal of Fluid Mechanics*, 174, 441–465.

[Maxey & Riley, 1983] Maxey, M. R. & Riley, J. (1983). Equation of motion for a small rigid sphere in a nonuniform flow. *Physics of Fluids*, 26, 883.

[Mezard et al., 1987] Mezard, M., Parisi, G., & Virasoro, M. (1987). *Spin Glass Theory and Beyond (World Scientific Lecture Notes in Physics)*, volume 9. World Scientific Publishing Company.

[Monin & Yaglom, 1971] Monin, A. & Yaglom, A. (1971). *Statistical Fluid Mechanics: Mechanics of Turbulence*, volume 1. Cambridge: MIT press.

[Mordant et al., 2004] Mordant, N., Crawford, A., & Bodenschatz, E. (2004). Three-dimensional structure of the lagrangian acceleration in turbulent flows. *Physical Review Letter*, 93, 214501.

[Obligado et al., 2011] Obligado, M., Missaoui, M., Monchaux, R., Cartellier, A., & Bourgoin, M. (2011). Reynolds number influence on preferential concentration of heavy particles in turbulent flows. In *Journal of Physics: Conference Series*, volume 318 (pp. 052015).

[Obukhov, 1941] Obukhov, A. (1941). On the distribution of energy in the spectrum of turbulent flow. *Izv. Akad. Nauk SSSR, Ser. Geogr. Geofiz.*, 5, 453–466.

[Opper & Saad, 2001] Opper, M. & Saad, D. (2001). *Advanced mean field methods : Theory and practice*. MIT Press.

[Ott & Mann, 2000] Ott, S. & Mann, J. (2000). An experimental investigation of the relative diffusion of particle pairs in three-dimensional turbulent flow. *Journal of Fluid Mechanics*, 422, 207–223.

[Ottino, 1989] Ottino, J. (1989). *The Kinematics of Mixing: Stretching, Chaos and Transport*. Cambridge University Press.

[Ouellette et al., 2006] Ouellette, N., Xu, H., Bourgoin, M., & Bodenschatz, E. (2006). An experimental study of turbulent relative dispersion models. *New Journal of Physics*, 8, 109.

[Parisi, 1979] Parisi, G. (1979). Toward a mean field theory for spin glasses. *Physics Letters A*, 73(3), 203–205.

[Pearson, 1905] Pearson, K. (1905). The problem of the random walk. *Nature*, 72(294), 318–342.

[Peterson & Dean, 2008] Peterson, R. & Dean, K. (2008). Forecasting exposure to volcanic ash based on ash dispersion modeling. *Journal of Volcanology and Geothermal Research*, 170(3–4), 230–246.

[Pilewskie, 2007] Pilewskie, P. (2007). Climate change: Aerosols heat up. *Nature*, 448(7153), 541–542.

[Pinsky & Khain, 1997] Pinsky, M. & Khain, A. (1997). Turbulence effects on droplet growth and size distribution in clouds—a review. *Journal of Aerosol Science*, 28, 1177–1214.

[Pope, 2000] Pope, S. (2000). *Turbulent flows*. Cambridge University Press.

[Post & Abraham, 2002] Post, S. & Abraham, J. (2002). Modeling the outcome of drop-drop collisions in diesel sprays. *International Journal of Multiphase Flow*, 28(6), 997–1019.

[Pumir et al., 2000] Pumir, A., Shraiman, B., & Chertkov, M. (2000). Geometry of lagrangian dispersion in turbulence. *Physical Review Letters*, 85, 5324–5327.

[Pumir et al., 1991] Pumir, A., Shraiman, B., & Siggia, E. (1991). Exponential tails and random advection. *Physical Review Letters*, 66, 2984–2987.

[Rast & Pinton, 2011] Rast, M. & Pinton, J. (2011). Pair dispersion in turbulence: the subdominant role of scaling. *Physical Review Letter*, 107, 214501.

[Richardson, 1926] Richardson, L. (1926). Atmospheric diffusion shown on a distance-neighbour graph. *Proceedings of the Royal Society of London. Series A, Containing Papers of a Mathematical and Physical Character*, 110(756), 709–737.

[Sahimi, 2011] Sahimi, M. (2011). *Flow and Transport in Porous Media and Fractured Rock: From Classical Methods to Modern Approaches*, volume 2nd Edition.

[Salazar & Collins, 2009] Salazar, J. & Collins, L. (2009). Two-particle dispersion in isotropic turbulent flows. *Annual Review of Fluid Mechanics*, 41, 405–432.

[Sawford, 2001] Sawford, B. (2001). Turbulent relative dispersion. *Annual Review of Fluid Mechanics*, 33(1), 289–317.

[Scatamacchia et al., 2012] Scatamacchia, R., Biferale, L., & Toschi, F. (2012). Extreme events in the dispersions of two neighboring particles under the influence of fluid turbulence. *Physical Review Letters*, 109, 144501.

[Schumacher, 2008] Schumacher, J. (2008). Lagrangian dispersion and heat transport in convective turbulence. *Physical Review Letters*, 100, 134502.

[Seinfeld & Pandis, 2006] Seinfeld, J. & Pandis, S. (2006). *Atmospheric chemistry and physics: from air pollution to climate change.* Somerset, NJ: John Wiley and Sons.

[Shaw, 2003] Shaw, R. (2003). Particle-turbulence interactions in atmospheric clouds. *Annual Review of Fluid Mechanics*, 35(1), 183–227.

[She & Lévêque, 1994] She, Z. & Lévêque, E. (1994). Universal scaling laws in fully developed turbulence. *Physical Review letters*, 72(3), 336–339.

[Sherrington & Kirkpatrick, 1975] Sherrington, D. & Kirkpatrick, S. (1975). Solvable model of a spin-glass. *Physical Review Letters*, 35, 1792–1796.

[Shraiman & Siggia, 1994] Shraiman, B. & Siggia, E. (1994). Lagrangian path integrals and fluctuations in random flow. *Physical Review E*, 49, 2912–2927.

[Shraiman et al., 2000] Shraiman, B., Siggia, E., et al. (2000). Scalar turbulence. *Nature*, 405(6787), 639–646.

[Sinai, 1982] Sinai, Y. (1982). The limit behavior of a one-dimensional random walk in a random environment. *Teoriya Veroyatnostei i ee Primeneniya*, 27(2), 247–258.

[Smyth et al., 2001] Smyth, W., Moum, J., & Caldwell, D. (2001). The efficiency of mixing in turbulent patches: inferences from direct simulations and microstructure observations. *Journal of physical oceanography*, 31(8), 1969–1992.

[Solomon, 1975] Solomon, F. (1975). Random walks in a random environment. *The annals of probability*, 3(1), 1–31.

[Spitzer, 1976] Spitzer, F. (1976). *Principles of Random Walks, 2nd edition*, volume 34. New-York:Springer-Verlag.

[Squires & Eaton, 1991] Squires, K. & Eaton, J. (1991). Preferential concentration of particles by turbulence. *Physics of Fluids A: Fluid Dynamics*, 3, 1169.

[Sreenivasan, 1991] Sreenivasan, K. (1991). On local isotropy of passive scalars in turbulent shear flows. *Proceedings of the Royal Society A Mathematical Physical and Engineering Sciences*, 434(1890), 165–182.

[Stevens & Feingold, 2009] Stevens, B. & Feingold, G. (2009). Untangling aerosol effects on clouds and precipitation in a buffered system. *Nature*, 461(7264), 607–613.

[Stokes, 1850] Stokes, G. (1850). *On the effect of the internal friction of fluids on the motion of pendulums*, volume IX.

[Sznitman, 2004] Sznitman, A. (2004). : (pp. 203–266).: Notes of course at school and Conference on Probability Theory, May 2002 - ICTP Trieste.

[Tabeling et al., 1996] Tabeling, P., Zocchi, G., Belin, F., Maurer, J., & Willaime, H. (1996). Probability density functions, skewness, and flatness in large reynolds number turbulence. *Physical Review E*, 53, 1613–1621.

[Taylor, 1921] Taylor, G. (1921). Diffusion by continuous movements. *Proceedings of the London Mathematical Society*, 20, 196–212.

[Thomson, 1987] Thomson, D. (1987). Criteria for the selection of stochastic models of particle trajectories in turbulent flows. *Journal of Fluid Mechanics*, 180(529-556), 109.

[Toschi & Bodenschatz, 2009] Toschi, F. & Bodenschatz, E. (2009). Lagrangian properties of particles in turbulence. *Annual Review of Fluid Mechanics*, 41, 375–404.

[Uhlenbeck & Ornstein, 1930] Uhlenbeck, G. & Ornstein, L. (1930). On the theory of the brownian motion. *Physical Review*, 36, 823–841.

[Valavanidis et al., 2008] Valavanidis, A., Fiotakis, K., & Vlachogianni, T. (2008). Airborne particulate matter and human health: toxicological assessment and importance of size and composition of particles for oxidative damage and carcinogenic mechanisms. *Journal of Environmental Science and Health, Part C*, 26(4), 339–362.

[Van Atta & Chen, 1970] Van Atta, C. & Chen, W. (1970). Structure functions of turbulence in the atmospheric boundary layer over the ocean. *Journal of Fluid Mechanics*, 44, 145–159.

[Van Kampen, 2007] Van Kampen, N. (2007). *Stochastic processes in physics and chemistry*. North Holland.

[Varadhan, 2004] Varadhan, S. (2004). Random walks in a random environment. *Proceedings Mathematical Sciences*, 114, 309–318.

[Wang & Maxey, 1993] Wang, L. & Maxey, M. (1993). Settling velocity and concentration distribution of heavy particles in homogeneous isotropic turbulence. *Journal of Fluid Mechanics*, 256, 27–27.

[Wang & Pan, 2008] Wang, M. & Pan, N. (2008). Modeling and prediction of the effective thermal conductivity of random open-cell porous foams. *International Journal of Heat and Mass Transfer*, 51(5–6), 1325–1331.

[Warhaft, 2000] Warhaft, Z. (2000). Passive scalars in turbulent flows. *Annual Review of Fluid Mechanics*, 32, 203–240.

[Yeung & Borgas, 2004] Yeung, P. & Borgas, M. (2004). Relative dispersion in isotropic turbulence. part 1. direct numerical simulations and reynolds-number dependence. *Journal of Fluid Mechanics*, 503, 92–124.

[Yoshimatsu et al., 2009] Yoshimatsu, K., Okamoto, N., Schneider, K., Kaneda, Y., & Farge, M. (2009). Intermittency and scale-dependent statistics in fully developed turbulence. *Physical Review E*, 79, 026303.

[Zeitouni, 2004] Zeitouni, O. (2004). Part II: Random walks in random environment. *Lectures on probability theory and statistics*, (pp. 1930–1930).

"Start where you are. Use what you have. Do what you can."

- Arthur Ashe -

Acknowledgements

Finally I have the pleasure to say *thanks* to all those people with who I have shared my doctoral experience in this smiling and sunny Nice.

I am thankful to my advisors Jérémie Bec and Alain Noullez for their continuous support during my Ph.D. In particular, I would like to express my gratitude to Jérémie whom, in fact, very patiently took charge of my entire Ph.D. I really appreciate his expertise, enthusiasm and sense of responsability from which I learned very much.

Besides my advisors, I would like to thank in advance the rest of the committee: A. Lanotte, M. Bourgoin, M.E. Brachet and A. Pumir for having kindly agreed to be a part of the jury.

My sincere thanks goes also to the guys of my group, Benjamin, Giorgio, Holger, Mamadou and Samriddhi, with whom I had the chance and the pleasure to work and increase my professional and personal experience.

In particular, I am especially grateful to Ben, my first official French teacher, for helping me to solve all kinds of problems that a person can have in a foreign country. It was a pleasure sharing the office with him and I cannot count the times we spent chatting and laughing over our misadventures! He is a very generous and good guy and I think I could not have had a better officemate.

I am also especially grateful to Samriddhi-da, a very dear friend. If I have been able to deal with all the difficulties of the last part of the Ph.D. it was also thanks to him. I cannot explain how much he has helped and encouraged me. Thanks for all of the coffees, laughs, amusing squabbles, badminton matches, complaints, jokes, the tedious Bob Dylan songs that I was forced to listen to, nice emails, lighthearted teasing, gifts, cups of tea, encouragements, thesis corrections, Mozart kugeln, bike tours, postacards, criticisms, dinners, suggestions ...everything has been very very fun :)

Together with Samriddhi I would also like to say thanks Dario, for the funny moments and the delightful evenings spent watching movies from the times of the Punic wars, and Purbasha, for cheering me up at distance!

A very very big thanks goes to my wonderful friends and rugby-mates Clémence, Clare, Marion, Naomi (la capitaine), Roxanne et Aurélien (le coach) for their friendship, which has meant to me more than I could ever express. I had the chance to share with them a lot of happy and funny moments (made from 0 up to 2351 m on the sea level) and even the glory of two well-deserved medals. I will treasure forever these memories. It has been great to know all of them and I am very grateful for all I have received and learned from them in terms of emotions and feelings :)

Thanks also to the other rugby-mates Erell, Lila, Marianne, Maud, Severine, and Georges for the fun trainings and the nice third half times.

I wish to thank the people of the internal service: Ghislain, Karima, Khaled and Nadia, (the amazing restaurant staff who is the only one in the world to combine good cookery and great cabaret at the same time); the secretaries Rose and Sylvie; the receptionists Isabelle and Nathalie (together with the lovely cat, Minette); and also Aziz, Christian, David, Fabrice, Françoise, Jean-Maria and Michel. Thank you all for the nice, small daily chats we had and for being always very kind and having time for me.

A very special thanks also goes to all of my friends and to *my family*, half in Italy and half in Morocco, for supporting me with love for this whole time.

To conclude, my greatest and deepest gratitude is for *Raffaele*, without whom none of this would ever have been possible. Indeed this manuscript represents the completion of a long period of study we have faced together supporting each other. Words are not enough to express what I have inside my heart but I truly thank him so much for everything he gave and did for me in all of these beautiful years.

Grazie !